AN ABSTRACT OF THE DISSERTATION OF

Tabeel A. Jacob for the degree of Doctor of Philosophy in Mechanical Engineering presented on September 1, 2020.

Title: Investigation of In-tube Non-equilibrium Condensation of Low Global Warming Potential Refrigerants

Abstract approved: _____

Brian M. Fronk

This work investigates the in-tube condensation of low global warming potential (GWP) zeotropic refrigerant mixtures R448A, R450A, R452A, R454B and R454C. These refrigerants have been proposed for a wide range of commercial heating, ventilation, air-conditioning applications, but their heat and momentum transport phenomenon were not well understood. Thus, in this study, pressure drop and quasi-local heat transfer coefficients were measured during condensation in a 4.7 mm horizontal tube at mass fluxes ranging from 100 kg m^{-2} s^{-1} to 500 kg m^{-2} s^{-1} at three different saturation conditions (40, 50 and 50 °C). The corresponding temperature glides for these mixtures range from 0.7 °C to 6.3 °C.

Past research has shown that a strong coupling between the heat and mass transfer exists for zeotropic condensation. As a result, the correlations developed for pure fluids generally translate poorly to predictions for mixtures. Therefore to determine

the best modeling method for low GWP mixtures, the measured data from this study were compared against predictions from various heat transfer models from the literature. The heat transfer coefficients for all five refrigerants are best predicted by the Cavallini et al. [21] correlation (Mean absolute percent error, MAPE = 8%), with the mixture effects accounted for using the Silver [96], Bell and Ghaly [12] correction. A comparison of the heat transfer and pressure drop of the new HFC/HFO mixtures against their HFC predecessors indicates that the low GWP mixtures may be considered as viable substitutes from a heat and momentum transport perspective. The two-phase frictional pressure drop for complete condensation of mixtures was also measured. The pressure drop for these low GWP refrigerants was predicted by the Cavallini et al. [19] correlation, with the MAPE equal to 24%.

In addition to the investigation of saturated condensation, an emphasis was placed on the superheated and subcooled condensation. A review of the literature reveals limited investigations on this topic, with only a handful of predictions models available for pure fluids. These models were developed based on various simplifying assumptions, which may be why they exhibit a poor agreement with the measured data for refrigerant mixtures. Therefore, a new model is introduced to predict the heat transfer in the superheated region. The model predicts superheated and complete condensation data with good accuracy, with MAPEs equal to 8% and 12%, respectively. Implementing this model allows for a more accurate representation of the superheated condensation phenomenon and by doing so, permits for a more compact condenser geometry. More broadly, this work will aid in the adoption of low GWP refrigerant technology.

Investigation of In-tube Non-equilibrium Condensation of Low Global Warming Potential Refrigerants

by

Tabeel A. Jacob

A DISSERTATION

submitted to

Oregon State University

in partial fulfillment of
the requirements for the
degree of

Doctor of Philosophy

Presented September 1, 2020
Commencement June 2021

Doctor of Philosophy dissertation of Tabeel A. Jacob presented on September 1, 2020.

APPROVED:

Major Professor, representing Mechanical Engineering

Head of the School of Mechanical, Industrial and Manufacturing Engineering

---

Dean of the Graduate School

I understand that my dissertation will become part of the permanent collection of Oregon State University libraries. My signature below authorizes release of my dissertation to any reader upon request.

Tabeel A. Jacob, Author

ACKNOWLEDGEMENTS

I would like to express my gratitude to my advisor, Dr. Brian Fronk for being a remarkable mentor, teacher, leader, and friend throughout my time in graduate school. His guidance and dedication to his work inspired me to discover my passion for thermal fluid sciences. Over the years, he has had an immeasurable impact on my training, as an engineer and as a young professional. For that, I will always be thankful to him.

I would like to acknowledge my Ph.D. committee members for their valuable feedback during the development of this study. Thank you, Dr. David Blunck, Dr. Wade Marcum, Dr. Kendra Sharp, and Dr. David Hurwitz.

I would like to thank all the current and past members of the Thermal Energy Systems and Transport (TEST) Lab for creating an inclusive and collaborative research environment. Even though we were all working on our independent projects, the willingness among group members to help each other answer questions, troubleshoot codes, provide feedback on presentations, and prepare for qualifying exams was truly heartwarming. In particular, I would like to acknowledge Saad Jajja and Paul Armatis for their support in overcoming the challenges that graduate school threw at us.

I would like to express my gratitude to ASHRAE for its support through the 2017 ASHRAE New Investigator Award and the 2019 Graduate Student Grant-in-Aid award. Also, this work would not have been possible without the financial support from the United States Agency for International Development (USAID) through the

U.S.-Pakistan Centers for Advanced Studies in Energy (USPCAS-E).

Finally, I am thankful to my parents (Nabila and Peter) and my brother (Sachal) for all their love and support. Thank you for playing such a crucial part in shaping the person I am today, and for encouraging me to pursue my passion for engineering. You have afforded me countless opportunities and have always prioritized my education, for which I am eternally grateful. I would also like to thank Aisha McKee, for all her love, support, and encouragement during all those good and not so good times in graduate school.

TABLE OF CONTENTS

TABLE OF CONTENTS (Continued)

TABLE OF CONTENTS (Continued)

LIST OF FIGURES

LIST OF FIGURES (Continued)

Figure Page

LIST OF FIGURES (Continued)

LIST OF TABLES

LIST OF TABLES (Continued)

LIST OF APPENDIX TABLES

Chapter 1: Introduction

Condensation of zeotropic mixtures is of interest to numerous industries including power generation, chemical process, and heating, ventilation, cooling, air conditioning, and refrigeration (HVAC&R). It differs from the condensation of pure fluids, such that the resistances of the heat and mass transfer in the vapor phase can no longer be considered negligible and the liquid/vapor interface temperature may deviate significantly from the equilibrium saturation temperature. Motivated by legislative actions on the HVAC&R industry mandating the use of new refrigerants, the goal of this research is to better understand the coupled heat and mass transfer during internal flow condensation of new, low global warming potential, zeotropic refrigerant mixtures. This will be accomplished by designing and conducting an experimental investigation of different zeotropic refrigerant mixtures to evaluate the heat transfer and pressure drop under representative operating conditions. Particular attention will be given to the heat transfer during the superheated and subcooled condensation regions. The heat transfer in these regions is conventionally assumed to be single-phase vapor and liquid, respectively. However, past experiments indicate that this assumption does not accurately describe the actual non-equilibrium heat transfer mechanisms, particularly for mixtures. The experimental data are used to assess the predictive capability of existing models for superheated, subcooled, and saturated condensation conditions, and to guide the development of more accurate predictive

methods for zeotropic refrigerants. The results from this study will (1) allow prediction of HVAC&R equipment performance when new refrigerants are "dropped-in" to replace phased out refrigerants, and (2) enable the more efficient design of next-generation condensers in multiple industries.

1.1 Motivation

International agreements and regulations have outlined the plans to phase out hydrofluorocarbon (HFC) refrigerants due to their environmental impact. These HFC refrigerants are currently being used in a wide range of commercial, automotive, and residential HVAC&R systems. Notably, the Kigali Amendment to the Montreal Protocol – with support from over 170 countries – aims to reduce the use of HFC refrigerants by more than 80% over the next 30 years. Similarly, aggressive regulations such as the F-gas Regulation No. 517/2014 [88], call for a 79% reduction in European market supply for HFCs from 2015 to 2030. Furthermore, it prohibits the use of refrigerants with Global Warming Potential (GWP) higher than 2500 for refrigeration equipment, beginning in the year 2020. The European Union directive 2006/40/EC [38] limits the GWP of all new cars below 150 after 2017. Therefore, there is an urgent need to find alternatives to HFCs which have significantly lower GWP.

The majority of the HVAC&R applications operate based on the vapor compression cycle. A simple vapor compression cycle consists of four main components: condenser, compressor, evaporator, and an expansion device. The refrigerant circu-

lates through the evaporator where it undergoes vaporization as energy is transferred from the space being cooled to the refrigerant. The refrigerant is then compressed to a relatively higher pressure and temperature by the compressor. After leaving the compressor, the refrigerant vapor undergoes complete condensation in the condenser as it rejects heat to the surroundings. Finally, the refrigerant expands to the evaporator inlet pressure in an expansion device. The selection of the working fluid is an important consideration during the design of these systems. The thermodynamic properties of the fluid dictate the operating pressures and required flow rates for different applications. The heat transfer and the pressure drop characteristics of the working fluid during phase change dictate the sizes of the condenser and evaporator. In addition, the pressure drop in these components is directly related to the power required by the compressor and consequently, the coefficient of performance (COP) of the system. Therefore it is critical to understand and compare the heat transfer and momentum transport phenomenon to their HFC predecessors. A drastic increase in the power consumption of the applications utilizing these new refrigerants could potentially offset the environmental benefits from using lower GWP fluids. Thus, any proposed alternatives to HFCs must have similar or better heat transfer and pressure drop characteristics to be commercially viable and environmentally friendly.

Pure Hydrofluoroolefins (HFOs) have been proposed as potential alternatives to HFCs for HVAC&R applications. Compared to pure HFCs, HFOs have significantly lower GWP. However, previous investigations on the condensation heat transfer of pure HFO refrigerants, such as R1234ze (GWP <1) and R1234yf (GWP <1)[7], have reported lower heat transfer coefficients compared to their HFC pre-

decessors [30, 85, 52, 34]. Furthermore, both R1234ze and R1234yf are classified as mildly flammable A2L refrigerants (ASHRAE [7]), which complicates their adoption. HFC/HFO refrigerant mixtures are another potential alternative to HFC refrigerants. They have the advantage of lower GWP than pure HFCs and lower flammability risk than some pure HFOs. The GWPs of commonly used refrigerants and their proposed HFO or HFO/HFC replacements are reported in Table 1.1. The corresponding temperature glides, discussed below, of the refrigerant mixtures are also reported in Table 1.1.

There is presently a lack of publicly available experimental condensation data available for these refrigerant mixtures. Because zeotropic condensation is a function of coupled heat (latent and sensible) and mass transfer effects, conventional condensation correlations for pure fluids cannot be accurately used to predict mixture condensation. Past studies[41] on the condensation heat transfer of zeotropic refrigerant mixtures have reported a degradation in the heat transfer coefficients as compared to the individual components of the mixture at the same operating conditions. It is, therefore, vital to understand the heat and mass transfer of these zeotropic refrigerant mixtures and to be able to predict their heat transfer and pressure drop to design next-generation condensers.

1.2 Zeotropic condensation phenomenon

Condensation of miscible refrigerant mixtures can be broadly classified into three categories, azeotropic, near-azeotropic, and zeotropic mixtures, based on the tem-

Table 1.1 GWPs of commonly used HFC refrigerants and their proposed HFC/HFO replacements [7]. The temperature glides are calculated at a pressure corresponding to $T_{sat,avg} = 50$ °C, from REFPROP 10 [70].

Refrigerant	**ASHRAE safety classification**	**Type**	**GWP**	**Replacement for**	**Temperature glide (°C)**
R134a	A1	HFC	1300	-	-
R404A	A1	HFC mixture	3943	-	0.3
R410A	A1	HFC mixture	3000	-	0.1
R1234yf	A2L	HFO	<1	R134A	-
R1234ze(E)	A2L	HFO	<1	R134A	-
R1233zd(E)	A1	HFO	1	R245fa	-
R448A	A1	HFC/HFO	1360	R404A	4.3
R450A	A1	HFC/HFO	547	R134a	0.6
R452A	A1	HFC/HFO	1952	R404A	3.0
R454B	A2L	HFC/HFO	467	R410A	1.2
R454C	A2L	HFC/HFO	148	R404A	6.3

perature glide they exhibit. For azeotropic mixtures, the dew point and the bubble point are the same, and therefore the temperature glide is equal to zero. The heat transfer and pressure drop behavior of azeotropic mixtures are generally well predicted by correlations and models developed for pure fluids [36, 16, 51]. Conversely, condensation of near-azeotropic and zeotropic mixtures is characterized by a non-isothermal phase change at a constant pressure. This occurs due to the difference in saturation temperatures of the constituent fluids. Equation 1.1 shows that temperature glide is the difference between the temperature at which condensation begins (dew point), and ends (bubble point) at a constant pressure.

$$\Delta T_{glide} = T_{dew} - T_{bubble} \tag{1.1}$$

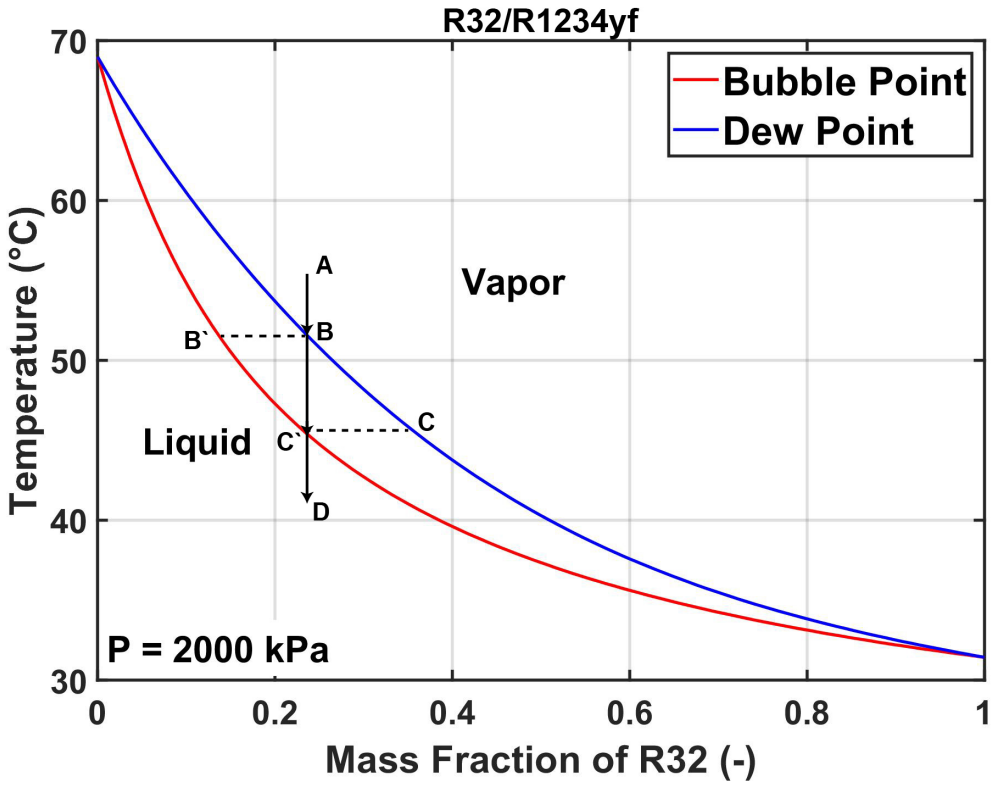

Figure 1.1: Phase diagram of R32/R1234yf mixtures at a constant pressure equal to 2000 kPa.

To further understand the nuances of the underlying coupled heat and mass transfer associated with condensation of zeotropic mixtures, it is instructive to analyze the constant pressure phase diagram of binary mixtures of R32 (HFC) and R1234yf (HFO). Two of the mixtures (R454B and R454C from Table 1.1) investigated in this study are in fact mixtures of R32 and R1234yf. In Figure 1.1, the x-axis increases with an increasing mole fraction of R32 and decreases with a mole fraction of R1234yf. The two plots in the figure show variations in the dew point temperature (blue line) and bubble point temperature (red line) with varying molar fractions.

As can be observed in Figure 1.1, the temperatures corresponding to 0 and 1 mole fraction of R32 are the saturation temperatures of R1234yf and R32, respectively, at a constant pressure equal to 2000 kPa. In this case, R32 is the more volatile component out of the two components. If a superheated ammonia/water mixture, as represented by point A on Figure 1.1, is cooled, sensible cooling of the mixture occurs until the dew point temperature is reached. As condensation commences (point B), preferential condensation of the less volatile component (R1234yf) occurs. This results in significantly different equilibrium compositions of the vapor and the condensate droplets. The mole fraction of R32 in the liquid condensate, which is represented by point B′ in Figure 1.1, is much lower than in the vapor phase (point B). As condensation proceeds, the composition of both the liquid and vapor phase continuously changes. As more energy is removed from the system, the mixture further cools down to the dew point temperature (point C′) and the concentration of the liquid approaches the original concentration of the superheated gas. Point C represents the concentration of the very last bubbles which will condense. As the mixture is further cooled below the dew point temperature to point D, no change in the concentration occurs.

The ideal process described above assumes thermodynamic equilibrium throughout the phase change. However, in reality, condensation of zeotropic refrigerants is inherently a non-equilibrium process. For the condensation to occur, temperature and concentration gradient must exist between the bulk liquid and vapor phases to drive the transport of individual components to the liquid/vapor interface. Figure 1.2 shows representative temperature and concentration distributions that develop

during film condensation of a binary mixture. As condensation proceeds, preferential condensation of the less volatile component occurs at the interface which increases the local concentration of the more volatile component. These concentration gradients promote the back diffusion of the more volatile component from the vapor interface to the vapor bulk and diffusion of the less volatile component from vapor bulk to the vapor interface. Thus, there is an additional mass transfer resistance to the condensation process. Similar to the vapor phase, a concentration gradient develops between the liquid interface and the bulk liquid as well.

Additionally, the increased concentration of the more volatile component at the interface will result in the depression of the liquid/vapor interface temperature. This is dissimilar to the condensation of pure fluids, during which the interface temperature (T_{int}) is equal to the bulk saturation temperature (T_{sat}) defined by the operating pressure. During condensation, the heat flux through the condensate film (q''_T) is equal to:

$$q''_T = \alpha(T_{int} - T_{w,in}) \tag{1.2}$$

where α is the film heat transfer coefficient, and $T_{w,in}$ is the tube wall temperature. For zeotropic mixtures, the maximum driving temperature occurs when the mass transfer is infinite and the T_{int} is equal to the local equilibrium saturation temperature T_{eq}. In reality, the interface temperature will be somewhere between the equilibrium saturation temperature and the bubble point temperature, T_{bubble}. The magnitude of the reduction in interface temperature directly depends on the local concentration at the interface, which depends on the vapor phase mass transfer rate. This depression of the interface temperature causes heat transfer degradation

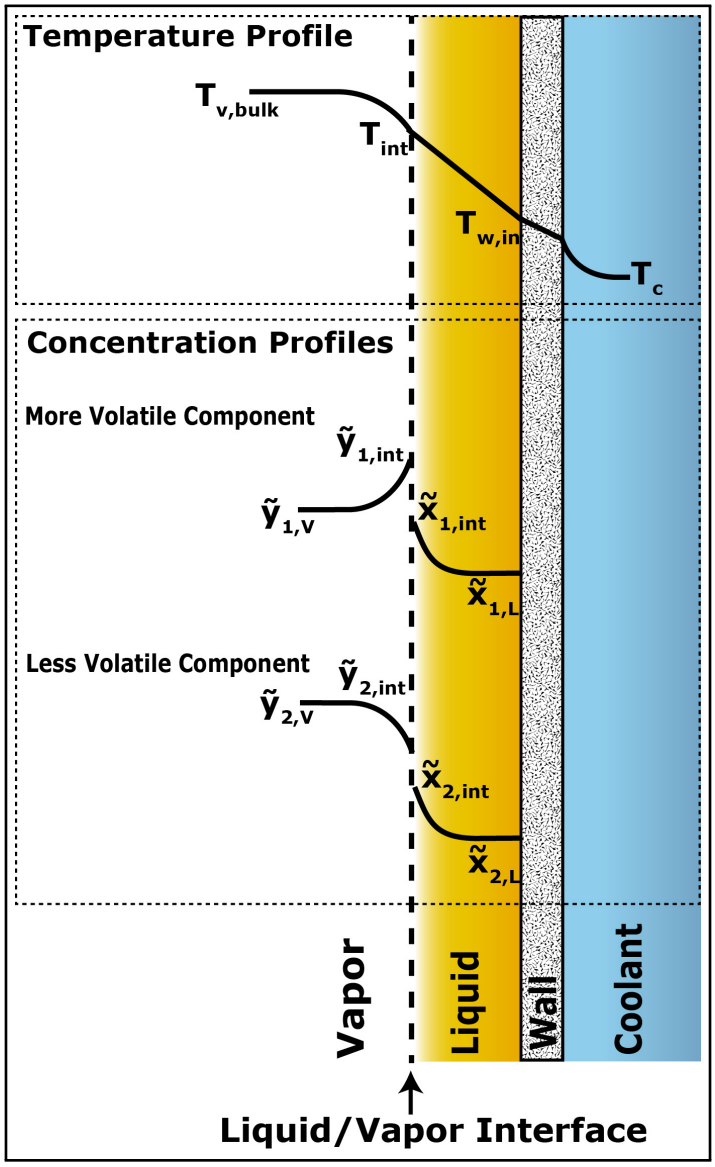

Figure 1.2: A schematic of film condensation of zeotropic binary mixture

because of the reduction in the driving temperature difference ($T_i - T_{w,in}$).

Thus, the heat and mass transfer are strongly coupled for zeotropic mixtures. Along with the heat transfer resistances (sensible and latent) in the liquid film, prediction methods for the vapor phase sensible resistance, and mass transfer resistances in both the vapor and liquid phases are required to understand and accurately model the process.

1.3 Superheated and subcooled condensation phenomenon

Conventionally, the heat transfer in a condenser is modeled by assuming a local thermodynamic equilibrium and then categorizing the flow as either superheated vapor, two-phase flow, or subcooled liquid based on the specific bulk enthalpy. Single- or two-phase heat transfer correlations are then used depending on the expected flow regime. Condensation is assumed to begin when the bulk enthalpy approaches the vapor saturation enthalpy and ends when the bulk enthalpy reaches liquid saturation enthalpy. However, past flow visualization experiments [77] on the cooling of pure superheated refrigerants have shown that vapor begins to condense as soon as the wall temperature drops below the saturation temperature, even when the bulk enthalpy is above the saturation vapor enthalpy. In this so-called superheated condensation region, the measured local heat transfer coefficients are much greater than those predicted by single-phase vapor correlations. This is visually illustrated in a schematic in Figure 1.3.

Similarly, condensation continues to occur even when the bulk enthalpy is less

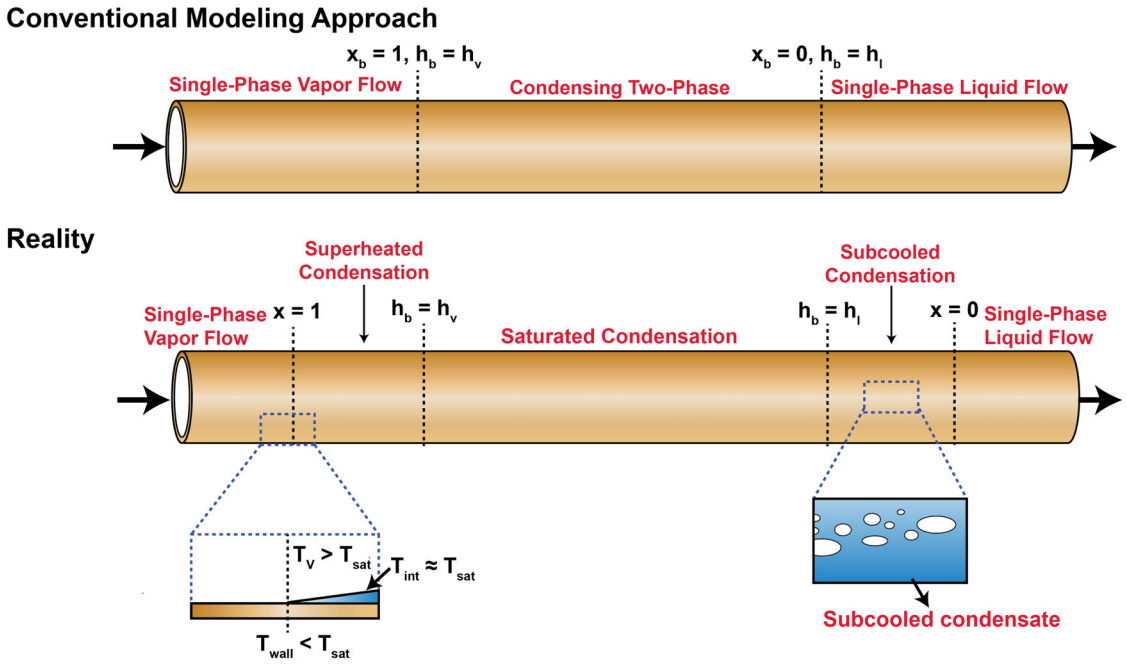

Figure 1.3: A schematic highlighting the differences in the condensation phenomena considered by the conventional modeling approach and the reality. The conventional modeling approach ignores superheated and subcooled condensation.

than the saturated liquid enthalpy. This discrepancy exists because the conventional equilibrium treatment ignores the radial variation in temperature for flow condensation in a tube. Thereby, the sensible cooling of the liquid condensate film throughout the condensation process is considered negligible. However, as indicated by the above discussion on film condensation of zeotropic mixtures, a driving temperature gradient must exist between the liquid, vapor, and the liquid/vapor interface. This is true for both single and multi-component fluids. Because the liquid film must be subcooled and the heat flux transferred in the two-phase regime is a combination of latent and sensible heat fluxes, complete condensation can not occur when the bulk enthalpy

reaches the saturated liquid enthalpy. Otherwise, a departure from the conservation of energy will occur.

As condensation occurs outside the bounds of the traditionally defined two-phase region, it is extremely important to understand the pressure drop and heat transfer for those conditions. These non-equilibrium effects are of increasing importance for high-temperature heat pumps and heat pump water heaters, where there may be significant desuperheating from the compressor outlet. For example, the review by Arpagaus et al. [6] indicates that the superheat for refrigerant entering the condenser in a high temperature heat pumps may be as high as 35 °C. Furthermore, accurately predicting superheated, and subcooled condensation heat transfer offers an opportunity to design more compact heat exchangers.

1.4 Dissertation organization

For a successful transition to low GWP refrigerant mixtures in the HVAC&R industry, it is critical that the heat and mass transfer of these refrigerants is well understood. Furthermore, this transition can also serve as an opportunity to develop a condenser modeling methodology that considers the effects of superheated and subcooled condensation. However, doing so requires further exploration of the phenomenon. Thus, this dissertation adopts a systematic approach to investigating the superheated, saturated and subcooled condensation of low GWP zeotropic refrigerant mixtures. The chapters in this dissertation are structured in the following manner:

1. Chapter 2 presents an in-depth discussion of the prior heat transfer and pressure drop investigations on the condensation of single- and multi-component fluids. Various modeling strategies used by previous investigators, based on equilibrium and non-equilibrium assumptions, are introduced. Informed by the existing literature, the scope and the objectives of the current study are finalized.

2. Chapter 3 provides the details of the experimental facility used in this study. Furthermore, the data reduction methodologies used to calculate quasi-local heat transfer coefficients and pressure drop in the test section are described.

3. Chapter 4 presents the heat transfer and pressure drop results. The measured data is compared against correlations from the literature.

4. Chapter 5 presents the development of a novel modeling methodology for predicting superheated, saturated, and subcooled condensation of low GWP refrigerant mixtures. This model is evaluated against measured data to determine its accuracy. Furthermore, the design of a condenser for a commercial refrigeration system is carried out, using both the conventional modeling approach and the novel modeling approach from this study. The difference in the resulting heat exchanger areas is highlighted.

5. Chapter 6 presents the conclusions and contributions from the study, and identifies the relevant topics for future research.

Chapter 2: Prior Work

In-tube condensation has been studied extensively due to its relevance in a range of industries including the nuclear, chemical process, and HVAC&R industry. A considerable amount of research effort has been directed towards investigating condensation of steam, as well as the adiabatic two-phase flow of water/air and oil/air mixtures, due to their relevance to power generation and petroleum industry [13, 95, 68, 71].

However, refrigerants typically operate at much higher reduced pressures and have significantly lower surface tension compared to water. Thus, empirical and semi-empirical prediction methods developed for condensation of steam often translate poorly to condensation of synthetic refrigerants. Furthermore, the operating conditions and geometries of the heat exchangers for these applications differ significantly.

Therefore, this review focuses specifically on the condensation of single-component and multi-component synthetic refrigerants and identifies the gaps in the literature that the present work addresses. This review begins with the pressure drop and condensation heat transfer of pure fluids, and the relevant heat transfer mechanisms associated with it. Studies on the condensation of zeotropic mixtures are then reviewed. Finally, prior work on the superheated and subcooled condensation of refrigerants is presented.

2.1 Pressure drop

For a steady condensing two-phase flow in a channel, the total pressure gradient consists of three terms (as shown in Carey [15] and Garimella and Fronk [45]):

$$\left(-\frac{dP}{dx}\right)_T = \underbrace{\left(-\frac{dP}{dx}\right)_g}_{\text{Hydrostatic pressure gradient}} + \underbrace{\left(\frac{dP}{dx}\right)_a}_{\text{Acceleration pressure gradient}} + \underbrace{\left(-\frac{dP}{dx}\right)_f}_{\text{Frictional pressure gradient}} \tag{2.1}$$

The hydrostatic pressure gradient accounts for any gravitational effects. Its magnitude depends on the orientation of the channel, the void fraction of the flow, and the liquid and vapor phase densities. The acceleration pressure gradient considers the pressure gain due to deceleration of the flow as it condenses from vapor to a denser liquid phase. It can be evaluated from a momentum balance on a given control volume.

During condensation, the vapor travels at a much higher velocity than the liquid due to a large phase density difference and to satisfy continuity. Rayleigh-–Taylor instabilities are observed at the interface between the vapor and liquid phases. Therefore, the frictional pressure drop occurs due to the combination of shear between the fluids and the wall, as well as the interfacial shear between the gas and vapor phases. Purely analytical determination of the frictional pressure gradient for condensing flows is challenging because of the formation of complex flow structures. Therefore, past researchers have developed empirical and semi-empirical relations to accurately estimate the frictional pressure gradient for specific fluids and geometries. This

is typically done by introducing two-phase multipliers (Φ) (originally proposed by Lockhart and Martinelli [72]). In general, the two-phase multipliers are a function of the channel geometry, flow quality, mass flux, and fluid properties. With a known two-phase multiplier, the frictional pressure drop can be calculated as:

$$\left(-\frac{dP}{dx}\right)_f = \Phi_{LO}^2 \left(-\frac{dP}{dx}\right)_{f,LO} \tag{2.2}$$

The term on the right hand side of Equation 2.2 represents the pressure gradient for single-phase liquid flowing at the same total mass flux as the two-phase mixtures.

2.1.1 Prediction methods

Several two-phase multiplier correlations have been introduced by researchers to account for different fluids, tube diameters and channel geometries [11, 75, 22, 23]. Among one of the most widely cited two-phase pressure drop correlations, the empirical Friedel [39] correlation was developed by considering adiabatic 25,000 frictional pressure drop data points with a wide range of fluids (water, refrigerants, air, oil, etc.) and tubes (12 mm $< D_h <$ 49 mm). It considers the two-phase Weber number (We_{TP}) and Froude (Fe_{TP}) number to account for surface tension and gravitational effects. The effect of mass flux is accounted by incorporating the vapor-only (f_{vo}) and liquid-only (f_{lo}) friction factors. The Friedel [39] correlation has been reported to show good agreement with condensation data for a variety of working fluids and operating conditions [16, 30, 105, 94]. For horizontal flow, the liquid only two-phase multiplier is defined as:

$$\Phi_{LO}^2 = C_1 + \frac{3.21 C_2}{Fr_{TP}^{0.0454} We_{TP}^{0.035}} \tag{2.3}$$

$$C_1 = (1-x)^2 + x^2 \left(\frac{\rho_l f_{vo}}{\rho_v f_{lo}} \right)$$

$$C_2 = x^{0.78}(1-x)^{0.224} \left(\frac{\rho_l}{\rho_v} \right)^{0.91} \left(\frac{\mu_v}{\mu_l} \right)^{0.19} \left(1 - \frac{\mu_v}{\mu_l} \right)^{0.7}$$

Müller-Steinhagen and Heck [83] developed an empirical correlation that was validated using a large database of experimental pressure drop (including the data used by Friedel [39] and Martinelli and Nelson [75]). This correlation uses the single-phase vapor and liquid pressure drops as bounds and thus, shows no discontinuity between the single-phase correlations and two-phase correlations when the quality equals one and zero.

Earlier research on two-phase pressure drop was focused on primarily on air/water and some air/oil mixtures [78]. However, the thermophysical properties of the these mixtures differ significantly from those of synthetic refrigerants that are of interest in this study. Haraguchi et al. [48] developed a correlation by analysing the pressure drop data of R22, R134a and R123 in an 8.4 mm horizontal tube. The correlation is defined in terms of the turbulent-turbulent Martinelli parameter (X_{tt}) and the vapor two-phase multiplier:

$$\Phi_V^2 = 1 + 0.5 \left[\frac{G}{\sqrt{gd\rho_v(\rho_l - \rho_v)}} \right]^{0.75} X_{tt}^{0.35} \tag{2.4}$$

$$X_{tt} = \left(\frac{\rho_l}{\rho_v} \right)^{0.571} \left(\frac{\mu_v}{\mu_l} \right)^{0.143} \left(\frac{1-x}{x} \right)$$

Soliman et al. [98] also developed a simple empirical correlation, by carrying out a curve fit on the Lockhart-Martinelli [75] data, for predicting pressured drop in the annular flow regime. The highest pressure drops during condensation occur in the annular regime, which is generally associated with high qualities and thus, relatively high vapor velocities. The correlation is valid for $0 < X_{tt} < 10{,}000$):

$$\Phi_V^2 = 1 + 2.85 X_{tt}^{0.523} \tag{2.5}$$

The Cavallini et al. [19] correlation (Equation 2.6) has a similar form as the Friedel [39] correlations and explicitly considered the effects of different tube surface roughness and liquid entertainment in the vapor core in shear dominated flows (i.e., annular flows). This model was primarily developed for annular flows in minichannels ($D_h = 0.5$ to 3.2 mm) but was also shown to be applicable to intermittent flows and macro tubes ($D_h = 8$ mm).

$$\left(-\frac{dP}{dx} \right)_f = \Phi_{LO}^2 2 f_{LO}^* \frac{G^2}{D_h \rho_L} \tag{2.6}$$

$$f_{LO}^* = 0.046 Re_{LO}^{-0.2}$$

$$\Phi_{LO}^2 = Z + 3.595 F H (1-E)^W$$

$$W = 1.398 P_r$$

$$Z = (1-x)^2 + x^2 \left(\frac{\rho_l}{\rho_v} \right) \left(\frac{\mu_l}{\mu_v} \right)^{0.2}$$

$$F = x^{0.9525} (1-x)^{0.414}$$

$$H = \left(\frac{\rho_l}{\rho_v}\right)^{1.132} \left(\frac{\mu_v}{\mu_l}\right)^{0.44} \left(1 - \frac{\mu_v}{\mu_l}\right)^{3.542}$$

Later, Del Col et al. [31] compared their experimental data from five different test sections, with different geometries (circular, square and irregular) and diameters (D_h = 0.76 to 2 mm), with the Cavallini et al. [19] model. They found that the model overestimated the contribution of surface roughness effects for low liquid-only Reynolds number (i.e., laminar region). Del Col et al. [31] argued that this is due to the fact that surface roughness effects on the pressure drop are comparatively negligible for laminar flows. Therefore, they proposed a modified definition of the liquid-only friction factor which accounted for the surface roughness effects only in the transition and turbulent regions.

Andresen et al. [5] collected condensation data for refrigerant blends R404A and R410A at near-critical pressures (P_r = 0.8, 0.9) in five channels sizes (0.76 <D <9.4 mm). The experimental data was generally overpredicted by the correlations from the literature. They hypothesized that this is because the ratio of the liquid/vapor densities and viscosities approaches unity at the critical point, and interfacial shear effects decrease. Thus, they proposed a two-phase multiplier correlation for predicting the pressure drop during condensation of HFC refrigerant mixtures at near-critical pressure.

2.1.2 Application to mixtures

Several past researchers have investigated if the two-phase frictional pressure drop models developed for pure or azeotropic fluids can be extended to zeotropic mixtures.

Koyama [66] collected pressure drop data for pure and three different mixtures (23 - 73% R22 by mole) of R22 and R114 inside an 8.32 mm spirally grooved horizontal copper tube. Their data was well predicted by the Lockhart and Martinelli [72] method for all fluids, regardless of the molar concentration.

Del Col and co-workers reported the pressure drop during adiabatic two-phase flow of both pure and mixtures of R32/R1234ze(E) (23/77, 50/50 and 75/25% by mass) with temperature glides equal to 10.9, 7.4, and 3, respectively °C [33, 32]. R32 is a HFC, while R1234ze(E) is a HFO refrigerant. The tests were conducted in a 0.96 mm micro-channel at $T_{sat,avg} = 40$°C and mass fluxes from $200\,\mathrm{kg\,m^{-2}\,s^{-1}}$ to $800\,\mathrm{kg\,m^{-2}\,s^{-1}}$. The resulting data for pure fluids and mixtures were well predicted by the Del Col et al. [31] model, with the Mean Absolute Percentage Error (MAPE) equal to 7.7%.

Azzolin et al. [8] measured the pressure drop of zeotropic refrigerants R455A (R32, R1234yf, and R744 at 21.5/75.5/3.0% by mass) and R452B (R32, R1234yf, and R125 at 67.0/26.0/7.0% by mass) in an 8 mm tube and 0.96 mm tube. The temperature glide of R455A and R452B are 9.8 °C and 1.1 °C, respectively. Two-phase adiabatic pressure drops agreed well with the Friedel [39] correlation, with a MAPE equal to 10.9%. Similar results have been reported in other studies on the condensation of mixtures [2, 105], which confirms that models developed for pure fluids can be successfully applied to zeotropic mixtures at similar operating conditions. In the present study, the pressure drop was measured in addition to heat transfer, and the observations from prior work were confirmed for the new refrigerants under consideration here. These results are discussed in Chapter 4.

2.2 Saturated condensation of pure fluids

The internal convective condensation behavior of pure saturated refrigerants has been widely studied and is fairly well understood [44, 16, 18, 62]. Several past researchers have developed semi-empirical heat transfer correlations that attempt to identify and model the dominant heat transfer mechanisms.

As condensation begins in a tube, a thin layer of condensate film develops around the surface. This layer of condensate continues to grow as more vapor condenses. In a horizontal tube, this results in the development of the annular flow regime. The liquid condensate travels at a much slower velocity than the vapor due to differences in densities and to satisfy continuity. The shear between the vapor and liquid phases causes the formation of interfacial waves as described by the Kelvin-Helmholtz instability theory. Generally, these waves tend to enhance heat transfer. In a horizontal tube, eventually the weight of the condensate can no longer be supported in the upper part of the tube and the effect of gravity becomes more significant, a pool of liquid begins to form at the bottom of the tube. This is defined as the stratified-wavy flow regime. In this regime, the vapor primarily condenses at the top of the tube and travels down the tube walls. Past researchers [21, 101] have similarly modeled this process using the Nusselt's [84] laminar falling film analysis. The heat transfer through the liquid pool is comparatively lower due to its higher thermal resistance. At relatively low qualities (high liquid mass fraction) and high vapor velocities, the transition to the intermittent regime may occur. This occurs when the magnitude of the interfacial waves becomes larger than the tube diameter and discrete liquid and vapor bubbles/slugs are formed. The heat transfer through this regime is a

combination of annular flow and single-phase liquid flow.

The dominant thermal resistance during the in-tube condensation of pure saturated vapors is the resistance through the liquid condensate. The main heat transfer mechanisms that occur depend on the prevailing flow regime (e.g. annular, intermittent, stratified-wavy). At the beginning of condensation, the thickness of the condensate is thin and its thermal resistance is relatively small. Therefore, the highest heat transfer coefficients are associated with higher qualities. As condensation proceeds, this resistance increases as the liquid condensate film thickness increases. Similarly, the heat transfer further deteriorates as liquid pool forms at the bottom of the tube in the stratified-wavy regime. Eventually, as the vapor quality approaches zero, the heat transfer coefficients are reduced to those of single-phase convective liquid flow.

Therefore, the ability to accurately predict heat transfer during condensation depends on being able to accurately identify the expected flow regime for a given set of operating conditions. Several flow regime maps have been introduced to determine the conditions at which these regimes occur and the transition criteria between them [99, 9, 14, 74]. Taitel and Dukler [99] were among the first researchers to develop transition criteria based upon the underlying physics, rather than just relying on empirical data. Earlier efforts focused on adiabatic two-phase flows such as air-water and air-oil mixtures [9]. These have shown to have limited applicability when extrapolated to condensing flows [14, 20]. Furthermore, the predictions from these flow maps do not always agree with each other, and different authors have introduced different names for similar flow structures. This is because the process of collecting

flow regime data often involves visually determining the regime and therefore, can be highly subjective.

Garimella and Fronk [45] state that the main relevant regimes for condensation modeling in large horizontal tubes are annular and stratified wavy regimes. This is because the transition between these regimes distinguishes whether the dominant heat transfer mechanisms are shear driven or gravity driven. This argument was also used as the basis of the semi-empirical heat transfer correlation by Dobson and Chato [36]. In their model, they considered the relative contribution of the shear and gravity effects during condensation. The height of the pool during gravity driven condensation was obtained by determining θ (Figure 2.1), the upper angle of the tube not wetted by the stratified liquid. The Zivi [112] model was used to determine the void fraction. Dobson and Chato [36] used condensation data of refrigerants (R-12, R-22, R-134a and R-32/R125 mixtures) in horizontal tubes ($3.14 < D < 7.04\,\text{mm}$) at varying mass fluxes ($25 < \text{G} < 800\,\text{kg m}^{-2}\,\text{s}^{-1}$) to guide development of their model.

The Thome et al. [101] multi-regime condensation model uses the flow regime map of El Hajal et al. [37] to identify the dominant heat transfer mechanisms occurring for a given flow. For annular, intermittent and mist flows, the heat transfer primarily occurs through the thin liquid film that develops between the vapor core and the inner surface of the tube. For stratified and wavy-stratified flows, the heat transfer is a combination of the falling film heat transfer, α_f at the upper surface of the tube and the convection heat transfer coefficient, α_c through the liquid pool. A visual representation of the falling film and pool are shown in Figure 2.1. Again, the depth of the liquid pool, as well as the areas associated with each mode of heat transfer

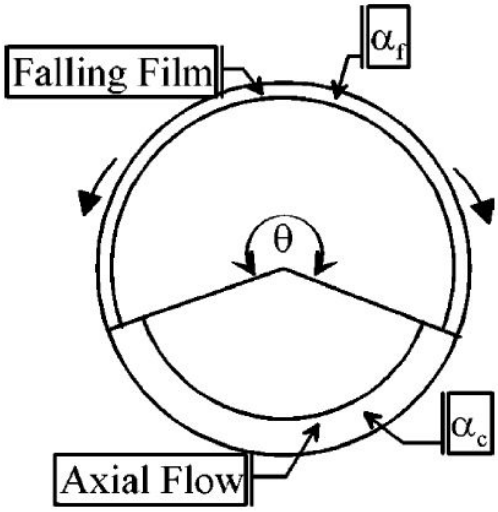

Figure 2.1: Schematic of the falling film and liquid pool during gravity driven condensation, from Thome et al. [101]

can be determined by evaluating θ. The resulting two-phase heat transfer coefficient can be modeled as:

$$\alpha = \left[\frac{\theta\alpha_f + (2\pi - \theta)\alpha_c}{2\pi}\right] \tag{2.7}$$

Another multi-regime model was introduced by Cavallini et al. [20] for the condensation of refrigerants. Later on, Cavallini et al. [21] presented a simplified, easier-to-implement version of the model which was developed from an extensive database of condensation heat transfer data in tubes with $D > 3$ mm. The model accounts for different flow regimes by categorizing them into either ΔT-dependent or ΔT-independent flows. ΔT is the temperature difference between the wall and the fluid saturation temperature. ΔT-independent flows include annular and intermittent flows, where the flow structure is shear dominated and heat transfer is primarily due

to convection. For ΔT-independent flows such as stratified and stratified-wavy flows, the role of gravitational force is more significant. The transition criterion in this model is defined in terms of transition dimensionless gas velocity J_G, which is based upon the turbulent-turbulent Lockhart−Martinelli parameter. The model showed good agreement with 4471 experimental data points (representative of hydrochlorofluorocarbon, HFC, hydrocarbon, ammonia, water, and carbon dioxide condensation), with the MAPE equal to 15%. The two relations proposed by Cavallini et al. [21] for temperature-independent and temperature-dependent regimes are shown in Eq. 2.8 and Eq. 2.9.

Δ T-independent:

$$\alpha_a = \alpha_{lo}\left[1 + 1.128x^{0.8170}\left(\frac{\rho_l}{\rho_v}\right)^{0.3685}\left(\frac{\mu_l}{\mu_v}\right)^{0.2363}\left(1 - \frac{\mu_v}{\mu_l}\right)^{2.144} Pr_L^{-.1}\right] \tag{2.8}$$

Δ T-dependent:

$$\alpha_d = [\alpha_a(J_G^T/J_G)^{0.8} - \alpha_{STRAT}](J_G/J_G^T) + \alpha_{STRAT} \tag{2.9}$$

$$\alpha_{STRAT} = 0.725\left[1 + 0.741\left(\frac{1-x}{x}\right)^{0.3321}\right]^{-1}\left[\frac{k_l^3\rho_l(\rho_l - \rho_v)gh_{lv}}{\mu_l D\Delta T}\right]^{0.25} + (1 - x^{0.087})\alpha_{lo}$$

where the α_{lo} is the single-phase liquid-only heat transfer coefficient evaluated using Dittus and Boelter [35] correlation. In Equation 2.9, the ΔT term is not known. Therefore, an iterative solution is required to calculate both the ΔT and α_d

for a given heat flux condition.

Other authors have relied on purely empirical approaches to predict condensation heat transfer coefficients. The highly cited Shah [90] correlation was developed by analyzing condensation data in horizontal tubes for a wide range of operating conditions and fluids. Later, Shah [89, 92, 91] presented revised versions of the correlation which were validated against a database containing condensation data for 33 fluids, tubes with diameters ranging 0.1 to 49 mm, reduced pressures ranging from 0.0008 to 0.946, and mass fluxes from 1.1 to 1400 kg m^{-2} s^{-1}. In the latest version of the correlation, three purely empirical regimes were defined. The heat transfer in regime I is evaluated using a two-phase multiplier type correlation for annular flow (similar to the one suggested in Shah [90]):

$$\alpha_I = \alpha_{lo}\left[\left(1+\frac{3.8}{Z^{0.95}}\right)\left(\frac{\mu_l}{14\mu_v}\right)^{0.0058+0557P_r}\right] \tag{2.10}$$

$$Z = (1/x-1)^{0.8}P_r^{0.8}$$

The heat transfer in regime III is evaluated in a similar manner as Nusselt's analysis [84]:

$$\alpha_{Nu} = 1.32Re_{LO}^{-1/3}\left[\frac{k_l^3\rho_l(\rho_l-\rho_v)g}{\mu_l^2}\right]^{1/3} \tag{2.11}$$

The heat transfer in regime II is a sum of α_I and α_{Nu}. The transition criteria between regimes are defined in terms of the dimensionless gas velocity and vapor-only Weber number. Despite their simplicity and lack of theoretical background, the correlations by Shah are able to predict the condensation heat transfer coefficients

fairly well. For this reason, the latest Shah [91] correlation was recommended in the ASHRAE [7] handbook for predicting condensation heat transfer coefficients of refrigerants.

2.2.1 Condensation of pure Hydrofluoroolefins (HFOs)

As discussed in the Chapter 1, new refrigerant mixtures comprised of HFCs and HFOs have been proposed as alternatives to high GWP HFCs. The condensation behavior of HFCs in mini- and micro-channels has been widely studied and is well understood [16, 67, 102, 94, 10]. On the contrary, the condensation of HFOs is still a relatively new area of research and has received much attention recently. Some of the notable HFOs include R1234ze(E), R1234yf, and R1233zd(E), which have a GWP equal to or less than 1. Therefore, their adoption in HVAC and power generation industries may greatly reduce the environmental impact of these industries. However, it is also critical to investigate the heat transfer performance of these refrigerants, as it is directly related to the size and COP of the system. It is also crucial to compare HFO performance to that of their HFC predecessors to determine their viability as substitutes. Therefore, a summary of the studies investigating the condensation of pure HFO is presented in this section.

Both R1234yf and R1234ze(E) have been proposed as potential replacements for R134a for applications in mobile air conditioning systems, refrigerators, energy-efficient chillers, etc. Del Col et al. [30] experimentally measured the local heat transfer coefficients of R1234yf in a 0.96 mm horizontal channel at a constant sat-

uration temperature equal to 40 °C. The measured heat transfer coefficients were well predicted by the Cavallini et al. [21] correlation. Furthermore, the heat transfer coefficients of R1234yf were 15 to 30% lower than those of R134a at the same operating conditions. This degradation increased with increasing quality and mass flux. This difference in performance is due to the fact that R1234yf has a thermal conductivity 18% lower than R134a. In addition, R1234yf has a lower liquid density and viscosity, and higher vapor density. This results in 10-12% lower pressure drop compared to R134a. [52] reported similar conclusions in their investigations in a horizontal multi-port test section with 1.16 mm hydraulic diameter.

Del Col et al. [34] compared the measured local heat transfer coefficients and frictional pressure drop values for pure R1234ze(E) in a 0.96 mm horizontal tube against R32, R134a and R1234yf. Experiments were conducted at mass fluxes ranging from 200 kg m^{-2} s^{-1} to 800 kg m^{-2} s^{-1}, and at a nominal saturation temperature equal to 40 °C. They concluded that the heat transfer coefficients of R1234ze(E) were comparable to those of R134a, while the resulting two-phase frictional pressure drop values for R1234ze(E) were 18-28% higher than for R134a at similar operating conditions. Among the 4 refrigerants tested, R1234yf exhibited the lowest heat transfer coefficients and R32 exhibited the highest heat transfer coefficients. The Cavallini et al. [21] and Del Col et al. [31] correlations exhibited good agreement with the experimental heat transfer coefficients and frictional pressure drop values, respectively.

Hossain et al. [51] also studied the condensation of R1234ze(E) in a 4.35 mm horizontal tube and compared its performance to refrigerants R32 and R410A. Tests were conducted at three different saturation conditions (35, 40 and 45 °C) and mass

fluxes ranging from 150 kg m^{-2} s^{-1} to 400 kg m^{-2} s^{-1}. Their results indicated that heat transfer coefficients for R1234ze(E) were 30% lower than R32 and pressure drop values were 26-50% higher than R32. Their heat transfer coefficient data was predicted well by the Haraguchi et al. [49] and Dobson and Chato [36] correlations. The pressure drop results were best predicted by the Miyara et al. [79] correlation.

In an independent past research project [53], we investigated the condensation of HFO R1233zd(E) as a potential replacement for HFC R245fa for application in Organic Rankine Cycle (ORC) systems. We collected heat transfer and pressure drop data for condensing R1233zd(E) in a 4.7 mm horizontal tube at 2 different saturation conditions (T_{sat} = 45 and 60 °C) and mass fluxes ranging from 100 kg m^{-2} s^{-1} to 400 kg m^{-2} s^{-1}. The measured data were then compared with various condensation correlations from the literature. Shah [90, 91], Cavallini et al. [21] and Thome et al. [101] correlations were all able to predict the experimental heat transfer coefficient well, with MAPEs less than 15%. The best performing correlations were then used to design an air-cooled condenser for a 1 MW ORC plant. A similar analysis was conducted for R245fa using experimentally validated correlations from the literature. Replacing R245fa with R1233zd(E) leads to 2.7% reduction in size but an 18.9% increase in the refrigerant pressure drop for equivalent power production.

Thus, it is clear from the review of literature that in general, the performance of pure HFO refrigerants is lower than that of their HFC predecessors, due to the differences in thermodynamic properties. These HFO refrigerants are not suitable for "drop-in" replacement into existing technologies. Critical components such as condensers must be redesigned and optimized for HFOs, which may result in the

increased footprint of the equipment or reduction in the COP. This further demonstrates the need for HFC/HFO refrigerant mixtures as working fluids. They offer the opportunity for greater performance benefits from HFCs while still reducing the impact on the environment from HFOs. While R1234yf and R1234ze(E) are proposed replacements for R134a in a variety of medium pressure applications, there are no pure HFOs available for replacing HFCs, R404A, and R10A, in high pressure applications such as industrial refrigeration and commercial HVAC. This necessitates the research into HFC/HFO mixtures for finding potential replacement candidates for these applications.

2.3 Non-equilibrium condensation of pure fluids

A large majority of the past research on the condensation of pure refrigerants has been focused on saturated condensation. For these studies, the fluid is assumed to be in equilibrium at each axial cross section along the tube, and the effects of superheated and subcooled condensation are considered negligible. This is done because:

- It simplifies the calculation procedure.
- It results in an oversized heat exchanger which may be desirable for a conservative design.
- Until recently, there has been a lack of validated methods for predicting non-equilibrium condensation heat transfer coefficients.

However, this assumption is not supported by our theoretical understanding of

heat transfer (Section 1.3). Furthermore, accurately predicting non-equilibrium condensation offers an opportunity to design more compact heat exchangers, resulting in economic savings and reduction in the footprint of the equipment.

One of the earliest theoretical models on superheated condensation was presented by Webb [104] in 1998. In his paper, Webb mentions the surprising lack of prior literature available on superheated condensation. He proposed that the heat transfer to a condensing superheated vapor, flowing inside of a tube, can be modeled as the sum of the sensible and latent component (Equation 2.12).

$$q''_{superheat} = q''_{sensible} + q''_{latent} \tag{2.12}$$

Equation 2.12 can be further rewritten in terms of the sensible and latent heat transfer coefficients, and their respective driving temperature differences:

$$\alpha_{superheat}(T_{sat} - T_{wall}) = \alpha_{sensible}(T_b - T_{sat}) + \alpha_{latent}(T_{sat} - T_{wall}) \tag{2.13}$$

$$\alpha_{superheat} = \alpha_{sensible}\frac{(T_b - T_{sat})}{(T_{sat} - T_{wall})} + \alpha_{latent}$$

where T_b and T_{wall} are the refrigerant bulk and tube wall temperatures. The sensible and latent heat transfer coefficients may be predicted using the Dittus and Boelter [35] and Shah [90] correlations, respectively. Webb [104] also suggested an expression to account for the mass transfer of vapor to the interface, similar to the Ackermann correction factor [1]. As the superheat approaches zero, the contribution of the sensible heat transfer coefficient disappears in Equation 2.13. The framework proposed by Webb [104] was an elementary effort on the topic and was not rigorously vali-

dated against experimental data. Furthermore, a procedure on how to predict the quality during superheated condensation was not included in the work. This quality is required as an input for most two-phase condensation models such as Shah [90].

In 2012, Kondou and Hrnjak [64] experimentally measured heat transfer coefficients during cooling of pure superheated CO_2 and R410A in a 6.1 mm tube. A wide range of superheats (0 - 40 °C), reduced pressures (0.55 - 0.95) and heat fluxes (3 to 20 kW m^{-2}) were tested. Some of their results are presented in Figure 2.2, which shows plots of measured and predicted heat transfer coefficients versus the bulk enthalpy for three different reduced pressures for each fluid. The experimental data is denoted with red markers, which were defined using the temperature difference between the bulk and tube inner wall in the superheated region. The blue lines in the plots show the predictions of the Cavallini et al. [21] correlation in the two-phase region and the Gnielinski [46] correlation (dotted line) in the single-phase region. The maximum heat transfer coefficients are associated with the saturation vapor enthalpy ($x = 1$, vertical green dotted line). The heat transfer coefficients in the two-phase region are well predicted. However, the heat transfer coefficients in the superheated condensation region (which corresponds to enthalpies higher than the saturation vapor enthalpy) are significantly under predicted by the Gnielinski [46] correlation. These results confirmed the existence of superheated condensation.

To improve predictions in the superheated region, Kondou and Hrnjak [64] proposed a similar prediction method as Webb [104], but modified the driving temperature associated with superheated condensation heat transfer coefficient $\alpha_{superheat}$ to $(T_b - T_w)$, instead of $(T_{sat} - T_w)$ (Equation 2.13). Kondou and Hrnjak [64] sug-

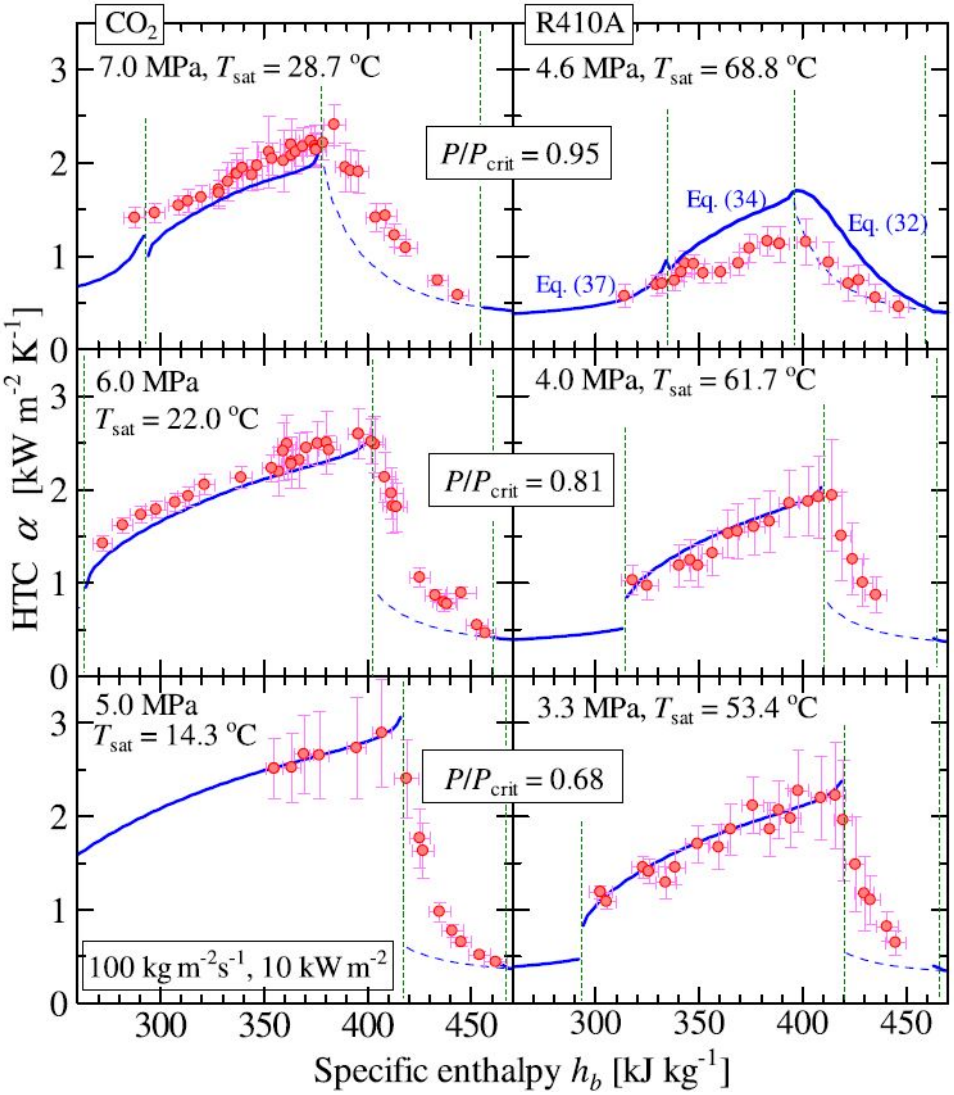

Figure 2.2: R410A and CO_2 heat transfer coefficients in the superheated and saturated condensation regions at reduced pressures 0.68, 0.81, and 0.95, from Kondou and Hrnjak [64]

gested using the Cavallini et al. [21] and the Gnielinski [46] equations for predicting the latent and sensible heat transfer coefficients. For the calculations in the superheated region, the bulk thermodynamic quality was assumed to be equal to 0.9999. A MAPE value was never evaluated to quantify the agreement with the correlation in the superheated condensation region.

Later, Agarwal and Hrnjak [4] tested various two-phase correlations (including the Thome et al. [101], Dobson and Chato [36] and Haraguchi et al. [49] correlations) to see if that would allow them improve the predictions from Kondou and Hrnjak [64] model. They compared their experimental data for superheated condensation of R32, R134a, and R1234ze(E). The superheat temperatures were varied from 5°C to 50°C. In the end, they found the Cavallini et al. [21] correlation to best predict their data, as originally proposed by Kondou and Hrnjak [64]. The resulting MAPE values in the saturated and superheated condensation regions were 12% and 23%, respectively.

Agarwal and Hrnjak [3] then further refined Kondou and Hrnjak's model by incorporating the areas associated with the vapor and liquid condensate during condensation. The thickness of the annular film in the superheated regime was evaluated by using Nusselt's falling film analysis. This is questionable because the main driving mechanism in Nusselt's falling film analysis is gravity, while shear forces are expected to dominate in the annular regime. Agarwal and Hrnjak [3] also extended their analysis to subcooled condensation. The new model allowed them to improve their agreement with data, with MAPE = 15.8% for all their data (including the superheated, two-phase, and subcooled regimes). Figure 2.3 shows a schematic of

the differences in the modeling approach of Kondou and Hrnjak [64] and [3], as well as the conventional method.

To be more generally applicable, a good heat transfer model must provide accurate predictions while also providing an accurate representation of the underlying physical mechanisms. For calculating heat transfer in the superheated region, both the Kondou and Hrnjak [64] and Agarwal and Hrnjak [3] models assume that the bulk quality x_b is approximately equal to one. However, in reality, the true quality x in this region is lower than one, since condensation is actively occurring. Furthermore, a discrepancy between the true quality and equilibrium quality exists in the two-phase region, which is not accounted for. Xiao and Hrnjak [108] attempted to address this issue by introducing the superficial quality (Equation 2.14).

$$x_{sup} = \frac{h - h_{end}}{h_{onset} - h_{end}} \tag{2.14}$$

where h_{onset} and h_{end} represent the bulk enthalpies at location where condensation begins and ends, respectively. The onset of condensation can be determined by evaluating the bulk refrigerant temperature at the point where the associated wall temperature will decrease below the saturation temperature. Upstream of this point, single phase vapor flow occurs and therefore, heat transfer can be predicted using single-phase correlations. Equation 2.15 shows this criteria in mathematical form:

$$T_{b,onset} = T_{sat} + \frac{q''}{\alpha_{onset}} \tag{2.15}$$

Xiao and Hrnjak [108] suggested the following empirical criteria for predicting

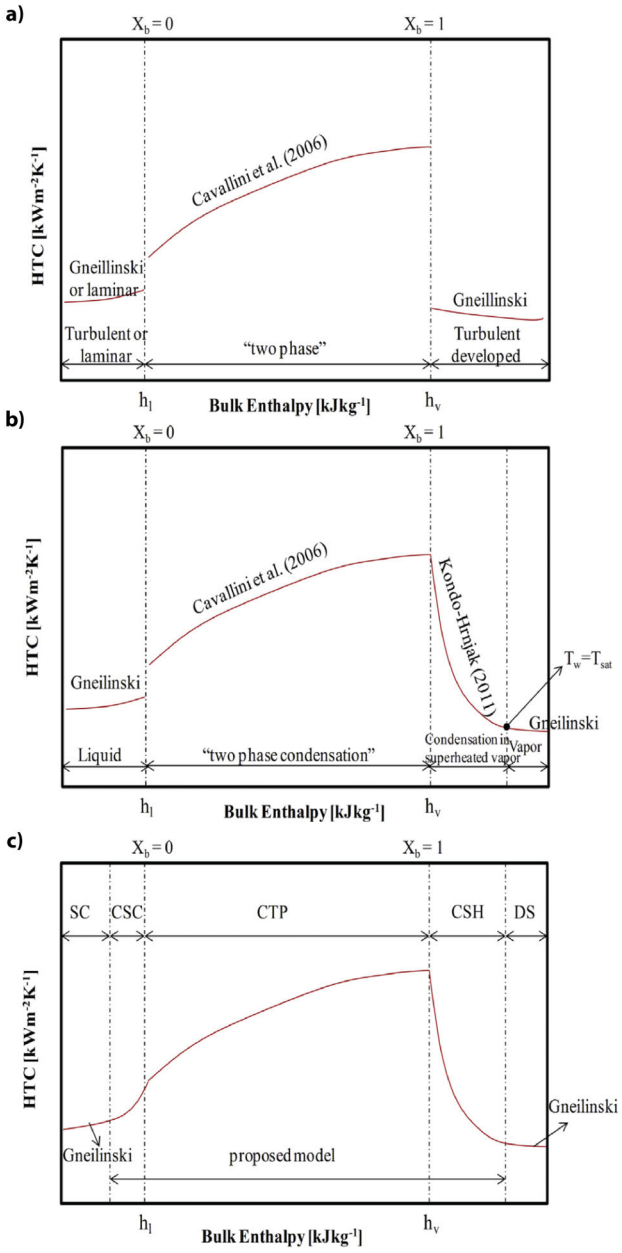

Figure 2.3: Predicted heat transfer coefficients versus bulk enthalpy using a) conventional approach b) Kondou and Hrnjak's [64] method c) Agarwal and Hrnjak's [3] method, from Agarwal and Hrnjak [3].

the end of condensation:

$$T_{b,end} = T_{sat} - 0.33\frac{q''}{\alpha_{end}} \tag{2.16}$$

By definition, the film heat transfer coefficient during condensation is defined as the ratio between total heat flux through the film divided by the temperature difference between the liquid/vapor interface and the tube wall surface (Equation 1.2). In the two-phase flow region, the liquid/vapor interface is equal to the saturation temperature for pure fluids. Furthermore, the resistance due to the convection in the vapor-phase is negligible and the dominant resistance is of the liquid condensate (as discussed in Section 2.2). Therefore, the heat transfer coefficients decrease as the liquid condensate resistance increases. However, this is not observed during superheated condensation, as the heat transfer coefficients increase until reaching a maximum at $x = 1$ and then decrease. Xiao and Hrnjak [107] attributed this discrepancy to the fact that the experimental heat transfer coefficients measured during superheated condensation are not the film heat transfer coefficients, but also comprise of the sensible vapor convective resistance. These so-called apparent heat transfer coefficients are evaluated by considering the bulk refrigerant temperature instead of the interface temperature. Therefore, Xiao and Hrnjak [108] introduced a condensation model to evaluate the film heat transfer coefficient. A peak for film heat transfer coefficients is observed at the onset of condensation and from thereon, they decrease as condensate film continues to grow. In the superheated and subcooled regions, Xiao and Hrnjak [108] suggested using Equation 2.17 to obtain the apparent heat transfer coefficient.

$$\alpha_{apparent} = \frac{T_{sat} - T_w}{T_b - T_w} \alpha_{film} \tag{2.17}$$

Based on two-phase visualization experiments, Xiao and Hrnjak modified the flow regime map of El Hajal et al. [37] to account for non-equilibrium effects during condensation of pure fluids [109, 110, 111].

A review of the literature reveals limited research on superheated condensation, primarily by Hrnjak and coworkers. There are even fewer investigations that address the superheated condensation of refrigerant mixtures. In general, the mixture effects are more pronounced for higher temperature glide mixtures [43]. Thus, in this study, we explore in detail the effects of superheated and subcooled condensation for mixtures. Furthermore, the applicability of superheated and subcooled condensation models to zeotropic mixtures is investigated.

2.4 Condensation of mixtures

Recently, the condensation of refrigerant mixtures has received an increased amount of attention in the quest to find the best low GWP fluids for use in HVAC&R industry. However, research on the condensation of mixtures dates back to the early twentieth century due to its application in other industries such as chemical process and power generation. In this section, modeling methods for predicting heat transfer coefficients and experimental studies on the condensation of mixtures in horizontal tubes are reviewed. Excellent reviews by Fronk and Garimella [41, 40, 45] provide an additional detailed discussion on zeotropic condensation.

2.4.1 Modeling methods

Zeotropic condensation is complex due to the coupled heat and mass transfer. The review by Fronk and Garimella [41] on zeotropic condensation indicates conventional condensation correlations for pure fluids cannot be accurately applied to mixtures. Unlike saturated condensation of pure fluids, the total heat rejected is a combination of sensible and latent heat. While the liquid/vapor interface temperature for these mixtures is often assumed to be equal to the equilibrium saturation temperature, in reality, the temperature is somewhere in between the equilibrium saturation temperature and bubble temperature, depending on the local interface concentrations. Fronk and Garimella [42] showed that deviation between these temperatures is significant for high glide mixtures, lowering the driving temperature difference and degrading heat transfer. Furthermore, the sensible heat transfer resistance in the vapor phase may significantly limit the resulting condensation process.

A non-equilibrium methodology, first introduced by Colburn and Drew [26] in 1937, has been shown to accurately capture the mechanisms of zeotropic condensation. As implied by the name, the local compositions and temperatures in vapor, liquid and at the interface are treated as different and tracked as condensation proceeds along the length of the condenser. The basic assumptions are (from Garimella and Fronk [45]):

- Thermodynamic equilibrium is assumed only at the interface.
- Heat and mass transfer in the vapor phase occurs in a thin film near the interface.

- Only the heat and mass transfer in the direction perpendicular to the film is considered.

For condensation of a binary mixture (schematic shown in Figure 1.2), the molar flux of the more volatile component ($\dot{N}_1$) to the interface is given as:

$$\dot{N}_1 = (\dot{N}_1 + \dot{N}_2)\tilde{y}_1 + \beta_v \frac{d\tilde{y}_1}{d\eta} \tag{2.18}$$

where $\tilde{y}_1, \beta_v, \eta$ are the molar concentration, mass transfer coefficient and distance from the interface. Equation 2.18 can be integrated across the vapor film to obtain the total condensing flux:

$$\dot{N}_T = (\dot{N}_1 + \dot{N}_2) = \beta_v ln \frac{Z - \tilde{y}_{1,i}}{Z - \tilde{y}_1} \tag{2.19}$$

where $Z = \dot{N}_1/\dot{N}_T$. With the knowledge of the total condensing flux and the composition, the latent flux can be determined as a function of the vaporization enthalpies:

$$q''_\lambda = \dot{N}_T Z \tilde{h}_{fg,1} + \dot{N}_T (1 - Z)\tilde{h}_{fg,2} \tag{2.20}$$

The sensible heat flux is evaluated by accounting for the effects of additional convection from mass transfer to the interface (similar to Ackermann [1]):

$$q''_{S,V} = \alpha_v (T_v - T_{int}) \frac{a}{1 - exp(-a)} \tag{2.21}$$

$$a = \frac{\dot{N}_1 \tilde{c}_{p,1} + \dot{N}_2 \tilde{c}_{p,2}}{\alpha_v}$$

The sum of the sensible and latent heat fluxes can then be used to determine the total heat duty transferred through the liquid film.

$$q''_{S,V} + q''_{\lambda} + q''_{S,L} = \alpha_f (T_v - T_{int}) \tag{2.22}$$

The Colburn and Drew [26] equations must be solved iteratively since the interface temperature is not known *a priori*. It must also be combined with heat and mass balances in both the liquid and vapor phases to provide closure. Lastly, accurate results from the model are contingent upon the accuracy of the underlying models used for predicting the heat and mass transfer coefficients for the relevant geometry of interest. This framework was revised by Price and Bell [86], who adopted a segmented approach for easier implementation during the design of condensers. To simplify the procedure, they assumed that the liquid film was well mixed, i.e., the concentration at the liquid interface is equal to the concentration of the entire liquid film. Other researchers have developed modifications to the above approach to account for application to various fluid mixtures including synthetic refrigerants [17, 103], CO_2/DME [2], ammonia/water[42], and other mixtures.

While the non-equilibrium method described above is a more realistic representation of the heat transfer process, it is computationally rigorous and difficult to implement as it requires an iterative solution. An alternative is the simpler equilibrium approach (also known as Silver, Bell and Ghaly, or SBG approach [12, 96]). The SBG approach assumes that the liquid and vapor are in equilibrium at the fluid bulk temperature, and the sensible heat from the bulk vapor is transferred to the interface via convection only, without two-phase enhancement. The additional resis-

tance due to mass transfer effects is not explicitly considered but rather correlated to the sensible resistance in the vapor phase, as shown in Equation 2.23.

$$\alpha_{mix} = \Big[\frac{1}{\alpha_{cond}} + R_{s,v}\Big]^{-1} = \Big[\frac{1}{\alpha_{cond}} + \frac{\dot{Q_{s,v}}}{\dot{Q_T}}\frac{1}{\alpha_v}\Big]^{-1} \tag{2.23}$$

where $\alpha_{cond}, R_{s,v}$ are the condensate film heat transfer coefficient evaluated using correlations for pure fluids with mixture thermodynamic properties and the sensible resistance of the vapor, respectively. $\dfrac{\dot{Q_{s,v}}}{\dot{Q_T}}$ is the ratio between the sensible heat removed from the vapor and the total heat removed. It can be approximated as:

$$\frac{\dot{Q_{s,v}}}{\dot{Q_T}} \approx \frac{x c_{p,v}(T_{dew} - T_{bubble})}{h_{lv}} \tag{2.24}$$

where h_{lv} is the latent heat of vaporization. The vapor phase heat transfer coefficient, α_v, is evaluated using the Dittus and Boelter [35] equation, assuming vapor only flow. Silver [96], Bell and Ghaly [12] argued that this would result in a conservative estimate of the heat transfer which is desirable since mass transfer effects are neglected. The SBG approach has enjoyed widespread use due to its simplicity and accuracy in predicting heat transfer coefficients for mixtures typically used in HVAC&R applications. However, caution must be exercised when implementing the SBG method. Fronk and Garimella [43] demonstrated that the SBG method fails to accurately predict heat transfer coefficients for high glide mixtures such as ammonia and water. Macdonald and Garimella [73] presented a criterion which can be used to determine the applicability of each type of model.

Several researchers in the past have adopted and modified the SBG method to

improve the predictions for various fluid mixtures and to account for heat transfer in various flow regimes [93]. Notably, Del Col et al. [29] modified the model of Thome et al. [101] to predict heat transfer coefficient of zeotropic mixtures. Del Col et al.'s model applied the additional SBG resistance to both the convective and the film heat transfer coefficients in Equation 2.7. For the convection in the pool, the effect of interfacial roughness on the vapor heat transfer coefficient α_v was included by introducing the interfacial friction factor f_i. They also introduced a non-equilibrium friction factor to the falling film heat transfer to account for non-equilibrium effects in the stratified flow regimes.

2.4.2 Experimental studies

The experimental studies on convective condensation of mixtures are reviewed in this section. In particular, an emphasis is placed upon the condensation of synthetic refrigerant mixtures in horizontal tubes, due to their relevance to the HVAC&R field. Furthermore, a discussion on the comparison between the experimental data from these studies and predictions from correlations in the literature is included.

Koyama [66] investigated the condensation of R22 and R114, and their mixtures in an enhanced copper tube with internal spiral groves ($D = 8.3$ mm). Experiments were conducted at saturation temperatures ranging from 40 °C to 65 °C. They found up to 20% degradation in the average heat transfer coefficients of the mixtures compared to pure refrigerants. By conducting a statistical analysis of their data, they proposed an empirical relation for heat transfer prediction. A similar approach

was adopted by Tandon et al. [100] after investigating R22 and R12 mixtures.

Smit et al. [97] investigated zeotropic condensation of five different mixtures of R22 and R142b (50% to 90% R22 by mass) in a 8.1 mm tube and a saturation pressure equal to 2.43 MPa. The glides for these mixtures ranged from 2.5 °C to 6.5 °C. They reported a degradation in heat transfer coefficients with an increase in R142b concentration. Particularly, the magnitude of degradation was more significant at lower mass flux ($40\,\mathrm{kg\,m^{-2}\,s^{-1}}$ to $350\,\mathrm{kg\,m^{-2}\,s^{-1}}$) than higher mass fluxes ($350\,\mathrm{kg\,m^{-2}\,s^{-1}}$ to $800\,\mathrm{kg\,m^{-2}\,s^{-1}}$), with up to 33% degradation at lower mass fluxes and only 7% degradation at higher mass fluxes. Their results were well predicted by the Dobson and Chato [36] correlation, after accounting for mass transfer effects using the SBG correction.

Shao and Granryd [93] studied the condensation behavior of refrigerants R32 and R134a, as well as three of their mixtures (26.5, 55 and 74.5% by mass of R-32). The experiments were performed in a circular copper tube with a 6 mm ID, at mass fluxes ranging from $131\,\mathrm{kg\,m^{-2}\,s^{-1}}$ to $389\,\mathrm{kg\,m^{-2}\,s^{-1}}$. The resulting temperature glides for the mixtures were within 3 - 5.8 °C. To account for the degradation in heat transfer of mixtures, Granryd [47] used a similar approach as Silver, Bell and Ghaly [96, 12]. He developed a correction method that takes into account the additional resistance due to mass transfer in both the gas and liquid phases, instead of just the gas phase. While the agreement was never quantified, the correlation seemed to predict their mixture data well.

In a two-part study, Fronk and Garimella [43, 42] conducted a comprehensive investigation of condensation of large temperature glide mixtures of ammonia and

water (80% and 90%) in mini-channels. The experiments were conducted at a fixed pressure equal to 1500 kPa and the corresponding temperature glides were equal to 78 °C and 93 °C. They recommended a model based on the non-equilibrium methodology by Colburn and Drew for predicting the heat transfer, as the equilibrium assumptions Silver [96], Bell and Ghaly [12] failed to capture the degradation in heat transfer of these mixtures.

Del Col et al. [33] performed an experimental investigation on the condensation behavior of binary mixtures of R1234ze(E) and R32 at two different mass compositions (77/23% and 54/46%). The corresponding temperature glides for these mixtures were equal to 11 °C and 8 °C, respectively. Experiments were conducted inside a horizontal tube with 0.96 mm I.D., at mass fluxes from 150 $\mathrm{kg\,m^{-2}\,s^{-1}}$ to 800 $\mathrm{kg\,m^{-2}\,s^{-1}}$ and saturation pressure equal to 13.7 bar and 17.7 bar. Measured heat transfer coefficients were 10 to 32% lower compared to heat transfer coefficients calculated assuming ideal linear interpolation between heat transfer coefficients of the pure individual components at similar conditions. The degradation increased with an increasing concentration of R1234ze(E), which was attributed to the mixture effects. They used the Cavallini et al. [21] model with Silver-Bell-Ghaly [12] correction, to account for mixture effects, to predicted heat transfer coefficients. Good agreement was observed with a Mean Absolute Percentage Error (MAPE) equal to 6.7%.

Azzolin et al. [8] investigated the condensation heat transfer coefficients and two-phase frictional pressure drop of R455A (R32, R1234yf and R744 at 21.5/75.5/3.0% by mass) and R452B (R32, R1234yf and R125 at 67.0/26.0/7.0% by mass) inside a 0.96 mm and an 8 mm tube. The ΔT_{glide} for R455A and R452B are 9.8 °C and 1.1

°C, respectively. Experiments were conducted at an average saturation temperature equal to 40 °C, at mass fluxes ranging from 100 to 600 kg m^{-2} s^{-1} for an 8 mm tube, and 200 to 800 kg m^{-2} s^{-1} for 0.96 mm tube. The heat transfer coefficients in the 0.96 mm tube were higher than those in the 8 mm tube. The heat transfer coefficients for both refrigerants and diameters were predicted with reasonable accuracy (MAPE values lower than 20%) by the Cavallini et al. [21] correlation with the Silver [96], Bell and Ghaly [12] approach used to correct for the additional heat and mass transfer resistances. Azzolin et al. [8] noted that the degradation in heat transfer due to mixture effects was more pronounced for the higher T_{glide} mixture, R455A. This is in line with the conclusions of Kondou et al. [65] who reported condensation and boiling heat transfer coefficients of two binary mixtures of R32/R1234ze(E) and two ternary mixtures of R32/R1234yf/R744 in a microfin tube. Both Kondou et al. [65] and Azzolin et al. [8] found the pressure drop of refrigerant mixtures to be well predicted by correlations for pure fluids [19, 39].

2.5 Summary of the research needs

The literature review reveals two critical gaps in the condensation heat transfer literature (1) there is limited investigation of HFC/HFO zeotropic mixture heat transfer and pressure drop, and (2) more broadly, there is limited investigation of refrigerant superheated and subcooled condensation, which is of increasing importance in HVAC&R applications.

A majority of the past studies on in-tube condensation have focused on the charac-

terization of single-component or azeotropic mixtures of HFCs. As described above, zeotropic condensation differs significantly due to coupled heat and mass transfer resistances and non-equilibrium effects. System-level experimental and simulated heat pump investigations have shown that HFC/HFO zeotropic mixtures are promising alternatives [81, 80, 82]. However, in addition to the thermodynamic considerations, the heat transfer and pressure drop of these refrigerants must be investigated to determine the effect on the resulting component sizes and system COPs. Currently, there is a lack of experimental data available for condensation of these refrigerants which can be used to test the applicability of the existing models and guide the development of improved models and correlations.

A review of prior studies reveals two methodologies that have been used to model condensation of zeotropic mixtures. The non-equilibrium framework by Colburn and Drew [26] tracks the compositions and temperatures of the vapor, liquid and the interface as condensation proceeds along the length of the heat exchanger. The Colburn and Drew [26] equations must be combined with heat and mass balances in both the liquid and vapor phases, and then must be solved in an iterative manner. Furthermore, predicting correlations for the liquid and vapor mass and heat transfer coefficients are required for this method to provide accurate results. On the other hand, the equilibrium approach of Silver, Bell and Ghaly [96, 12] simplifies the computational procedure of predicting heat transfer coefficients by assuming equilibrium between the vapor and liquid phases. This method also requires an accurate underlying predicting correlation for the film heat transfer coefficient. Moreover, the applicability of this method may be limited to low-temperature glide mixtures only.

Thus, the predictions from this approach must be compared against experimental HFC/HFO mixture data to determine if it is accurately able to capture the mixture effects, or if more sophisticated approaches are needed.

Finally, conventional two-phase models for pure fluids assume a local equilibrium during condensation along the length of a heat exchanger. The heat transfer in the two-phase regime is then defined in terms of the thermodynamic quality of the flow. While this assumption may be appropriate for pure fluids with low inlet superheat, significant deviations from this assumption occur during condensation of highly superheated mixtures. Condensation occurs as soon as the wall temperature drops below saturation and continues to occur even when the thermodynamic quality approaches 0. Previous research indicates that the heat transfer in the so-called superheated and subcooled condensation regions is much higher than those predicted by single-phase vapor correlations. There is limited literature on this topic, primarily by Hrnjak and coworkers. They have recently introduced empirical and semi-empirical methods in an attempt to predict the heat transfer of single-component refrigerants in these regimes. The first two models Kondou and Hrnjak [64], Agarwal and Hrnjak [4] were heavily empirical and not based on real physical parameters. The subsequent model of Xiao and Hrnjak [108] removed some of the empiricism but has not been validated for refrigerant mixtures. The non-equilibrium effects during zeotropic mixture superheated condensation are expected to play an even more significant role than for pure fluid superheated condensation. In his doctoral thesis, Xiao [106] found that his non-equilibrium model for single-component fluids significantly over predicted the results for R32/R1234ze(E) mixture condensation, and acknowledged

the need for more work in this area.

2.6 Objectives of the current study

Based on the research needs from above, the objectives of the current investigation are:

1. Design and build an experimental facility capable of measuring local heat transfer coefficients during complete condensation of refrigerant mixtures.

2. Conduct condensation experiments for refrigerant mixtures (R448A, R450A, R452A, R454B and R454C) at representative saturation temperatures, mass fluxes and heat fluxes.

3. Assess the predictive capabilities of current heat transfer and pressure drop correlations, as well as the equilibrium and non-equilibrium methodologies for mixtures. Based on the results, provide recommendations for the best performing correlations for the design of HVAC&R equipment.

4. Develop and validate a heat transfer model, based on real physical parameters, to predict the heat transfer in the superheated and subcooled condensation regions.

Chapter 3: Experimental Approach

This section provides a description of the experimental facility and the measurement technique used in this study. This is followed by the details of the data reduction methodology that was used to determine the quasi-local condensation heat transfer coefficients and total two-phase frictional pressure drop from the measured values.

3.1 Design Considerations

An in-depth review of the literature reveals that the experimental techniques used in the in-tube condensation studies to obtain quasi-local heat transfer can generally be divided into two main categories:

1. The fluid is superheated at the test section inlet, and then undergoes complete condensation in the test section. Local heat transfer coefficients are measured by dividing the test section into segments.

2. The fluid is pre-conditioned such that it enters the test section as a two-phase mixture of vapor and liquid. The inlet quality is determined from an energy balance on the preheater. In the test section, the fluid undergoes a relatively small quality change. The local heat transfer associated with the average quality in the test section is then measured through various means.

A major shortcoming of the second technique for mixture condensation is that the phase compositions at the test section inlet cannot be determined unless thermodynamic equilibrium is assumed. This assumption also fails to accurately capture the effects of subcooling of condensate and superheating of the vapor at the test section inlet. Furthermore, it is not possible to accurately quantify the mixing effects that occur between the preheater and the test section. It is also difficult to implement the non-equilibrium framework of Colburn and Drew [26] for the second configuration since the inlet conditions must be determined using the equilibrium assumption. Therefore, the facility in the present study was designed based on the first technique. Additional details of this measurement technique are provided in the following sections.

However, this methodology does not provide a constant heat flux to the entire test section. For each experimental condition, the local heat flux is evaluated by performing an energy balance on the coolant and then dividing by the heat transfer surface area. The heat flux can vary significantly as condensation proceeds along the length of the tube due to changing condensation heat transfer coefficient and/or driving temperature difference. These experiments are conducted to represent realistic operating conditions in which a refrigerant is condensed in a heat exchanger by a secondary fluid. For the experiments, the coolant flow rates were kept high to ensure that coolant-side thermal resistance did not become a limiting resistance for the process. In addition, the water inlet temperatures were set to ensure that the driving temperature differences between the wall and refrigerant saturation were greater than 30 °C. Thus, the non-constant heat fluxes throughout the test section

did not affect the resulting measured heat transfer coefficients.

Finally, with this technique, the test section is further divided into sub-segments to measure the quasi-local heat transfer coefficients along the length of the test section. As part of this work, extensive testing was conducted to determine the optimal lengths for test section segments. Reducing the spacing i.e, building shorter segments, allows for data collection with a higher resolution. However, this also results in a smaller temperature change on the water-side for a given effects, increasing the uncertainty in the measurement. Therefore, 19 cm long segments were implemented for the current technique to measure data with a high-resolution which still maintaining low uncertainty (on average under 10%).

3.2 Experimental setup

A schematic and photograph of the condensation facility are shown in Figure 3.1. The refrigerant flows in the primary loop which uses a post cooler, positive displacement pump, and evaporator to condition the flow into the test section. This facility does not utilize a compressor or lubricating oil. At state point 1 in Figure 3.1a, the refrigerant is in a superheated state as it enters the test section, which is a counter-flow tube-in-tube heat exchanger. The refrigerant flows in the inner tube of the test section and is completely condensed by the cooling water flowing in the annulus. Sight glasses are located before and after the test section to ensure that no liquid is present at the inlet and no bubbles are present at the outlet. At state point 2, the liquid refrigerant flow is directed towards another tube-in-tube heat exchanger

where it is further subcooled using a Neslab Merlin M150 recirculating chiller. The chiller temperature can be adjusted from 5 °C to 35 °C.

The refrigerant is then pumped through the system using a GC series magnetic drive gear pump from Micropump, with a M25 gear set. This gear set enables a nominal volumetric flow rate of 0.9 L min^{-1} to 7.2 L min^{-1}. At state point 4, the refrigerant enters the evaporator section where it is completely vaporized and superheated. The evaporator section is heated using three cartridge heaters from Watlow with 12.7 mm (0.5 inch) diameter and 2300 W heating capacity each. The power supplied to the heaters is adjusted using a silicon controlled rectifier (SCR) to ensure that the refrigerant is superheated as it reaches state point 1. An inline tube static mixer, with 21 spiral blades, is placed between the test section inlet and the evaporator outlet to ensure that non-equilibrium effects are not present and the superheated vapor is well mixed. The pressure in the refrigerant loop is controlled using a piston accumulator connected to a nitrogen cylinder, which enables the system volume to be varied.

The cooling water in the test section is circulated using a GJ series magnetic drive gear pump from Micropump with N27 gear set. The water pump is coupled with a DC variable speed drive and is able to achieve flow rates from 0.5 L min^{-1} to 6.5 L min^{-1}. Volumetric flow rate, temperature and adjacent pressure measurements are obtained to calculate the mass flow rate of the water. After the water leaves the test section, it is cooled in a copper-brazed 316 stainless steel plate heat exchanger using a NESLAB Merlin M150 recirculating chiller.

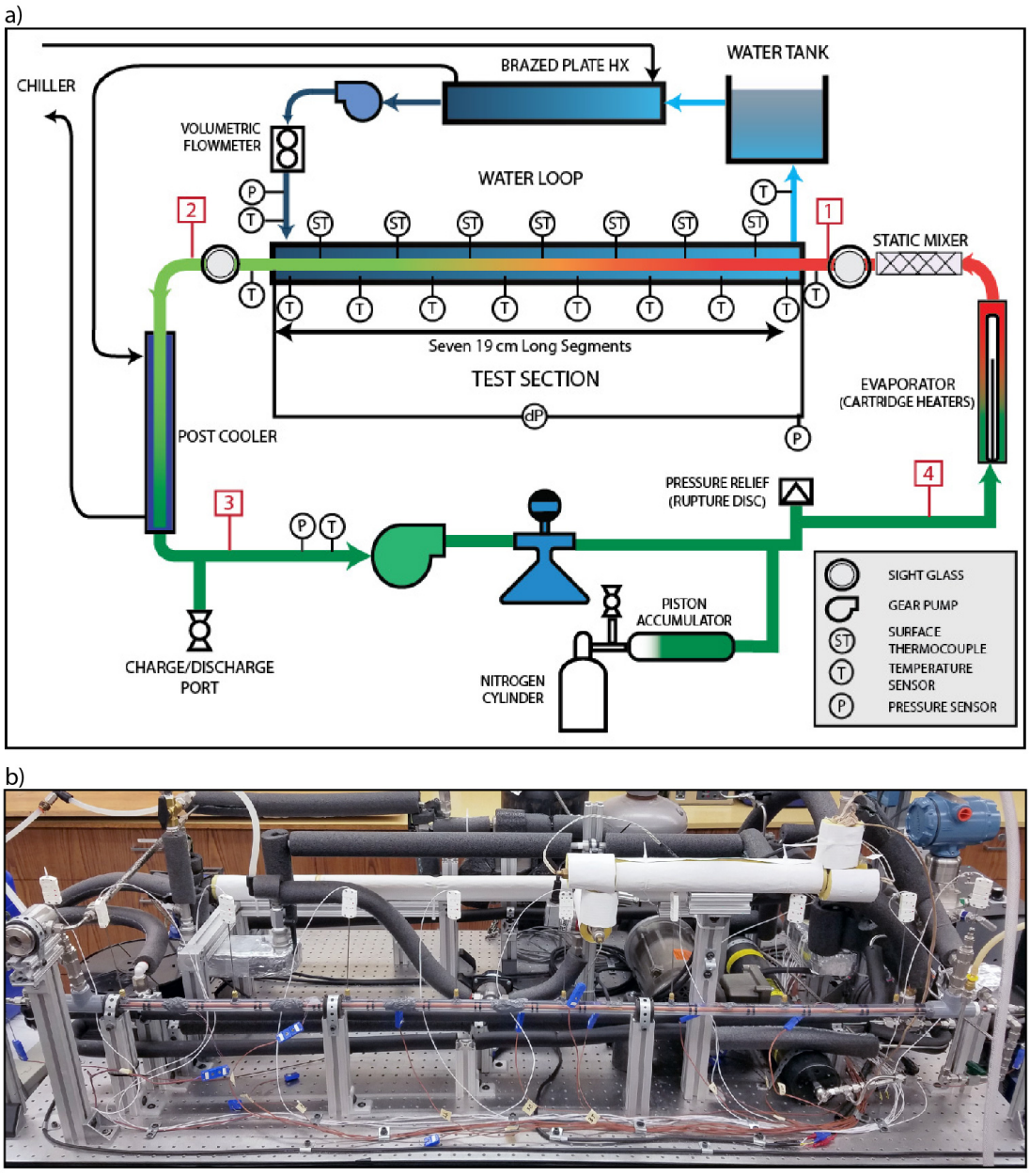

Figure 3.1: Condensation Facility (a) Schematic (b) Photograph

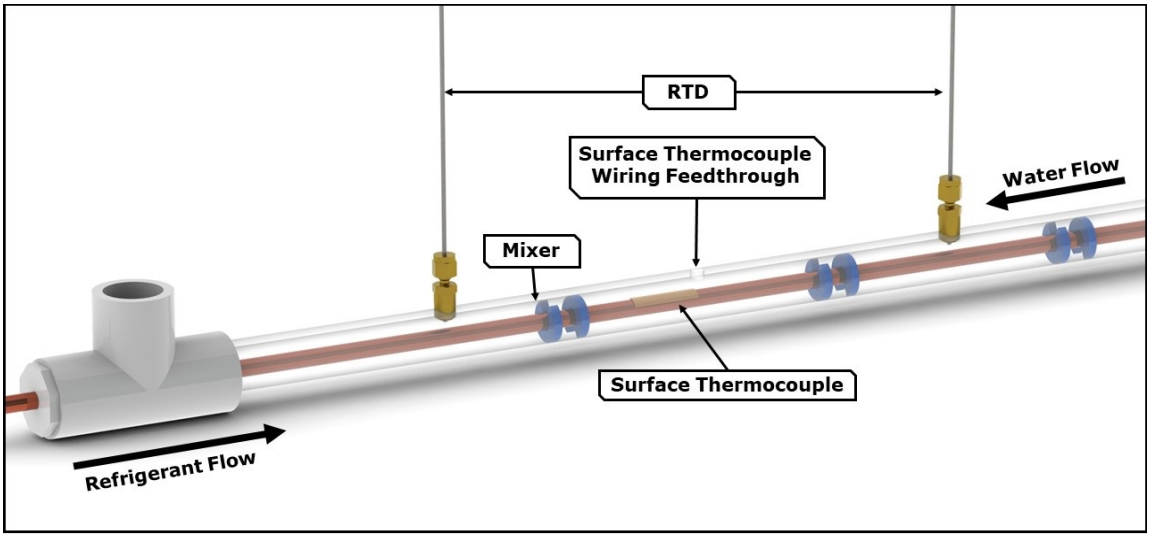

Figure 3.2: Rendering of the segments in the test section

3.3 Test section

The inner tube of the tube-in-tube test section is a copper tube with an inner diameter equal to 4.7 mm and outer diameter equal to 6.3 mm. The outer tube is constructed of clear PVC with an inner diameter equal to 15.8 mm and outer diameter equal to 21.3 mm. The high thermal resistance of PVC reduces the heat loss to the surroundings and the clear tube provides visual assistance during the placement of the temperature sensors in the test section.

The test section is divided into seven segments. Each section is approximately 19 cm long. Figure 3.2 shows a visual representation of one of the segments. Quasi-local heat transfer coefficients and the average quality are evaluated in each segment as condensation proceeds along the tube. This is accomplished by measuring the water inlet and outlet temperature at each segment, and the copper tube surface temperature. As shown in Figure 3.2, the water temperature change is measured

using calibrated RTDs, which are immersed in the coolant flow path and secured using tube fittings. To ensure that the temperature measured by the RTDs is approximately the bulk temperature of the water, the sensors are located at the center of the annulus between the inner and outer tubes. 3D printed mixers constructed from polylactic acid (PLA) were used to ensure that the water is fully mixed prior to the temperature measurements (Figure 3.2). Furthermore, the mixers were placed at least 5 cm away from the RTDs so that any nonuniformities due to mixing were not captured in the measurement.

The surface temperatures are measured at the center of each section using self-adhesive surface thermocouples with a polyimide base. The thermocouple design has an increased surface area to facilitate conduction heat transfer between the copper tube and thermocouple tip. The polyimide base is relatively thin (0.5 mm) and provides minimal resistance to the heat flux normal to the copper surface. A thermal resistance network analysis was conducted to compare the difference in the measured temperatures with and without the thermal resistance of the polyimide base. For the experimental conditions in this study, the difference was less than $\pm$ 0.05 °C, which is well within the uncertainty of the sensor ($\pm$ 0.5 °C). Thus, for simplicity, the resistance of the polyimide base was considered negligible. The surface thermocouples wiring is routed through drilled holes in the PVC tube and sealed with epoxy.

3.4 Facility charging process

After the experimental facility was built, isopropyl alcohol (IPA) was circulated in the facility to remove any impurities leftover from the manufacturing processes of the components. After discharging the IPA, the system was then purged with nitrogen.

To charge the system with the refrigerant, a vacuum was pulled on the system down to 0.027 kPa (0.2 torr) to remove any liquid or gas impurities from the system. The refrigerant is then allowed to enter the system via a standard refrigerant hose. The refrigerant was charged as a liquid using two different methods:

1. Whenever available, refrigerant tanks with a Y-Valve assembly with a dip tube were used. These tanks feed the refrigerant from the bottom of the tank where the liquid is present, instead of feeding the refrigerant from the top of the tank.

2. When refrigerant tanks with dip tubes were not available, the tanks were charged in an inverted orientation.

Following this procedure guaranteed that the composition of the refrigerant in the experimental loop is as close to the intended composition by the manufactures. The refrigerants used in this study were obtained directly from the manufacturer. They had never been reclaimed or been mixed with lubricants. The system does not utilize a compressor and therefore no lubricants were introduced. The pump is a magnetically coupled pump with no lubrication of the wetted components. This provided confidence that the working fluid being charged into the facility was the intended refrigerant for testing.

3.5 Data reduction

As discussed earlier, the test section is divided into seven segments. For each experimental condition, the system was allowed to reach a steady state. This was defined as the point when fluctuations in the temperature, absolute pressure, differential pressure, and mass flow sensor readings were less than 0.1 °C, 10 kPa, 0.1 kPa and 0.1 g s^{-1} for a duration of 4 minutes. Temperature, pressure and flow rate measurements were then collected for 4 minutes at 1 Hz. Heat transfer coefficients, frictional pressure drop, and the corresponding uncertainties were calculated from the methods described below. Data processing was conducted in the Engineering Equation Solver [87] software using refrigerant property data from REFPROP 10 [70].

3.5.1 Heat transfer coefficients

For a given segment in the test section, the total heat lost by the refrigerant is assumed to equal the heat gained by the water. The heat gained by the water in each segment can then be evaluated from an energy balance (Equation 3.1).

$$\dot{Q}_i = \dot{m}_w \cdot (h_{w,out} - h_{w,in})_i \tag{3.1}$$

where $\dot{m}_w, h_w, \dot{Q}$ are the water mass flow rate, enthalpy, and heat duty gained in segment number i. Water properties are evaluated based on the measured temperature and pressure. On the refrigerant side, the enthalpy of the superheated refrigerant at the test section inlet is evaluated based on temperature, pressure and

bulk composition of the refrigerant. The heat duty evaluated using Equation 3.1 is used to determine the refrigerant bulk enthalpy for subsequent segments along the test section:

$$h_{ref,out,i} = h_{ref,in,i} - \frac{\dot{Q}_i}{\dot{m}_{ref}} \tag{3.2}$$

The average quality (Equation 3.3) and equilibrium saturation temperature (Equation 3.4) in a segment where two-phase flow occurs can be evaluated from REFPROP [70].

$$x_{ref,avg,i} = f(P,\ h_{ref,avg,i},\ y_1,\ y_2...) \tag{3.3}$$

$$T_{ref,sat,avg,i} = f(P,\ h_{ref,avg,i},\ y_1,\ y_2...) \tag{3.4}$$

where x, P, y are the thermodynamic quality, pressure and bulk concentrations. The quasi-local film heat transfer coefficient associated with the thermodynamic quality in Equation 3.3 is equal to:

$$\alpha_{cond,i} = \frac{q''}{(T_{int,i} - T_{wall,inner,i})} \tag{3.5}$$

where q'', T_{int}, T_{wall} are the heat flux normal to tube surface, liquid-vapor interface temperature and inner tube wall temperature. For low-temperature glide mixtures, the liquid-vapor interface temperature can be approximated as the equilibrium saturation temperature [41, 43]. For superheated and subcooled regions, the role of

sensible heat transfer is significant in addition to the latent heat transfer. It is critical to evaluate the "apparent" heat transfer coefficient (which provides information about the sensible and latent heat transfer) instead of just the film heat transfer coefficient. Therefore, for superheated and subcooled regions, the bulk temperature was used, instead of the interface temperature, to evaluate the local heat transfer coefficients.

The inner wall temperature is evaluated by using a thermal resistance analogy and the measured outer wall surface temperature (Equation 3.6), assuming 1-dimensional conduction. An analysis comparing the thermal resistances indicated that axial conduction effects could be considered negligible, as 99.9% of the total heat was transferred in the direction normal to the tube surface.

$$T_{wall,inner,i} = T_{wall,outer,i} + \frac{\dot{Q}_i ln \frac{D_{inner}}{D_{outer}}}{2\pi l_i k_c} \tag{3.6}$$

Here $D_{inner}, D_{outer}, k, l$ are the inner and outer diameter, the thermal conductivity of copper, and length of the segment, respectively.

For heat flux and inner wall temperature calculations, the surface area occupied by the water mixers was assumed to be adiabatic. This is because the thermal conductivity of polylactic acid is very low (0.13 W m^{-1} K^{-1}, ASTM C518) compared to that of copper and, therefore, the heat transferred through the mixers is negligible compared to the total heat duty transferred. This was further confirmed by comparing the thermal resistances of the copper tube in the area that is directly exposed to water and the area that is exposed to the mixers. The resistance of the area exposed

to the mixers was several orders of magnitude higher and therefore, the heat transfer in this region is expected to be negligible.

To minimize the heat loss in the test section, the outer PVC tube was insulated using a 1.9 cm thick polyethylene insulation. The insulation was wrapped using zip ties to ensure that there were no air gaps present. During 167 experiments conducted in this study for five different refrigerants, the calculated heat lost by the refrigerant (evaluated using the measured inlet and outlet temperatures in the test section) was on average 2% ($\approx$ 29 W) higher than the heat gained by the water. This indicated that the heat loss in the test section was indeed minimal. Additionally, the coolant temperatures during the experiments were maintained such that the temperature difference between the coolant and ambient was never more than 15 °C, which also minimized the heat loss. This was done by adjusting the coolant flow rate and inlet temperature.

In addition, a heat loss analysis based on thermal resistance networks was conducted for the experimental condition with the highest overall heat loss. The heat loss from the coolant was estimated by determining the resistances due to convection through water, conduction through the PVC tubing (thickness = 0.55 cm), and polyethylene insulation (thickness = 1.9 cm), and air convection over the insulation. A conservative $\pm$200% uncertainty was assigned to each of the resistances. The evaluated heat loss was less than 1% of the total heat duty for the segment with the highest temperature difference between the ambient and the coolant. The difference in the calculated heat transfer coefficients from these heat duties is low (0.2%). Therefore, for simplicity, the heat loss was neglected during the calculation of heat

transfer coefficients.

3.5.2 Frictional pressure drop

A Rosemount 3051S MultiVariable pressure transducer is used to measure the absolute inlet pressure and the differential pressure across the test section. With the current measurement technique, local pressure drop data is not available. Our primary focus with this study was to investigate the heat transfer of these low GWP mixtures. Therefore, pressure drop taps were not incorporated along the length of the test section because they may disrupt the flow. Since local pressure drop data is not available, it is difficult to fully account for the role of superheated and subcooled condensation on the total measured pressure drop in the test section. Furthermore, there is a lack of validated methods available in the literature for predicting mixture pressure drop in these regions. Therefore, the pressure drop calculation methodology described in this section follows the conventional modeling method. In the superheated vapor and subcooled liquid regions, single-phase pressure drop Churchill [24] correlation is used to estimate the pressure drop. The contributions from the additional latent effects are considered by assigning a conservative $\pm 25\%$ uncertainty to the friction factor in these regions.

Equation 3.7 shows that the pressure drop measured by the sensor is the sum of the pressure drop due to two-phase frictional flow (ΔP_{fric}) and single-phase gas ($\Delta P_{v,tube}$) and liquid flow ($\Delta P_{v,tube}$). Additionally, there is a pressure gain due to the momentum change of the flow from vapor to liquid.

$$\Delta P_{fric} = \Delta P_{measured} - \Delta P_{v,tube} - \Delta P_{f,tube} + \Delta P_{deceleration} \tag{3.7}$$

To obtain the lengths corresponding to each fluid phase, a second-order polynomial fit was performed on the thermodynamic qualities (obtained from energy balances in each segment) with respect to their locations along the tube for each test case. This resulted in a function correlating thermodynamic quality to the location along the tube for each experiment. The statistical R^2 values were higher than 0.99 for all experiments. For a representative case for R448A condensation ($G = 600\,\mathrm{kg\ m^{-2}\ s^{-1}}$ and $T_{sat} = 50\,^{\circ}\mathrm{C}$), the measured pressure drop was 7.2 kPa and the resulting expression for quality as a function of length was defined as:

$$x = 1.331 - 1.575L + 0.4414L^2 \tag{3.8}$$

where x is the thermodynamic quality and L is the length along the tube. The locations corresponding to the start and end of the condensation (neglecting non-equilibrium condensation) were then obtained by evaluating the above function for $x = 1$ and $x = 0$ respectively. The single-phase vapor flow region was defined from the start of the test section to the location where condensation begins, while the single-phase liquid flow region was defined from the end of the condensation region to the end of the test section. For the representative case, single-phase vapor, two-phase flow and single-phase liquid lengths were 0.22 m, 1.14 m and 0.27 m long, respectively.

The pressure drop values associated with single-phase flow in tubes were deter-

mined using the Churchill [24] equation which takes into account the flow operating conditions and the surface roughness of the tube to evaluate the friction factor. It is valid for laminar, transition, and turbulent flow. The absolute surface roughness of copper was assumed to be 2×10^{-6} m based on reported values in the hydraulics design handbooks [28, 50, 69]. A conservative $\pm 25\%$ uncertainty was assigned to the calculated friction factors. For the representative case, the pressure drop due to single-phase vapor and liquid flow were 1.79 kPa and 0.25 kPa, respectively.

The pressure gain due to flow deceleration was evaluated by carrying out a momentum balance from the test section inlet to outlet, as shown in Equation 3.9.

$$\Delta P_{deceleration} = \rho_v V_v^2 - \rho_l V_l^2 \tag{3.9}$$

Finally, Equation 3.7 can be used to evaluate the frictional pressure drop by substituting in the values for the calculated variables on the right side of the equation. For the representative case, the resulting calculated pressure gain and frictional pressure drop were equal to 2.98 kPa and 8.1 kPa, respectively.

3.5.3 Uncertainty analysis

Table 3.1 lists the ranges and the values of systematic uncertainty, U_{sys} associated with the sensors used in this study. As shown in Equation 3.10, the total uncertainty in each of the measured variables is the root of the sum of squares of the systematic uncertainty and random uncertainty, U_{rand}.

$$U_{tot} = \sqrt{U_{sys}^2 + U_{rand}^2} \tag{3.10}$$

Systematic uncertainty of a sensor is dictated by the manufacturing process, physical traits and type of the sensor, repeatability, data acquisition capabilities, calibration process, etc. Random uncertainties occur due to the fluctuations and noise in the measured values even when the system is at steady state. These may occur due to a wide range of factors e.g. turbulence, Rayleigh–Taylor instabilities, bubble formation and collapse in the evaporator, pump displacement, etc. The random uncertainties were quantified statistically by assuming a normal distribution in the data.

$$U_{rand} = \frac{SD\ t_{95}}{\sqrt{N}} \tag{3.11}$$

where the SD, t_{95}, N are the standard deviation in the data for each sensor collected over 4 minutes, t-value corresponding to the 95% confidence interval and the number of total readings, respectively.

Uncertainty propagation in the calculated variables is evaluated using the procedure suggested by Kline and McClintock [63]. The uncertainty in the evaluated mass flux was due to the uncertainty in the refrigerant mass flow rate and tube diameter ($\pm$0.01 mm). The average uncertainty in the evaluated mass fluxes was on average $\pm$0.4%. Similarly, the uncertainty in the calculated thermodynamic quality was low (on average equal to $\pm$1.7%). A major source of uncertainty in the quality and heat transfer coefficients was from the measured water temperatures, which were used to

evaluate the heat duty in each segment. The calibration procedure for these sensors is described in the following section.

For heat transfer calculations, the pressure in the test section was assumed to be equal to the absolute pressure measured at the test section inlet. The uncertainty due to this assumption was quantified by evaluating the root mean square of the systematic uncertainty of the pressure sensor (5.7 kPa) and the measured pressure drop for that data point. The resulting value was then used as the new total systematic uncertainty for that data point. In general, the contribution of pressure uncertainty to the total uncertainty in heat transfer coefficients was low (on average 0.5%).

Table 3.1 Instrument ranges and uncertainties

Measurement	**Range**	**Systematic Uncertainty**
RTD (water temperature)	-200 – 500 °C	±0.05 °C
Surface temperature	-200 – 500 °C	± 0.5 °C
Type T thermocouple	-200 – 500 °C	± 0.5 °C
Refrigerant mass flow meter	0 – 30 g s^{-1}	± 0.1%
Water volumetric flow meter	0.04 – 7.5 L min^{-1}	± 0.5%
Pressure	0 – 10 MPa	± 5.68 kPa
Differential pressure	0 – 62 kPa	± 0.05 kPa

3.5.4 Calibration of temperature sensors

As discussed earlier, the heat duty in an individual segment in the test section is evaluated using the measured temperatures on the waterside. For a given segment, the water temperature change between the inlet and outlet was typically less than 2 °C. Therefore, it was critical to measure the water temperatures with low uncertainty to maintain a low propagated uncertainty in the evaluated heat transfer coefficients.

This is achieved by calibrating the RTDs based on the procedure outlined by Coleman and Steele [27].

Class A 3-wire platinum RTDs, with a 100 Ohm nominal resistance, were used to measure the water temperatures. The uncertainty specified the manufactures for these sensors was ±0.15 °C at 0 °C. This uncertainty was further reduced by calibrating the RTDs in a Fluke 7109A portable calibration bath. The bath is capable of achieving temperatures ranging from -25 to 140 °C. It has a stability and uniformity equal to 0.01 °C and 0.02 °C. In addition to the internal temperature sensor in the bath, an external high accuracy probe (Fluke 5615-A) with uncertainty equal to ±0.012 °C at 0 °C was used to measure the temperatures in the calibration bath.

The RTDs were calibrated over a small temperature range (5 - 40 °C) to minimize uncertainty. During the calibration, the bath was allowed to stabilize at five different temperatures within the calibration temperature range (including 5 and 40 °C). The RTDs and the external reference probe were tied together and immersed in the bath. The temperature measured by the RTDs was collected and stored using the DAQ system. Thus, using this procedure also eliminates any systematic errors introduced by the DAQ system. For each setpoint temperature, the readings from the RTDs and the reference probe were collected for 4 minutes. The RTD measurements were then compared to the reference probe and corrected using the LabVIEW software. After the corrections were made, the bath was allowed to stabilize again at three new temperatures within the calibration temperature range. Finally, the measurements from the reference probe and the RTDs were then compared again. The resulting uncertainty in the temperature measurements after this calibration process was equal

to:

$$U_{systematic,RTD} = \sqrt{U_{probe}^2 + U_{bath,stability}^2 + U_{bath,uniformity}^2 + U_{error}^2} \tag{3.12}$$

where the U_{probe} the uncertainty of the reference probe, and $U_{bath,stability}$ and $U_{bath,uniformity}$ are the stability and the uniformity of the bath. U_{error}^2 was the maximum difference between the reference probe and the RTD during verification. The resulting systematic uncertainty for all the RTDs was less than 0.05 °C. Therefore, for simplicity, a conservative uncertainty of 0.05 °C was used for all the data reduction in this study.

Chapter 4: Results and Discussion

Heat transfer and pressure drop results are presented in this section along with details of the initial facility validation. Condensation tests for five different mixtures (R404A, R450A, R448A, R452A) were conducted in the test facility.

4.1 Facility validation

Before collecting mixture condensation data, a thorough validation of the test facility was conducted to gain confidence in the proper operation of all components and sensors in the facility. These tests were conducted using R134a as the working fluid since its heat transfer and pressure drop are well understood [16, 67, 102, 94, 10]. The validation process included the following tests:

- Single-phase liquid and vapor pressure drop tests
- Energy balance tests
- Single component condensation tests

Single-phase liquid and gaseous pressure drop tests with R134a were performed to assess the predictive capabilities of the minor loss correlations used in Equation 3.7, as well as the accuracy of the refrigerant mass flow and differential pressure sensors. Eleven total pressure drop values were measured for liquid refrigerant flowing at

mass fluxes ranging for $200 < G < 1700\,\mathrm{kg\ m^{-2}\ s^{-1}}$ and vapor refrigerant flowing at mass fluxes ranging for $200 < G < 500\,\mathrm{kg\ m^{-2}\ s^{-1}}$. For each test, the measured pressure drop was compared with the predicted pressure drop from the Churchill [24] correlation. The agreement between the predicted and measured pressure drop values was quantified by evaluating the Mean Percentage Error (MPE, Equation 4.1)) and the Mean Absolute Percentage Error (MAPE, Equation 4.2)). Overall, good agreement was observed between measured and expected values (MAPE = 10.4% and MPE =10.4%).

$$MPE = \frac{100\%}{n} \sum_{n=1}^{n} \frac{P_{predicted} - P_{measured}}{P_{measured}} \tag{4.1}$$

$$MAPE = \frac{100\%}{n} \sum_{n=1}^{n} \frac{|P_{predicted} - P_{measured}|}{P_{measured}} \tag{4.2}$$

Similarly, single-phase energy balance tests were conducted to compare the energy lost by the refrigerant with the energy gained by the water. The refrigerant inlet temperature and mass were varied at ranges representative of the test conditions. During these tests, the water flow counter-current to the refrigerant was allowed to reach a steady state. The resulting differences in heat duties were less than 1.2% on average, and 3.4% maximum. This provided confidence in the accuracy of the measured water volumetric flow rate, inlet and outlet temperatures, and refrigerant mass flow rate.

Lastly, condensation heat transfer experiments were conducted with pure R134a. Condensation data were obtained for a range of mass fluxes ($100\,\mathrm{kg\ m^{-2}\ s^{-1}}$ to 600 $\mathrm{kg\ m^{-2}\ s^{-1}}$) and saturation conditions (45 and 55 °C). The results were compared

against predictions from several established heat transfer and two-phase frictional pressure drop correlations from the literature. The local heat transfer coefficients (Shown in Figure 4.1) and pressure drop were best predicted by the Cavallini et al. [21] correlation (MAPE = 7.8%) and the Haraguchi et al. [48] correlation (MAPE = 9.5). Additional details can be in found in Jacob et al. [58].

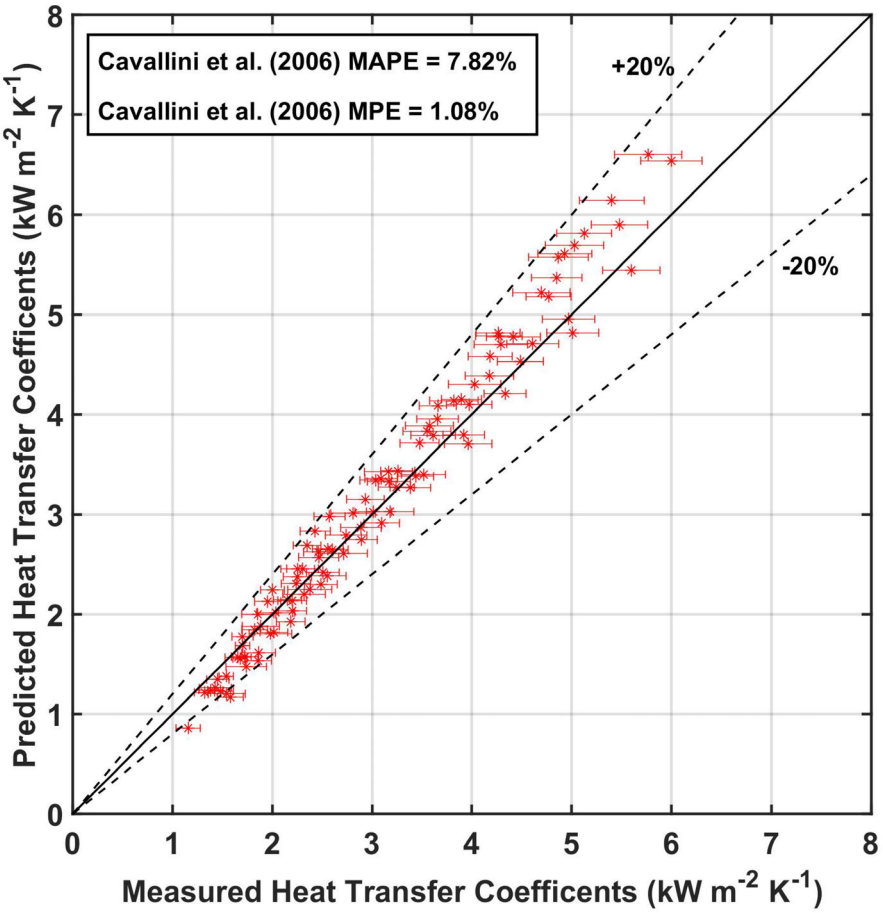

Figure 4.1: Measured R134a heat transfer coefficients versus predictions from the [21] correlation

Good agreement between measured the measured R134a heat transfer coefficients and the literature provided confidence in the validity of the measurement technique, as well as the proper operation of the experimental facility and its sensors. Therefore, the existing facility was then used to investigate the condensation of the low GWP mixtures.

4.2 Test matrix and public databases

Table 4.1 shows the test matrix of the experimental conditions at which heat transfer and pressure drop data for the low GWP mixtures were collected.

Table 4.1 Experimental test matrix

Average saturation temperature (°C)	**Mass flux** (kg m^{-2} s^{-1})				
	100	200	300	400	500
40	x	x	x	x	x
50	x	x	x	x	x
60	x	x	x	x	x

x = data collected

To aid in the adoption of low GWP mixtures and to support future modeling efforts for these refrigerants, all the measured and calculated variables from this study have been made shared publicly through the Figshare platform. The links for accessing these databases and associated publications are listed below. In addition to the research on refrigerant mixtures, condensation of low GWP refrigerant R1233zd(E) was also investigated which has been proposed for application in organic Rankine cycles. Thus, the database for R1233zd(E) has also been included.

1. R450A[57, 58] – doi.org/10.6084/m9.figshare.7611674.v1
2. R448A and R452A[59, 60] – doi.org/10.6084/m9.figshare.10024739.v2
3. R454B [56] – doi.org/10.6084/m9.figshare.12921407
4. R454C [54] – doi.org/10.6084/m9.figshare.12235454.v1
5. R1233zd(E) [55, 53] – doi.org/10.6084/m9.figshare.11608359.v1

4.3 Two-phase frictional pressure drop

The complete condensation pressure drop for each experimental condition was evaluated using the procedure outlined in Section 3.5.2. Due to the limited sensitivity and accuracy of the transducer at low differential pressures, the experiments with measured pressure drop values lower than 0.5 kPa are not reported in this study. The experiments resulted in a total of 94 data points. The average uncertainty in the measurement was 17%. Figure 4.2 shows the ratios of the two-phase frictional pressure drop over the total measured pressure drop measured in the test section. On average, the two-phase frictional pressure drop was 78% of the measured value after accounting for the minor losses and acceleration gain due to the momentum change of the flow. For experiments with low minor losses (i.e. shorter single-phase regions), the two-phase pressure drop was higher than the measured value, due to the pressure gain as the fluid decelerates. This can be observed in Figure 4.2.

The measured two-phase frictional pressure drop data were compared with predictions from models and correlations from the literature. These included the Friedel

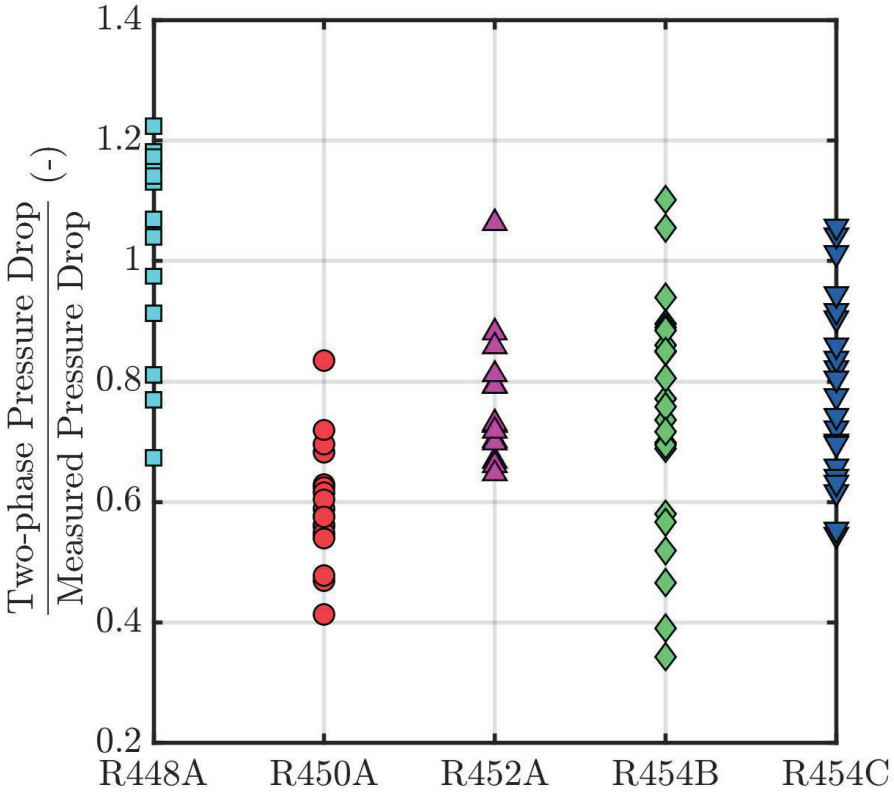

Figure 4.2: Two-phase frictional pressure drop over total measured pressure drop in the test section for R448A, R450A, R452A, R454B and R454C.

[39], Haraguchi et al. [48], Andresen et al. [5] and Cavallini et al. [19] correlations. Among the correlations listed, all except the Friedel [39] correlations were specifically developed for condensation of refrigerants in round mini-channels. The Friedel [39] correlation was developed based on adiabatic frictional pressure drop of two-phase flow and has been reported to show good agreement with condensation data by past researchers [16, 105, 94]. All four correlations provided a relationship for $\frac{dP}{dL}$ in terms of thermodynamic quality, x. As shown in Equation 4.3, the second-order polynomial fit (Equation 3.8) for the thermodynamic quality with respect to the length was

substituted into the $\frac{dP}{dL}$. This expression was then integrated over the saturated condensation region to evaluate the total two-phase frictional predicted pressure drop for that experimental condition.

$$\Delta P_{predicted} = \int_{L_{x=o}}^{L_{x=1}} \frac{dP\big[x(L)\big]}{dL} dL \tag{4.3}$$

The plots of the comparison with the correlations from the literature are shown in Figure 4.3. In addition, Table 4.2 shows the MAPE and MPE values for each individual refrigerant, as well as for the entire data set. Overall, the Cavallini et al. [19] correlation is able to predict the frictional pressure drop the best with a MAPE equal to 24%. Individually, it is able to predict the data for all of the refrigerants with MAPE values lower than 30%. In addition, it best predicted the pressure drop data for R454B and R454C. Recall that the Cavallini et al. [19] correlation has a similar form as the Friedel [39] correlation, but it also incorporates the effects of different tube surface roughnesses and liquid entertainment in the vapor core in shear dominated flows.

Overall, the Friedel [39] and Haraguchi et al. [48] correlations are also able to predict the pressure drop with a satisfactory agreement, except for R454B. The Haraguchi et al. [48] correlation best predicted the pressure drop data for R448A and R450A. For R452A, both the Haraguchi et al. [48] and the Friedel [39] correlations showed good agreement with the data, with MAPE equal to 17.8% and 14.2%, respectively. Figure 4.3 shows that the Haraguchi et al. [48] correlation slightly over predicts the R452A data (MPE = 13.9%), while the Friedel [39] correlation under predicts the data (MPE = -13.8%).

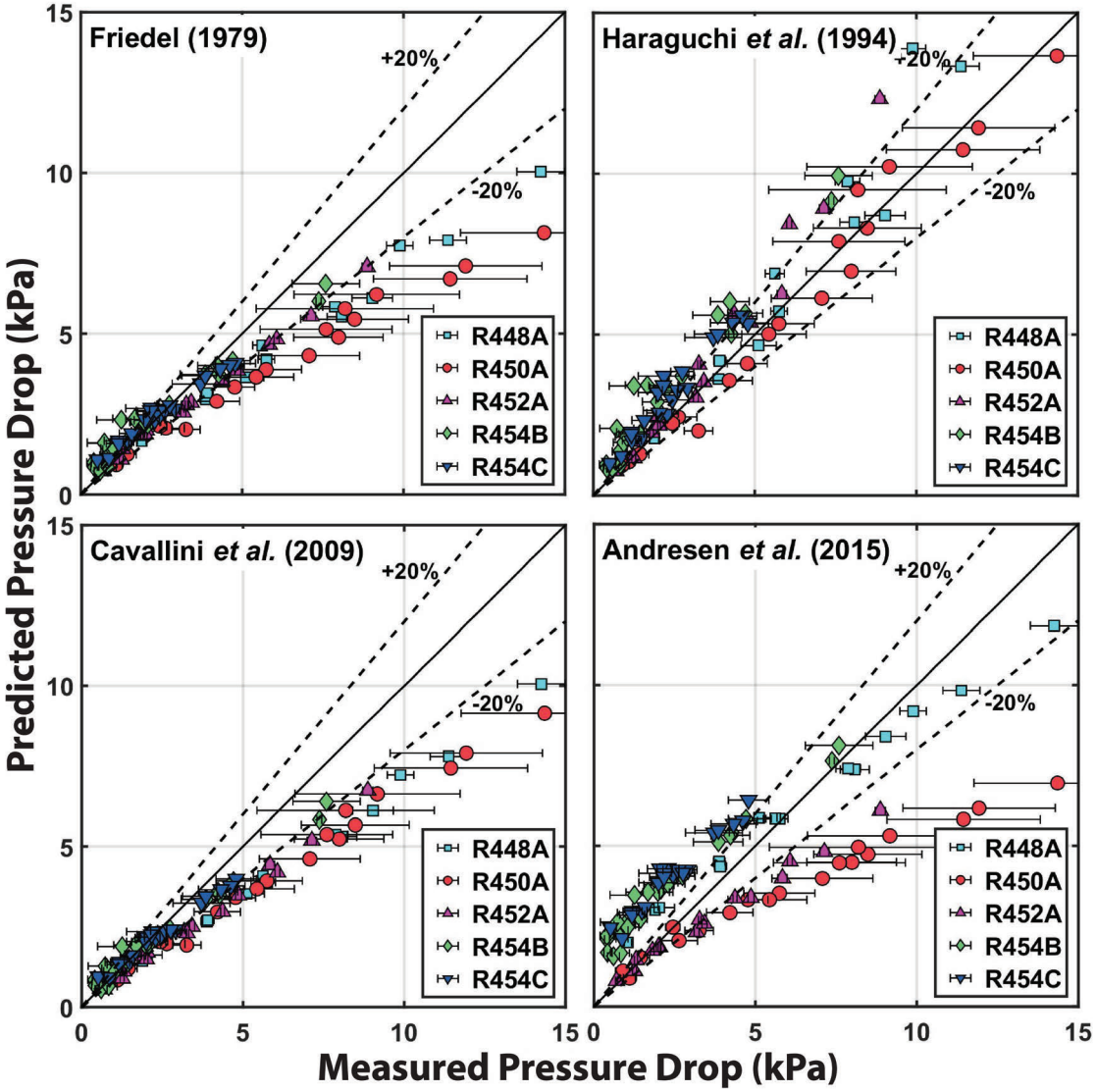

Figure 4.3: Comparison of predicted versus measured two-phase frictional pressure drop for different correlations from the literature

Generally, the Andresen et al. [5] correlation does not accurately predict the measured refrigerant data. It both under-predicts (R450A and R452A) and over-predicts (R448A, R454B, and R454C) the pressure drop data. This correlation was developed refrigerant blends operating at relatively higher reduced pressure ($P_r > 0.8$). At these pressures, the ratio of liquid over vapor densities approaches unity and the interfacial shear becomes less significant. In the current study, the corresponding reduced pressures range from 0.23 to 0.70. The highest reduced pressures are associated with R452A ($0.44 < P_r < 0.70$). The Andresen et al. [5] correlation exhibits the best agreement with R452A data, with MAPE equal to 20%. However, this trend between the reduced pressure and the predictions from Andresen et al. [5] correlation is not consistent. The second highest reduced pressures are associated with R454B ($0.42 < P_r < 0.67$), but its calculated frictional pressure drop is not well predicted by Andresen et al. [5] correlation (MAPE = 133%). Therefore, based on these findings, the Andresen et al. [5] correlation can only be recommended for predicting R452A pressure drop data at the operating conditions investigated here.

In addition to the poor agreement with the Andresen et al. [5] correlation, R45B data is generally not predicted well by the existing correlations. Table 4.3 shows the best performing pressure drop correlation for each refrigerant and their corresponding MAPE values. R454B data is best predicted by the Cavallini et al. [19] correlation, with a MAPE equal to 27%. In comparison, the data for all other refrigerants are predicted with corresponding MAPE values less than 15%. However, the cause of this discrepancy is not clear. This indicates that there is a need for additional investigation on local two-phase frictional pressure drop of R454B to better understand

its phase change behavior.

Table 4.2 Comparison of the measured two-phase frictional pressure drop and the predicted pressured drop

	R448A		**R450A**		**R452A**		**R454B**		**R454C**		**Overall**	
Model	MAPE(%)	MPE(%)	MAPE(%)	MPE(%)	MAPE(%)	MPE(%)	MAPE(%)	MPE(%)	MAPE(%)	MPE(%)	MAPE(%)	MPE(%)
Friedel [39]	23	-16	30	-29	14	-12	41	35	20	15	27	1
Haraguchi et al. [48]	15	11	10	-6	18	17	66	66	39	39	32	28
Andresen et al. [5]	40	33	34	-30	20	-16	133	133	97	97	71	51
Cavallini et al. [19]	29	-24	29	-29	24	-24	27	14	14	1	24	-10

Table 4.3 Best performing pressure drop correlation for each refrigerants (R448A, R450A, R452A, R454B and R454C)

Refrigerant	**Model**	**MAPE (%)**
R448A	Haraguchi et al. [48]	15
R450A	Haraguchi et al. [48]	10
R452A	Friedel [39]	14
R454B	Cavallini et al. [19]	27
R454C	Cavallini et al. [19]	14

4.4 Heat transfer coefficients

The experiments from this study resulted in a total of 962 heat transfer data points. 157 heat transfer coefficients were measured for R448A, 135 for R450A, 136 for R452A, 222 for R454B, and 312 for R454C. Among these data, 14% were in the superheated region, 73% were in the saturated region and 13% were in the subcooled condensation region. The uncertainty in the measured heat transfer coefficients was low, on average 8%. Table 4.4 shows the average and maximum uncertainties for each refrigerant. A major source of uncertainty in the quality and heat transfer coefficients was from the measured water temperatures, which were used to evaluate the heat duty in each segment. The highest measurement uncertainties were associated with lower thermodynamic qualities and low refrigerant mass fluxes, as well as the subcooled region. At these conditions, the heat duty in a given segment was comparatively lower, which resulted in a lower temperature change of the coolant and higher corresponding uncertainty. The resulting data from the experiments are presented in the following sections, along with the discussion and comparison with various prediction models from the literature.

Table 4.4 Average and maximum uncertainties in the calculated heat transfer coefficients for R448A, R450A, R452A, R454B and R454C

Refrigerant	**Average Uncertainty**	**Maximum Uncertainty**
R448A	8.1	39
R450A	8.0	38
R452A	9.5	43
R454B	6.8	27
R454C	8.2	39

4.4.1 Superheated condensation

Figures 4.4 and 4.5 show the plots of the temperature difference between dew point temperature and the calculated inner tube wall surface temperature versus the bulk enthalpy in the so-called superheated region for R454B and R454C. The uncertainty in these temperature differences was low (on average equal to 0.5 °C). For all the data points, the measured tube wall temperature is at least 15 °C lower than the dew point temperature, which hints to the presence of latent effects in this region. However, these measured data points represent the segments upstream of the saturated two-phase region, which is why the associated bulk enthalpy is higher than the saturation enthalpy. The corresponding heat transfer coefficients in the superheated condensation region at mass fluxes varying from 100 kg m^{-2} s^{-1} to 500 kg m^{-2} s^{-1} are also shown in Figures 4.4 and 4.5. As discussed earlier, the conventional approach would suggest that the heat transfer coefficients in this region can be modeled using single-phase heat transfer correlations. Therefore, predictions from the Gnielinski [46] correlation for single-phase turbulent heat transfer are also included in Figure 4.4 and Figure 4.5 for the range of mass fluxes investigated. These plots show that measured heat transfer coefficients are significantly under-predicted by the single-phase Gnielinski [46] correlation, suggesting the presence of "superheated" condensation. In the superheated zone, the heat transfer coefficients increase with increasing mass flux and decreasing bulk enthalpy (i.e., as the system moves closer to a bulk saturated vapor). For a given mass flux, they are maximum near the vapor saturation enthalpy. This is consistent with the results of Hrnjak and co-workers [64, 3, 108].

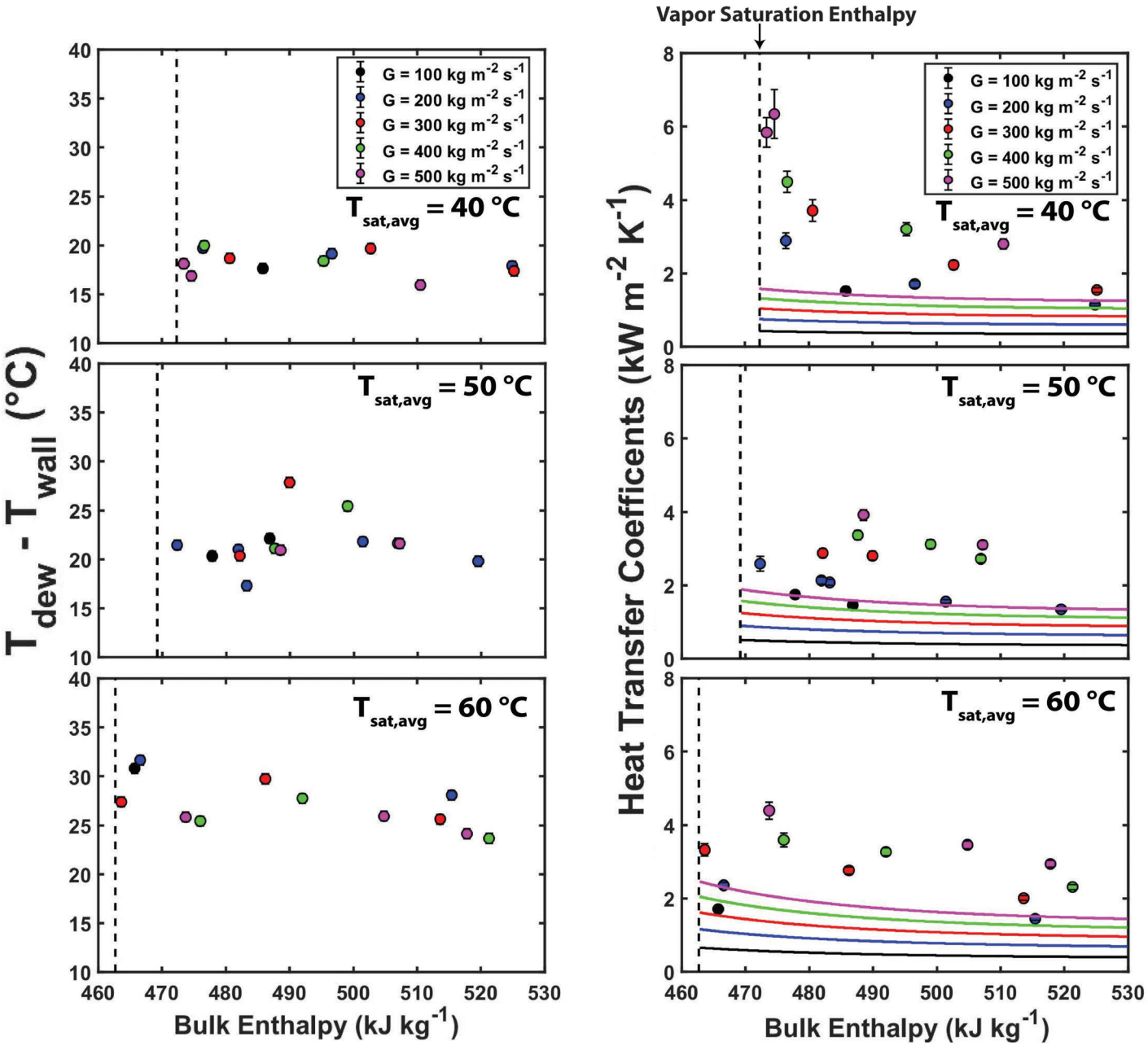

Figure 4.4: **Left**: Temperature difference between dew point temperature and the inner tube wall surface temperature versus the bulk enthalpy. **Right**: Superheated condensation heat transfer coefficient versus bulk enthalpy for R454B at mass fluxes ranging from 100 kg m^{-2} s^{-1} to 500 kg m^{-2} s^{-1} and average saturation temperature of 40, 50 and 60 °C. The lines represent single-phase vapor heat transfer coefficients predicted using Gnielinski [46] correlation.

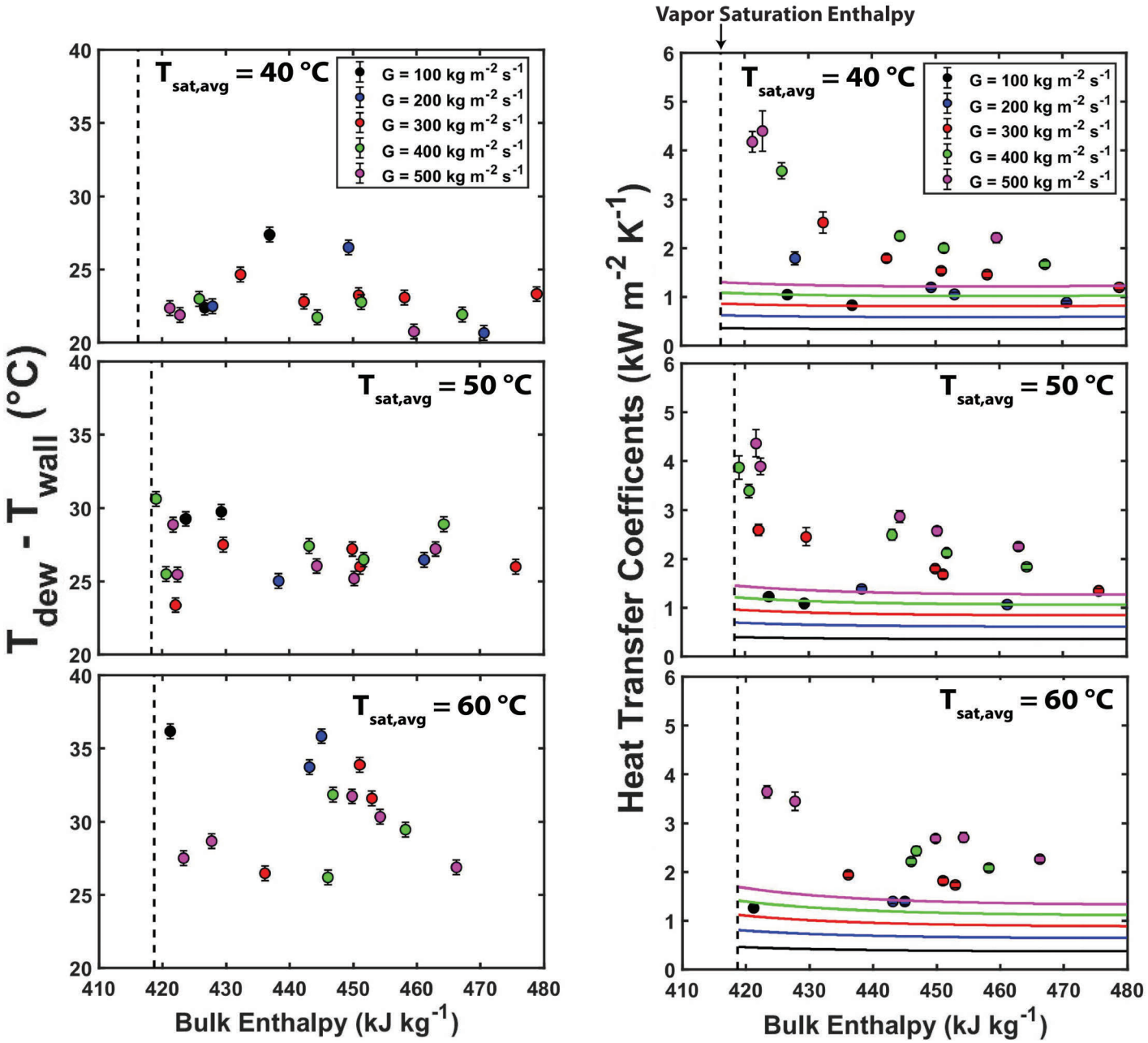

Figure 4.5: **Left**: Temperature difference between dew point temperature and the inner tube wall surface temperature versus the bulk enthalpy. **Right**: Superheated condensation heat transfer coefficient versus bulk enthalpy for R454C at mass fluxes ranging from 100 kg m^{-2} s^{-1} to 500 kg m^{-2} s^{-1} and average saturation temperature of 40, 50 and 60 °C. The lines represent single-phase vapor heat transfer coefficients predicted using Gnielinski [46] correlation.

The results in Figure 4.4 and Figure 4.5 are similar to those for the other three refrigerants tested in this study (R448A, R450A, R452A). The results indicate that single-phase correlations are not an appropriate method to predict the heat transfer coefficient in the superheated regime. This is evident in Table 4.5, which shows the MAPE (56%) and MPE (-56%) values for the Gnielinski [46] compared against the data for all five refrigerants.

In addition to the comparison with the single-phase heat transfer correlation, the measured data were also compared with the existing superheated condensation models [64, 3, 108]. These models of Hrnjak and co-workers were developed for pure refrigerants and therefore, do not account for the mixture effects during condensation. One of the goals of the present study is to assess the application of these models to superheated mixture condensation of mixtures and assess if the Silver, Bell and Ghaly (SBG) correction can be used to improve predictive capability. Thus, the measured data were compared with the superheated condensation models, with and without considering the mixture effects using the SBG correction. Recall that the SBG correction requires the quality as an input (Equations 2.23 and 2.24). For Kondou and Hrnjak [64] and Agarwal and Hrnjak [3] models, a constant value equal to 0.9999 was used, while the superficial quality was used as an input in Equation 2.24 for the Xiao and Hrnjak [108] model. Table 4.5 and Figure 4.6 shows the comparison with three different superheated condensation models, as well as the single-phase Gnielinski [46] correlation.

Overall, the measured data is well predicted by all the superheated condensation models from the literature, once the mixture effects are accounted for. The model of

Table 4.5 Predictive capability of different heat transfer correlations in the superheated region for R448A, R450A, R452A, R454B and R454C

	Without SBG		**With SBG**	
Model	MAPE(%)	MPE(%)	MAPE(%)	MPE(%)
Gnielinski [46]	56	-56	–	–
Kondou and Hrnjak [64]	31	31	20	19
Agarwal and Hrnjak [3]	27	27	17	16
Xiao and Hrnjak [108]	25	25	16	14

Xiao and Hrnjak [108] is able to predict the superheated condensation data the best, with a MAPE equal to 16%. This model describes the local flow structure in the superheated region as annular and uses a modified form of the Dittus and Boelter [35] correlation to determine the thermal resistance associated with the liquid film. This model has a similar structure to the Thome et al. [101] model, which utilizes the film Reynolds number and corrects for the enhancing effects of interfacial roughness.

4.4.2 Saturated Condensation

The saturated condensation region exists in segments where the bulk enthalpy is higher than the liquid saturation enthalpy and lower than the vapor saturation enthalpy. These data were collected downstream of the location where the superheated condensation data were measured. Figures 4.7 to 4.11 show the measured heat transfer coefficients versus the thermodynamic quality for different mass fluxes and saturation temperatures. The data show that the heat transfer coefficients increase with increasing thermodynamic quality and mass flux, as expected. Heat transfer coefficients decrease with increasing saturation temperature. The trends observed in

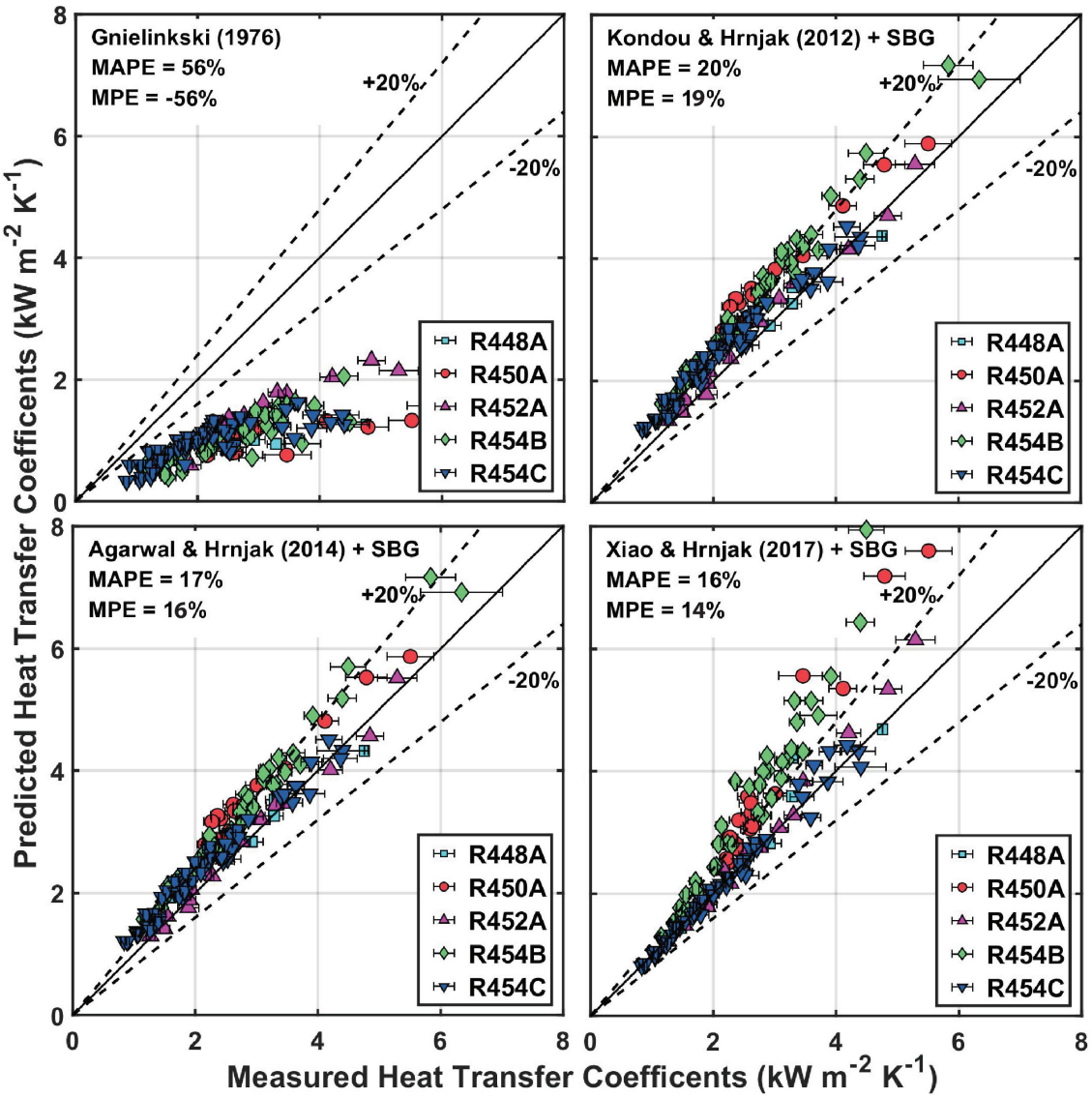

Figure 4.6: Predictive capability of different heat transfer correlations in the superheated region for R448A, R450A, R452A, R454B and R454C

the data match well with the trends associated with the condensation phenomenon for similar geometries in the literature.

The experimental data were compared with several well established saturated correlations from the literature (introduced in Section 2.2). Among these correlations are the Shah [91] and Cavallini et al. [21] correlation, which have been recommended in the 2017 ASHRAE Handbook: Fundamentals [7] for predicting refrigerant condensation. All of the correlations considered in this section are based on the equilibrium assumption (i.e., they do not consider the superheated and subcooled condensation). A comparison of the measured data and the non-equilibrium models of Hrnjak and co-workers is presented in Section 4.4.4.

The results from the comparison between the measured data and the correlations are summarized in Table 4.6. MAPE and MPE values were evaluated for two different cases, 1) where mass transfer effects were not considered and 2) where mass transfer effects were accounted for using the SBG correction. When mixture effects were not considered, all of the correlations over predicted the data as indicated by positive MPE values. The application of SBG correction improved the predictive capabilities of all the correlations. Figure 4.12 visually shows the differences in resulting MAPEs with and without the application of the SBG correction. The effect of the SBG correction was more significant for the Shah [90, 91] and Dobson and Chato [36] correlations. Conversely, the application of SBG correction to Thome et al. [101] correlation resulted in minimal differences in MAPE. This is because the magnitude of the heat transfer coefficients from Thome et al. [101] correlation was relatively smaller. It only slightly over predicts the mixture data (MPE = 4.8%) compared to

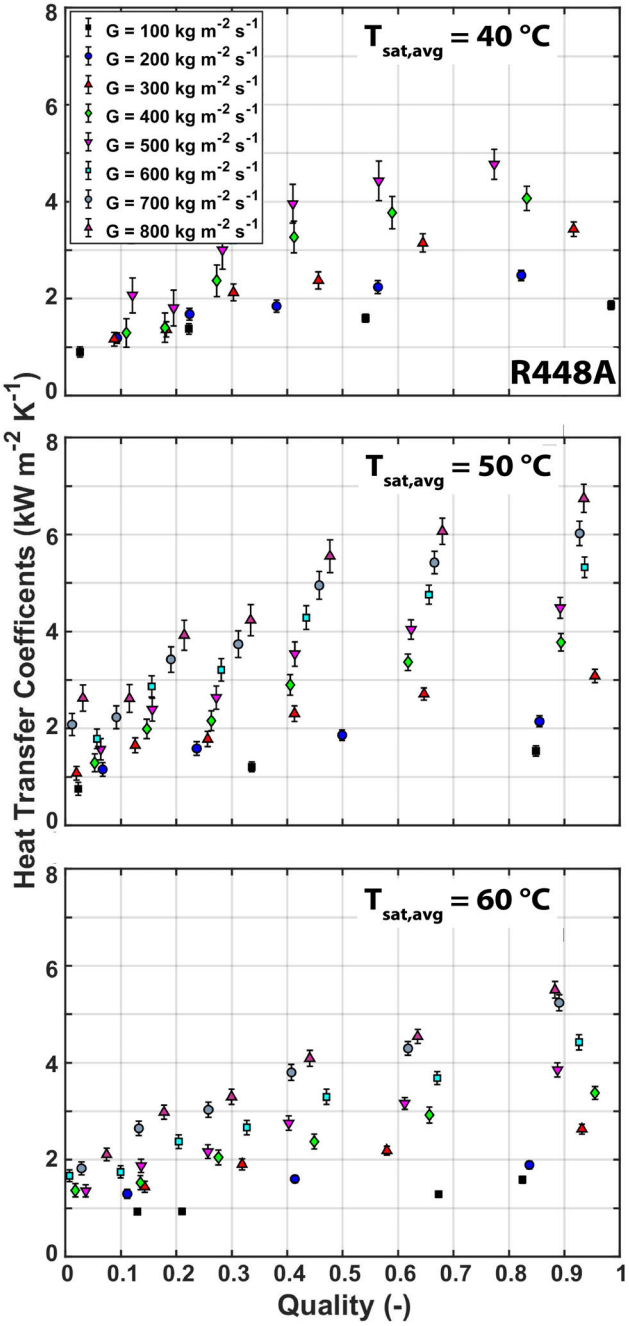

Figure 4.7: Saturated condensation heat transfer coefficient versus thermodynamic quality for R448A at G = 100 kg m^{-2} s^{-1} to 800 kg m^{-2} s^{-1} and at $T_{sat,avg}$ = 40, 50 and 60 °C

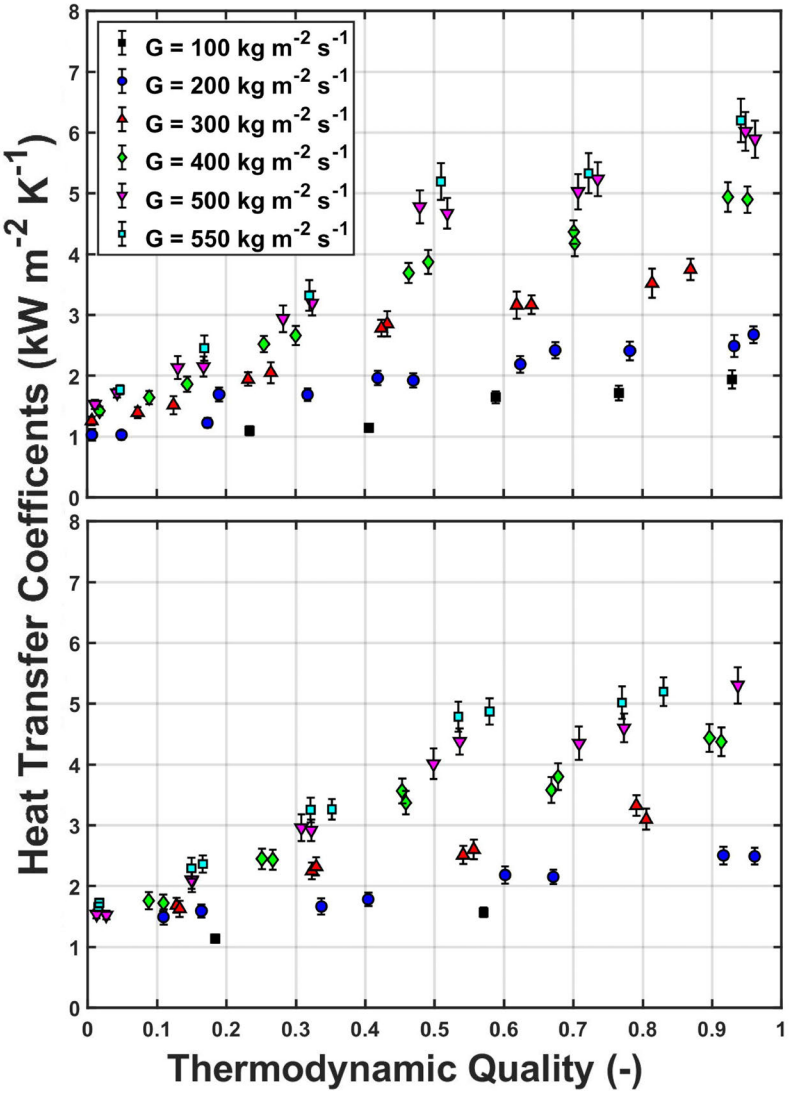

Figure 4.8: Saturated condensation heat transfer coefficient versus thermodynamic quality for R450A at G = 100 kg m^{-2} s^{-1} to 550 kg m^{-2} s^{-1} and at $T_{sat,avg}$ = 45 and 55 °C

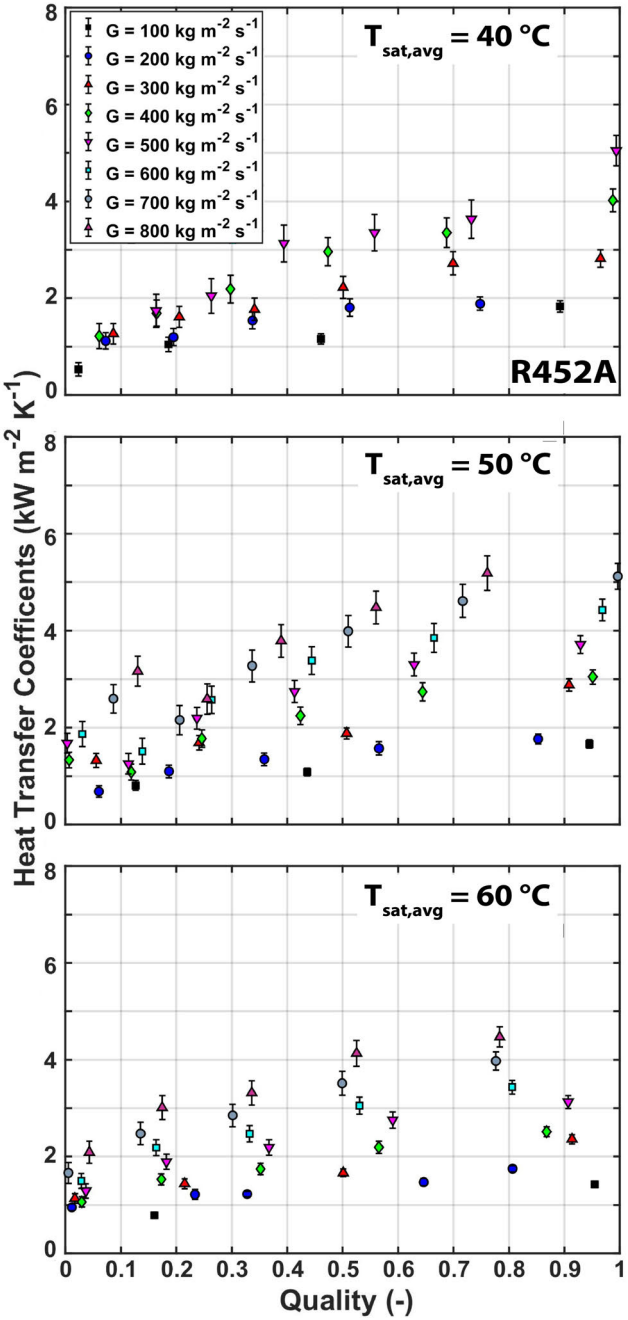

Figure 4.9: Saturated condensation heat transfer coefficient versus thermodynamic quality for R452A at G = 100 kg m^{-2} s^{-1} to 800 kg m^{-2} s^{-1} and at $T_{sat,avg}$ = 40, 50 and 60 °C

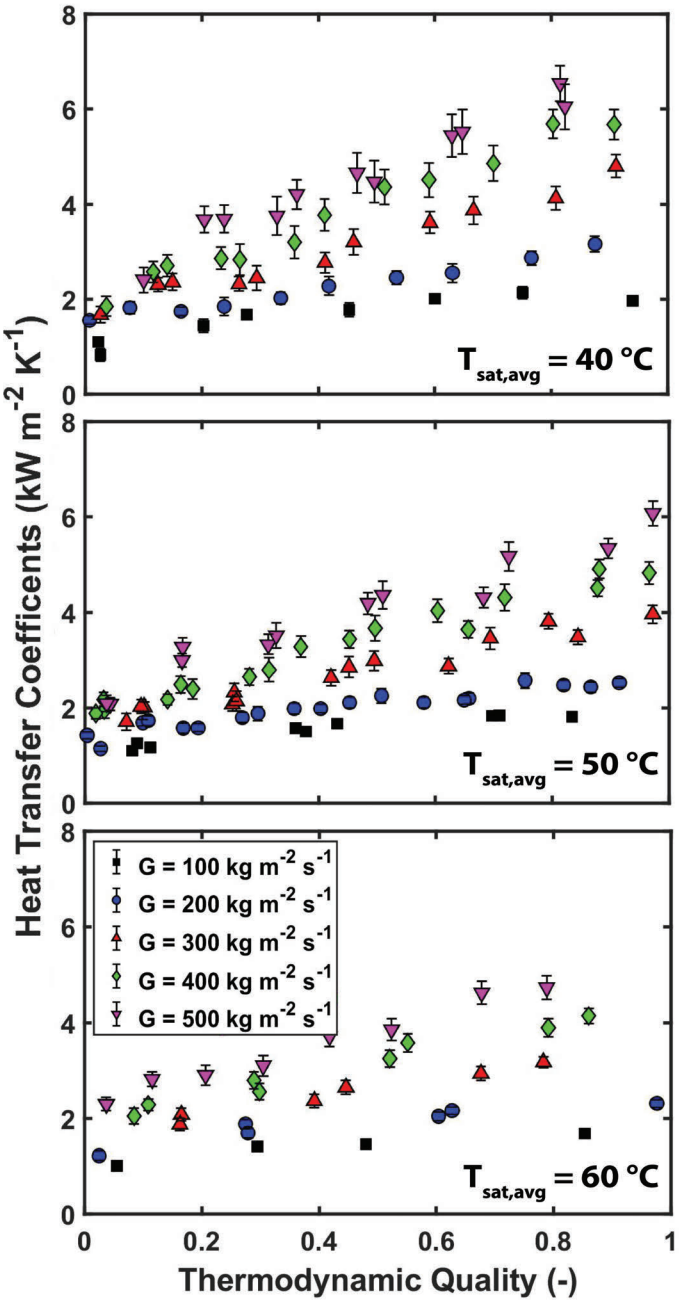

Figure 4.10: Saturated condensation heat transfer coefficient versus thermodynamic quality for R454B at G = 100 kg m^{-2} s^{-1} to 500 kg m^{-2} s^{-1} and at $T_{sat,avg}$ = 40, 50 and 60 °C

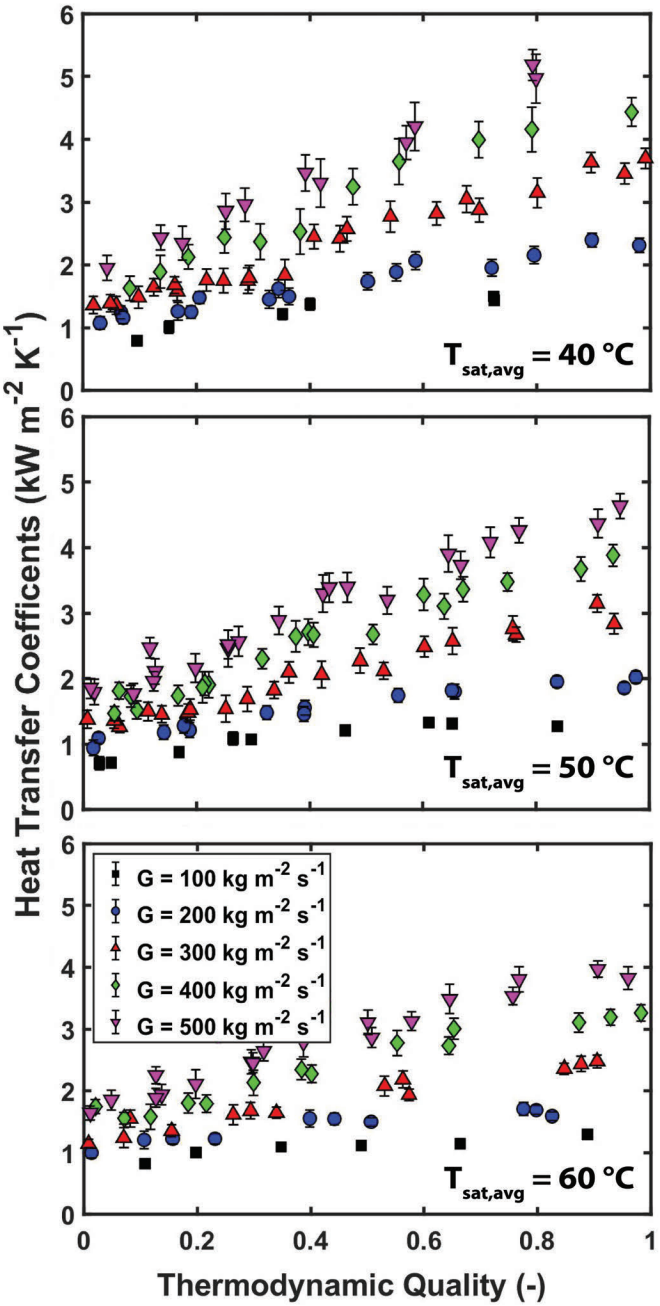

Figure 4.11: Saturated condensation heat transfer coefficient versus thermodynamic quality for R454C at G = 100 kg m^{-2} s^{-1} to 500 kg m^{-2} s^{-1} and at $T_{sat,avg}$ = 40, 50 and 60 °C

the other correlations.

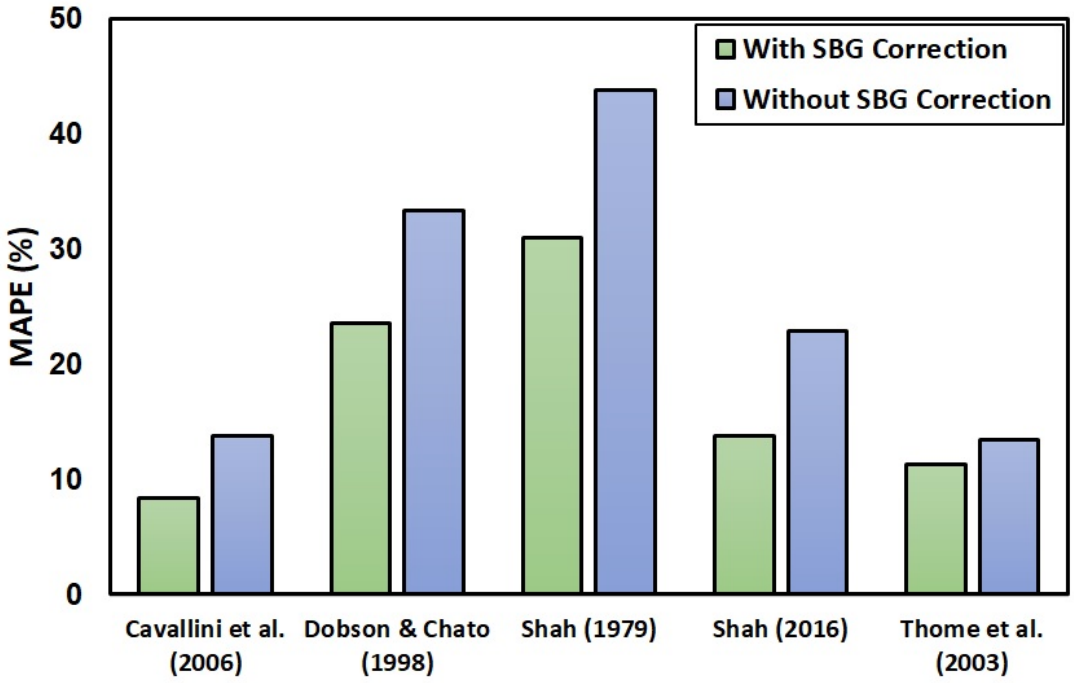

Figure 4.12: Predictive capability of different condensation correlations against experimental R448A, R450A, R452A, R454B and R454C data, with and without the Silver [96], Bell and Ghaly [12] (SBG) correction

Figure 4.13 shows plots of measured versus predicted heat transfer coefficients for all six models with the SBG correction. The measured data for all five refrigerants is best predicted by the Cavallini et al. [21] correlation with the SBG correction, with the MAPE and MPE values equal to 8% and 4%. On average, the application of the SBG approach to the Cavallini et al. [21] correlation resulted in an 8.8%, 1.3%, 7.2%, 3.2%, and 12.2% reduction in the predicted heat transfer coefficients for R448A, R450A, R452A, R454B, and R454C, respectively. The degradation due to mixture effects was more significant for higher temperature glide mixtures. In addition, this

degradation was highest at the highest mass fluxes and higher thermodynamic qualities. This is consistent with the understanding of zeotropic condensation in the literature (presented in Section 2.4).

Table 4.6 Predictive capability of different heat transfer correlations in the saturated region for R448A, R450A, R452A, R454B and R454C, with and without the Silver [96], Bell and Ghaly [12] (SBG) correction

	Without SBG		**With SBG**	
Model	MAPE(%)	MPE(%)	MAPE(%)	MPE(%)
Shah [90]	44	42	31	29
Dobson and Chato [36]	33	29	24	17
Thome et al. [101]	13	5	11	-1
Del Col et al. [29]	–	–	11	0
Cavallini et al. [21]	14	12	8	4
Shah [91]	23	22	14	12

The correlations by Thome et al. [101], Del Col et al. [29] and Shah [91] also predicted the data quite accurately, with the MAPEs below 15%. The modification of the earlier correlation Shah [90] to the Shah [91] correlation improved the predictability significantly from 31% MAPE value to 14%. In particular, the older Shah [90] correlation over predicted the heat transfer coefficients in the annular regime, which occurs at high qualities and mass fluxes.

Overall, the analysis conducted confirms that the existing correlations with the SBG correction are adequately able to predict the heat transfer coefficient of HFC/HFO refrigerant mixtures for the range of conditions investigated here.

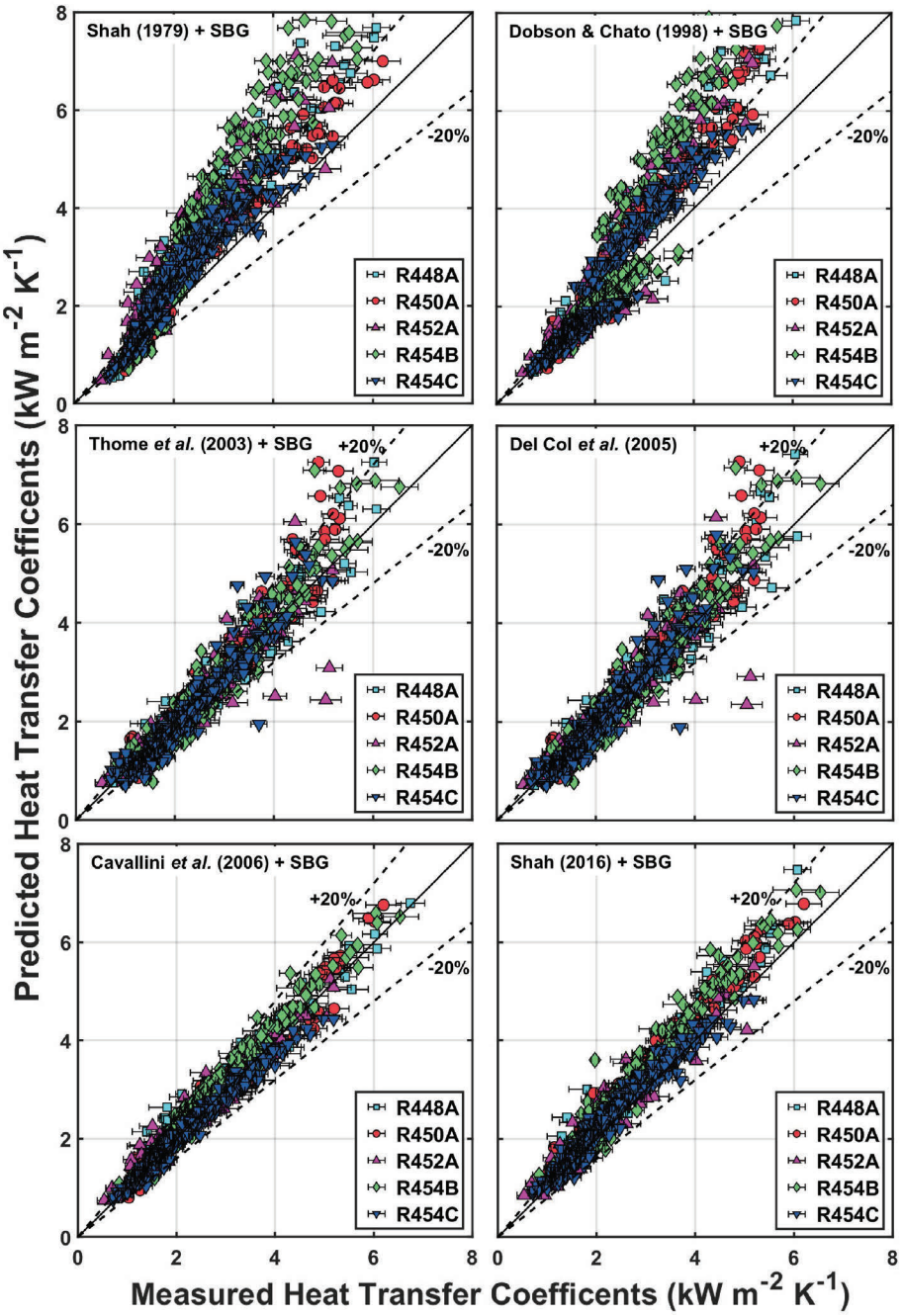

Figure 4.13: Predictive capability of different heat transfer correlations in the saturated region for R448A, R450A, R452A, R454B and R454C with the Silver [96], Bell and Ghaly [12] (SBG) correction

4.4.3 Subcooled condensation

The subcooled condensation region exists downstream of the saturated condensation region. The local refrigerant bulk enthalpy in this region is lower than the enthalpy of the liquid saturation enthalpy. Agarwal and Hrnjak [3] were among the first researchers to consider this zone in their heat transfer model. They argued that the conventional approach ignores the subcooling of the liquid condensate film during condensation modeling in the saturated region. However, in reality, the temperature of the condensate must be lower than the saturation temperature for heat transfer to occur. This implies that there is a sensible liquid heat load in the saturated region, in addition to the latent heat load. Therefore, to satisfy the first law of thermodynamics, non-condensed vapor bubbles are expected to be present in the flow beyond the point where bulk enthalpy is equal to the liquid saturation enthalpy. As these vapor bubbles eventually condense downstream, the heat transfer in the subcooled region is expected to be higher than that predicted by the single-phase heat transfer correlations. In the current study, subcooled heat transfer coefficients were measured for all five low GWP refrigerants for a wide range of experimental conditions. The Reynolds numbers corresponding to liquid flow at the test section outlet were always greater than 2385. This occurred for the lowest mass flux condition for R450A. For a majority of the experiments in this study, the Reynolds numbers at the test section outlet were much greater than 2300. Thus, turbulent flow occurred in the subcooled region for the experimental conditions investigated in this study.

Figure 4.14 shows a comparison between the heat transfer coefficients measured in the subcooled region against those predicted by the single-phase Gnielinski [46]

correlations. The measured data agree with the correlation extremely well, with the MAPE equal to 17.9%. There seems to be a limited enhancement in heat transfer in this region. However, it is important to note that this does not confirm or disprove the presence of latent effects in this region. A visualization study is required to conclude if there are, in fact, bubbles present in the subcooled region. However, these results do indicate that the contribution of these latent effects to the heat transfer is not significant. It is possible that condensation of the remaining bubbles occurs in this region. However, the heat transfer in this region is limited by the dominating thermal resistance of the liquid, which accounts for the majority of the cross-sectional area in the subcooled region. This explains why the heat transfer is well predicted by the single-phase heat transfer correlations. A comparison between the subcooled data and the complete condensation models is presented in the following section.

In addition to comparison with the Gnielinski [46] correlation, the subcooled condensation data were also compared against predictions from the single-phase Churchill [25] correlation. The Churchill [25] correlation provides predictions in the laminar and transition regimes, in addition to the turbulent region. The resulting MAPE was 17.6%. Therefore, if the flow in the subcooled region is not turbulent, the Churchill [25] correlation may be appropriately used instead.

4.4.4 Complete condensation

To be generally applicable, a good heat transfer model must provide accurate predictions for not just the saturated condensation region, but also for the superheated

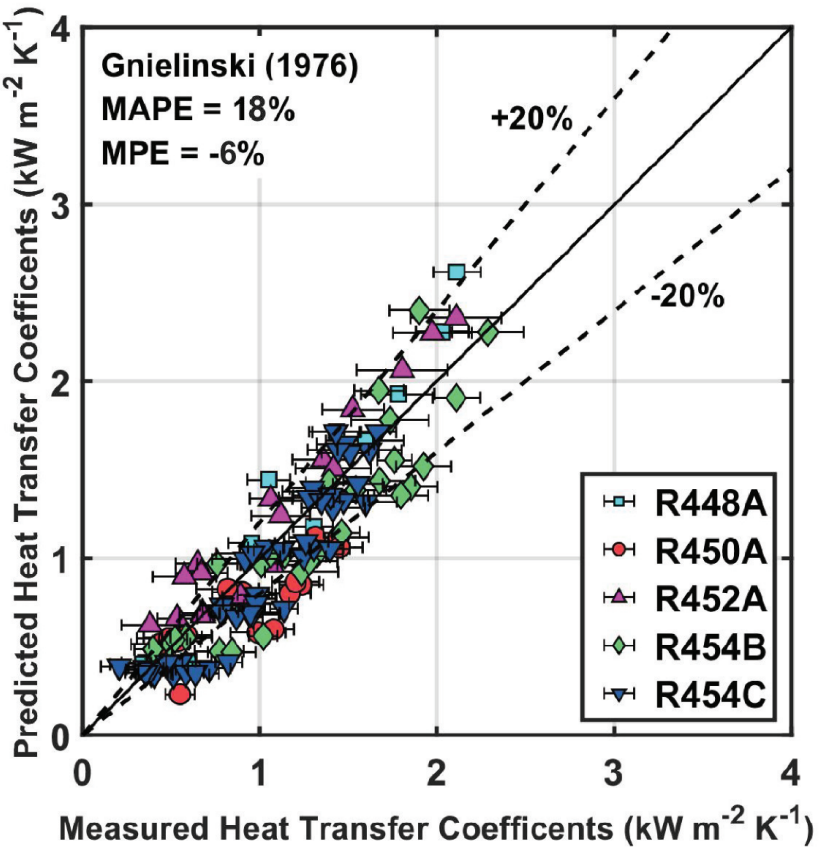

Figure 4.14: Predictive capability of the single-phase [46] correlation in the subcooled region for R448A, R450A, R452A, R454B and R454C

and subcooled condensation regions. As shown earlier, the latent effects in the superheated region are significant. Therefore, this section assesses the predictive capability of the non-equilibrium models of Hrnjak and co-workers for complete condensation by comparing them against the measured data.

Among the two-phase models discussed in the superheated condensation section, the model of Kondou and Hrnjak [64] does not provide predictions in the subcooled region. Therefore to compare each model with the complete data set, the Gnielinski

[46] correlation was used for predicting subcooled condensation with the Kondou and Hrnjak [64] model. Similarly, it is insightful to compare the predictive capabilities of the traditional equilibrium approach (which ignores the latent effects in superheated and subcooled regions) against the non-equilibrium two-phase models. The Cavallini et al. [21] correlation showed an excellent agreement with the saturated condensation data, with a MAPE equal to 8%. Therefore for the traditional approach, the saturated condensation data were predicted using the Cavallini et al. [21] correlation, and the subcooled and superheated condensation data were predicted using the Gnielinski [46] correlation. Mixture effects were accounted for using the SBG correction. The resulting comparison is shown in Figure 4.15 and summarized in Table 4.7.

Table 4.7 Predictive capability of different heat transfer models in the superheated, saturated and subcooled condensation regions for R448A, R450A, R452A, R454B and R454C

	With SBG	
Model	MAPE(%)	MPE(%)
Cavallini et al. [21] + Gnielinski [46]	16	-6
Kondou and Hrnjak [64] + Gnielinski [46]	11	5
Agarwal and Hrnjak [3]	41	35
Xiao and Hrnjak [108]	57	57

The results show an opposite trend compared to that of the superheated condensation results. Overall, the Kondou and Hrnjak [64] model with the Gnielinski [46] correlation is able to predict the data the best, with a MAPE equal to 11%. This is partly because Kondou and Hrnjak [64] also recommended using the Cavallini et al. [21] correlation for predictions in the saturated condensation region which, as noted earlier, predicts the saturated condensation data very accurately. Conversely, the

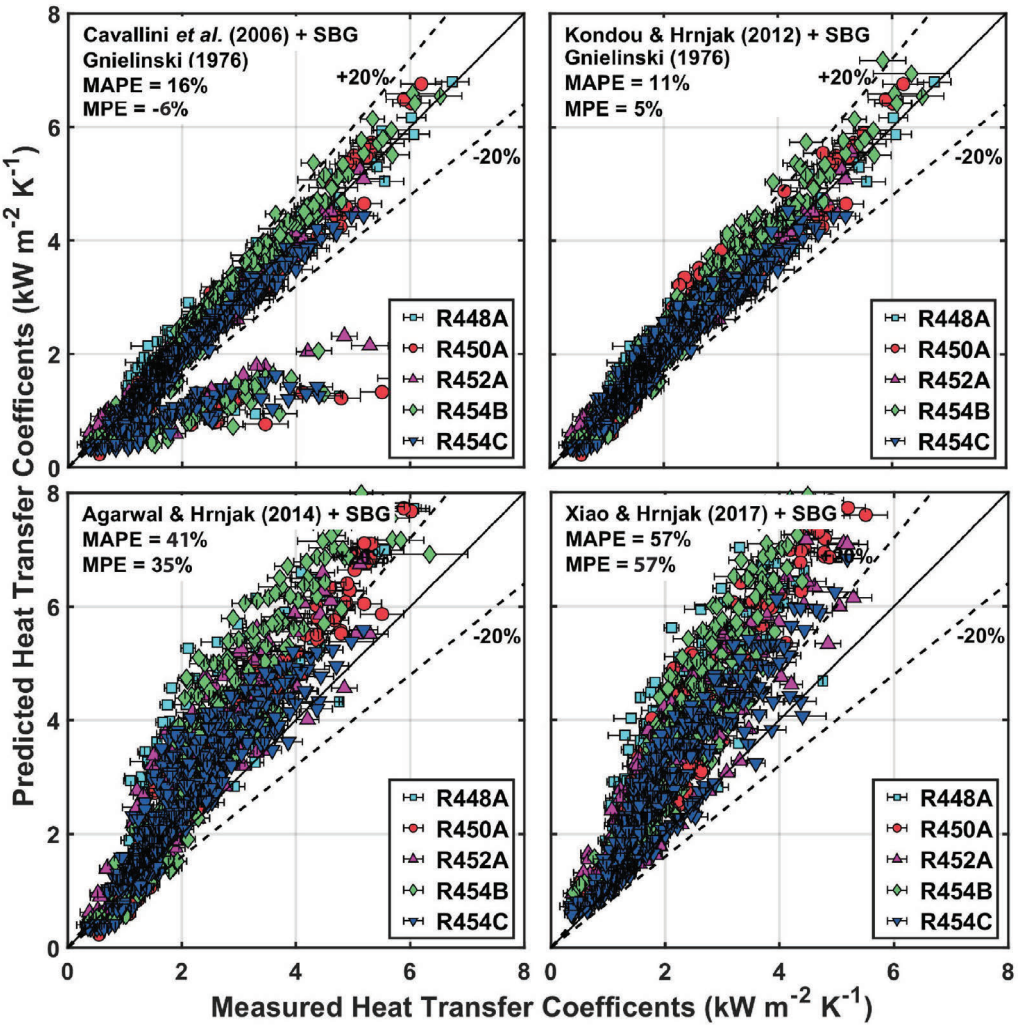

Figure 4.15: Measured heat transfer coefficients versus predictions from different models in the superheated, saturated and subcooled condensation regions.

models of Agarwal and Hrnjak [3] and Xiao and Hrnjak [108] significantly over predict the data in the saturated region. This is consistent with Xiao's doctoral thesis Xiao [106], where he reported that his non-equilibrium model significantly over predicted the results for R32/R1234ze(E) mixture condensation. Further limitations of these models are discussed in the following section.

It interesting to note that the overall MAPE for the traditional approach is lower than those associated with the models of Agarwal and Hrnjak [3] and Xiao and Hrnjak [108], despite the poor agreement in the superheated region. However, there is a significant advantage of using the non-equilibrium Kondou and Hrnjak [64] model over the traditional approach due to the much better agreement in the superheated region.

4.4.5 Limitations of the past complete condensations models

The group of Hrnjak et al. has been one of the first to attempt to model condensation through the superheated to saturated and finally subcooled regions. However, as presented, they are difficult to implement for condenser design due to an iterative solution scheme, some inconsistencies in nomenclature between the various models, and potential typographical errors.

In addition, the analysis in the previous section shows that the applicability of these models to refrigerant mixtures is limited. Only the model of Kondou and Hrnjak [64] is able to accurately predict the condensation of HFC/HFO mixtures across all condensation regions. A major shortcoming of the earlier models [3, 64] is that

they assume a constant quality equal to 0.9999 in the superheated zone. While the agreement between experimental data and predictions is reasonable in this zone, the constant quality assumption does not capture the underlying physical mechanisms. More importantly, their model for superheated condensation does not accurately represent the heat transfer process that occurs (further justification provided below in the modeling Chapter 5).

Xiao and Hrnjak [108] attempted to rectify this issue by introducing the superficial quality (Equation 2.14). They identify the location at which condensation ends using Equation 2.16. The criterion they used to determine this location was: the highest temperature in the liquid condensate drops below the saturation temperature. However, neither the paper nor Xiao's thesis adequately describes how this parameter was derived and therefore, its theoretical basis is not clear.

The implementation of the superficial quality further introduces other complications to the design procedure. To implement Xiao's [108] model and to determine the superficial quality along the length of the condenser, the local heat flux must be known *a prior* or solved by iteration for all regions (including the single-phase vapor and liquid flow regions). Of particular challenge is that the end of condensation, calculation of the bulk temperature (Equation 2.16) requires knowledge of the saturation temperature, a single-phase heat transfer correlation for the liquid flow and the local heat flux. The bulk temperature corresponding to the end of condensation enables calculation of the bulk enthalpy at the end of condensation, necessary for calculating the superficial quality used in upstream calculations. For practical condensation problems, the heat flux is unknown and not constant, and thus there

are two unknowns. To determine the end of condensation, more information about the thermal resistance from the tube wall to the ultimate thermal sink would be required. This would provide additional equations to provide closure to the problem. However, this complicates the implementation of this approach.

Most importantly, the models of Agarwal and Hrnjak [3] and Xiao and Hrnjak [108] significantly over predict the measured data in the present study (Figure 4.15). These models were developed for pure fluid, which may be one reason for the poor prediction of the zeotropic mixtures in this study. However, these discrepancies between the measured data and predictions do not appear to be solely attributed to the degradation due to mixture effects.

Consider the plots shown in Figure 4.16. The top graph in Figure 4.16 shows the measured heat transfer coefficients of R32, R1234ze(E), and their mixtures from Xiao's doctoral thesis [106]. The bottom graph shows the predicted heat transfer coefficients from the Cavallini et al. [21] correlations for pure R32 and R1234ze(E), at the same operating conditions ($G = 200$ kg m^{-2} s^{-1}, $D = 4.4$ mm and $T_{sat} = 30$ °C). The x-axes in the two plots are not the same, as the top shows the superficial quality while the bottom plots show the thermodynamic quality. Since Xiao [106] did not report the heat flux associated with 4.16(a), it is not possible to determine the corresponding thermodynamic qualities. Nonetheless, it is insightful to compare the magnitudes of the heat transfer coefficients for both the plots. Recall that for both the modeling methods, the highest heat transfer coefficients are observed for corresponding thermodynamic qualities close to 1. Xiao [106] measured heat transfer coefficients up to approximately 9 kWm^{-2}K^{-1} and 6.5 kWm^{-2}K^{-1} for R32

and R1234ze(E), respectively. However, the Cavallini et al. [21] correlations predicts much lower heat transfer coefficients, with the maximum equal to 5.1 $kWm^{-2}K^{-1}$ for R32 and 4 $kWm^{-2}K^{-1}$ for R1234ze(E). In the literature, the Cavallini et al. [21] correlation has been shown to predict the performance of both these refrigerants accurately for a wide range of operating conditions [76, 33, 34]. This discrepancy is larger than would be expected and can help explain the large deviation between their developed model and the data presented here. Among the three journal papers detailing the models from Hrnjak and co-workers, only Kondou and Hrnjak [64] compared their data against the existing conventional two-phase models in the saturated region to validate the accuracy of their experimental methods. Their experimental facility was then modified to incorporate a visualization section. However, after this modification, neither Agarwal nor Xiao provided a validation of their experimental methods in their publications. None of their subsequent peer-reviewed papers compare the data in the saturated region to the existing two-phase models. In addition, there have been no other condensation studies in the literature which have compared their data to these models by Hrnjak and co-workers. Therefore, it is not possible to confirm whether their measured heat transfer coefficients were accurate or not. However, this may provide a plausible explanation for why the models of Agarwal and Hrnjak [3] and Xiao and Hrnjak [108] over predict the measured data from the current study.

Given these factors, a new model is needed to accurately predict the condensation of HFC/HFO mixtures in the superheated, saturated, and subcooled regions. This model must be based on realistic physical parameters and easy to implement so it is

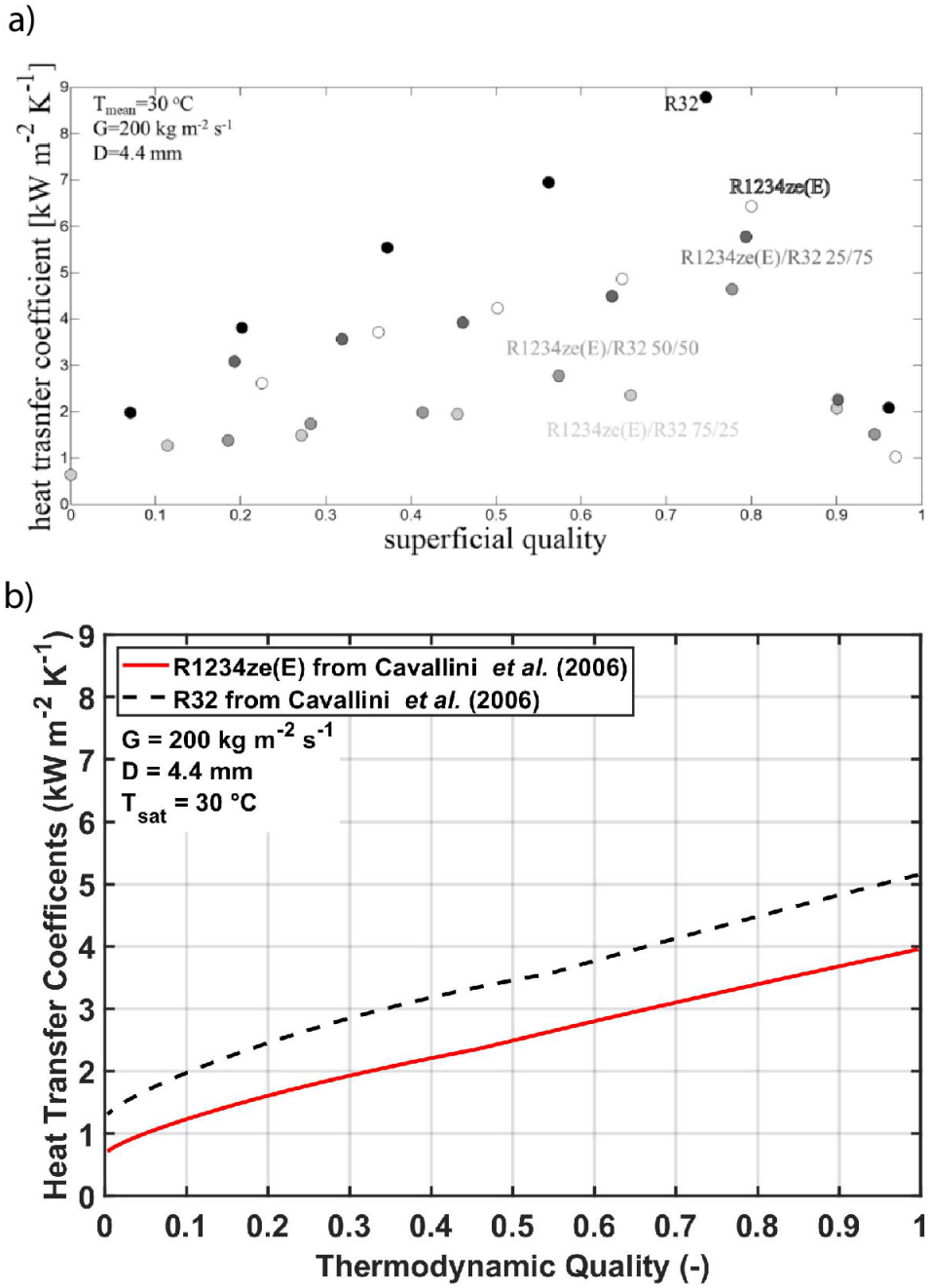

Figure 4.16: a) Heat transfer coefficients of R32 and R1234ze(E) measured by Xiao [106], b) Heat transfer coefficients of R32 and R1234ze(E) predicted by Cavallini et al. [21]

accessible to designers in the HVAC&R industry.

4.5 Comparison with the HFC predecessors

Table 4.8 shows that the five low GWP refrigerants investigated in this study have been proposed to replace three different HFC refrigerants for various medium- and high-pressure applications. In addition to a comparison with various predicting correlations from the literature, it is also insightful to compare the performance of the HFO/HFC replacements with their HFC predecessors. This will help determine if they are viable substitutes. Therefore, the best performing correlations were used to compare the heat transfer and pressure drop of these refrigerants in the saturated condensation regime. The resulting comparison is presented in this section.

Table 4.8 A list of the HFC refrigerants and their applications, along with their proposed HFO/HFC replacements

HFC	**Proposed Replacement**	**Application**
R13a	R450A	Medium-pressure applications such as heat pumps, air-cooled and water-cooled chillers, and vending machines
R404A	R448A, R452A and R454C	High-pressure applications such as commercial and transport refrigeration
R410A	R454B	High-pressure applications such as building air-conditioning, chillers, and heat pumps

4.5.1 R134a comparison

Condensation heat transfer performance and frictional pressure drop of R134a and R450A were simulated at identical operating conditions using the best performing correlations. The corresponding refrigerant mass flux was equal to 400 kg $m^{-2}s^{-1}$. Both R134a and R450A heat transfer coefficients were evaluated using the Cavallini et al. [21] correlation with the Silver, Bell and Ghaly correction applied to account for mass transfer effects for R450A. The Haraguchi et al. [49] correlation was used to evaluate the frictional pressure gradients for both refrigerants.

The resulting heat transfer coefficients and frictional pressure gradients are reported in Figure 4.17. The reduction in heat transfer coefficients of R450A compared to R134a occurs mainly at high qualities and the maximum reduction is less than 5% for all qualities. However, the resulting pressure gradient of R450A is significantly higher (Average 8%, max = 13%) than the pressure gradient for R134a. This difference is higher at higher qualities. R450A, compared to R134a, operates at lower working pressures, has a higher vapor viscosity, and lower liquid and vapor density (Table 4.9). This is in line with the findings of Del Col et al. [34], who found the pressure drop of R1234ze (a component of R450A) to be 18-28% higher than that of R134a (a component of R450A). These results indicate that the additional pressure drop must be taken into account during the design of newer refrigeration systems and HVAC&R equipment which use R450A as a replacement for R134a.

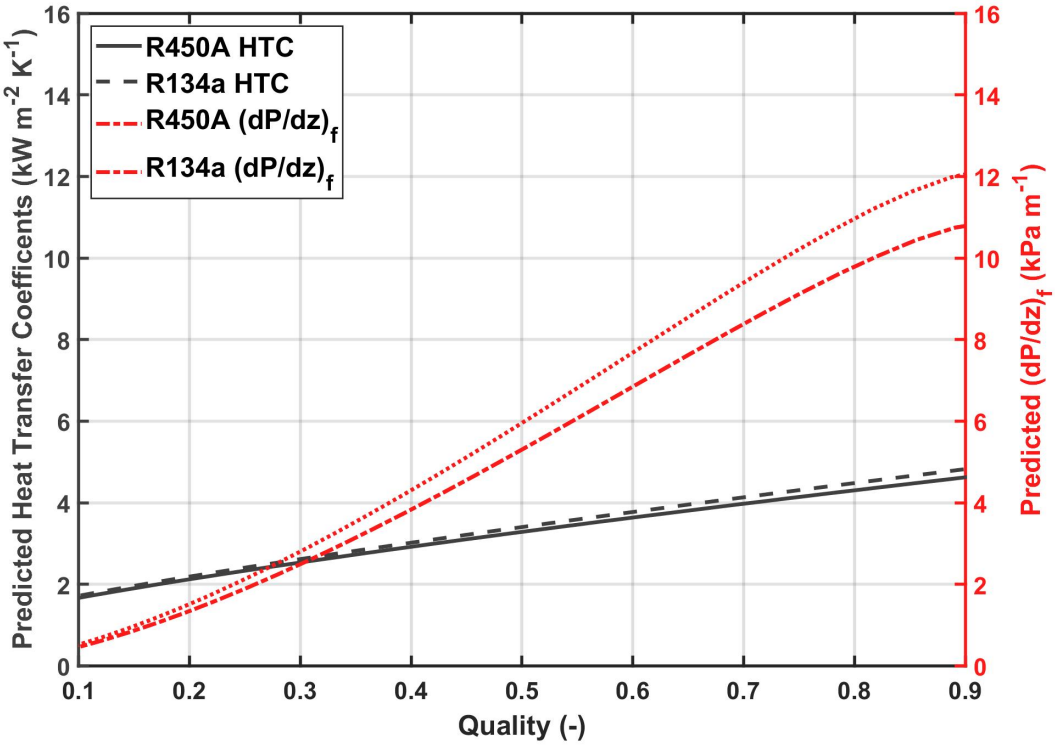

Figure 4.17: Heat transfer and pressure drop for R450A vs R134a at G = 400 kg m^{-2} s^{-1} tube with ID = 4.7 mm.

Table 4.9 Comparison of Properties at $T_{dew} = 55\,°C$, from REFPROP 10 [70]

	P_{sat}(kPa)	h_{fv}(kJ kg^{-1})	ρ_l/ρ_v	μ_l/μ_v	$\sigma \times 10^{-3}$(N m^{-1})
R134a	1492	145.7	14.2	10.0	4.3
R450A	1304	141.1	15.3	9.54	4.6

4.5.2 R404A comparison

Since R448A, R452A and R454C are proposed replacements for R404A, it is insightful to compare their performance with each other and to R404A. Figure 4.18 provides a comparison of the predictions from Cavallini et al. [21] correlation for each refrigerant at two different mass fluxes (G = 200 and 600 kg m^{-2} s^{-1}). The predictions show that the heat transfer performance of all three low GWP substitutes (R448A, R452A and R454C) is comparable to that of R404A; with the heat transfer coefficients of R404A being slightly higher than those of R452A and slightly lower than those of R448A and R454C. Among these fluids, R448A has the highest liquid phase thermal conductivity and R404A has the lowest at similar operating conditions. Even though the liquid phase thermal conductivity of R448A and R452A is higher than R404A, the heat transfer coefficients are very similar, which may be attributed to the degradation due to mixture effects.

It is not possible to compare the experimental pressure drops from this study directly due to the differences in lengths associated with the condensation region (Eq. 3.7) during experiments. Therefore, the correlations that best predicted the data for each fluid were used to compare the two-phase frictional pressure gradients associated with the condensation of each refrigerant. Figure 4.19 shows the frictional pressure gradient of R404A, R448A, R452A and R454C at two different mass fluxes

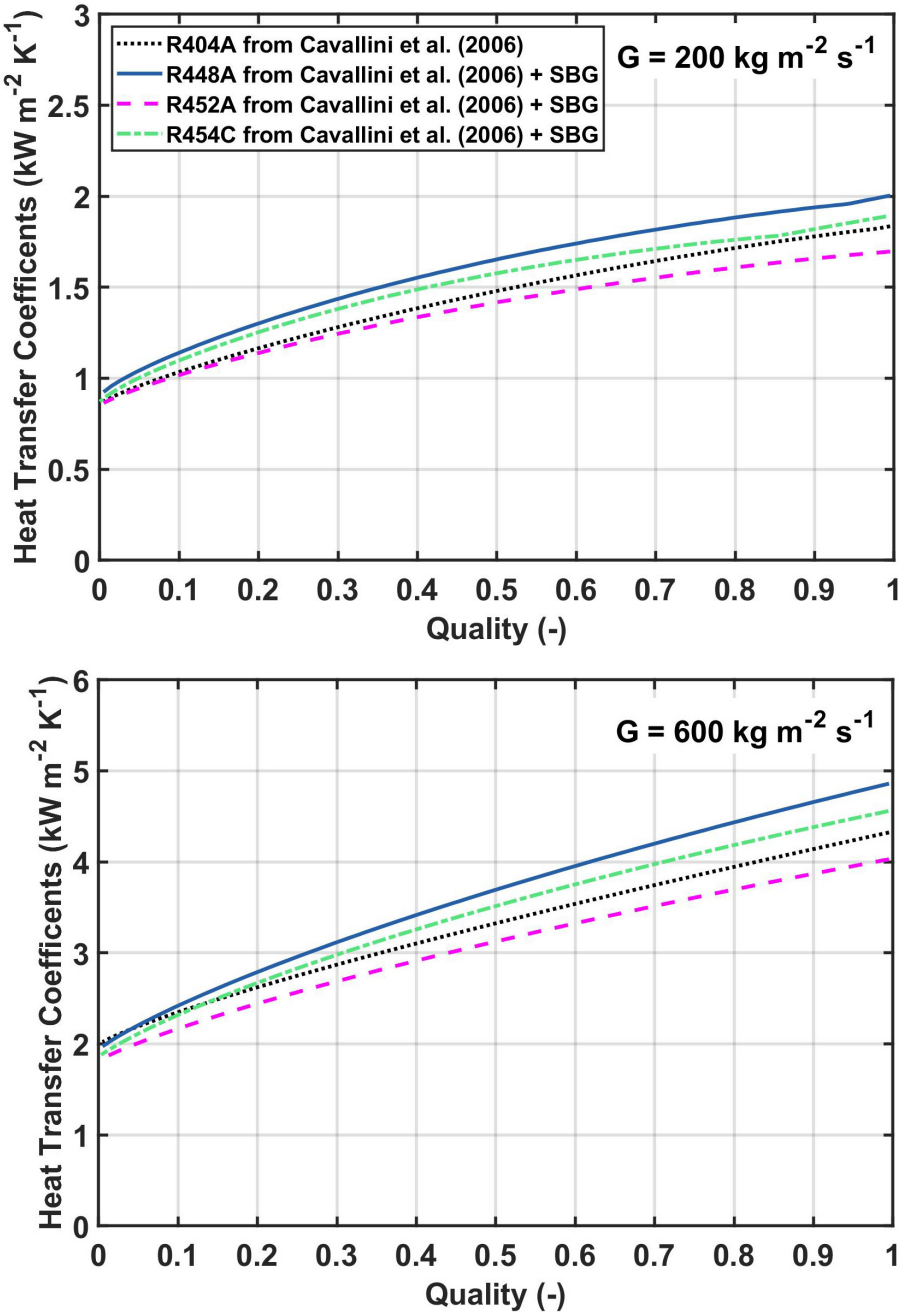

Figure 4.18: Condensation heat transfer coefficients of R448A, R452A and R454C at two different mass fluxes (G = 200 kg m^{-2} s^{-1} and 600 kg m^{-2} s^{-1}, $T_{sat,avg}$ = 60 °C) . The experimental data is compared with predictions from the Cavallini et al. [21] correlation for R404A, R448A and R452A

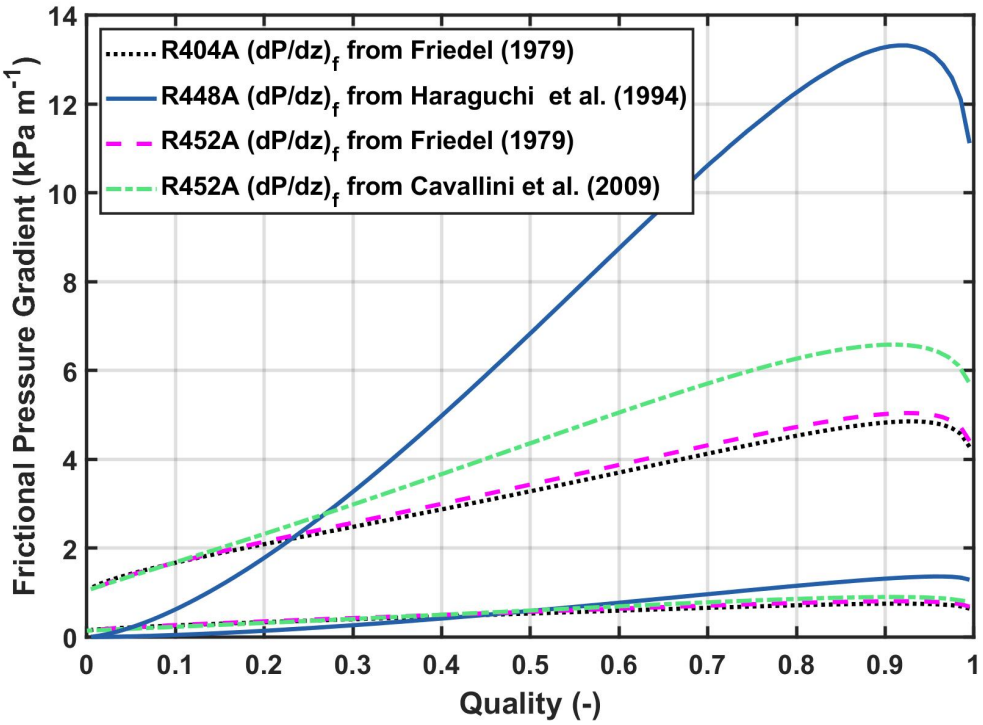

Figure 4.19: Predicted two-phase frictional pressure drop of R404A, R448A, R452A and R454C at two different mass fluxes (G = 200 kg m^{-2} s^{-1} and 600 kg m^{-2} s^{-1}, $T_{sat,avg}$ = 60 °C)

(G = 200 & 600 kg m^{-2} s^{-1}). R448A had the highest pressure drop, and R404A the lowest. For G = 600 kg m^{-2} s^{-1}, the pressure drop of R448A is on average 81% higher than that of R404A. The pressure drop of R452A and R454C are on average 3.3% and 27.6% higher than that of R404A, respectively.

The transport and thermodynamic properties of these refrigerants can help explain these observed differences. R448A and R452A have a higher liquid phase viscosity compared to R404A (Table 4.10). During condensation, higher liquid phase viscosity results in a greater amount of shear between the liquid and the wall, as well

Table 4.10 Thermophysical Properties of R404A, R448A, R452A and R454C at $T_{sat,avg} = 40\,°C$, from REFPROP 10 [70]

	ΔT_{glide} °C	P_{sat} (kPa)	h_{fv} (kJ kg^{-1})	ρ_l (kg m^{-3})	ρ_v (kg m^{-3})	$\mu_l \times 10^6$ (kg m^{-1}s^{-1})	$\mu_v \times 10^6$ (kg m^{-1}s^{-1})	$k_l \times 10^3$ (W m^{-1} K^{-1})	$\sigma \times 10^3$ (N m^{-1})
R404A	0.3	1822	120	964	102.1	102.4	13.4	56.6	2.7
R448A	4.7	1776	151	1013	81.3	109.7	13.7	73.3	3.7
R452A	3.4	1832	117	1033	104.7	105.8	14.2	60.3	2.8
R454C	6.8	1590	143	959	75.4	101.9	13.2	69.5	3.4

as between the liquid and the vapor phases. R448A and R452A have higher liquid phase densities and lower vapor phase densities than R404A. Similarly, compared to R404A, R454C has a similar liquid phase density and a lower vapor phase density. During the condensation process, this results in higher velocity vapor flow and lower velocity liquid flow compared to R404A at the same mass flow rate. The increased difference in velocities of the phases will result in a greater magnitude of interfacial shear between the phases. The combination of both of these factors results in higher pressure drops of R452A R448A and R454C when compared to R404A at equal mass fluxes.

The latent heats of vaporization for R448A and R454C are significantly higher than that of R452A and R404A. In practice, this would result in lower mass flow rates compared to R404A in a vapor compression system utilizing these fluids. Table 4.11 shows the mass flow rates of each refrigerant required to produce 1 kW of cooling assuming an evaporating temperature equal to 0 °C. The resulting mass flow rate of R404A was approximately 18% and 12% higher than those for R448A and R454C.

The mass flow rates in Table 4.11 were then used to calculate the heat transfer

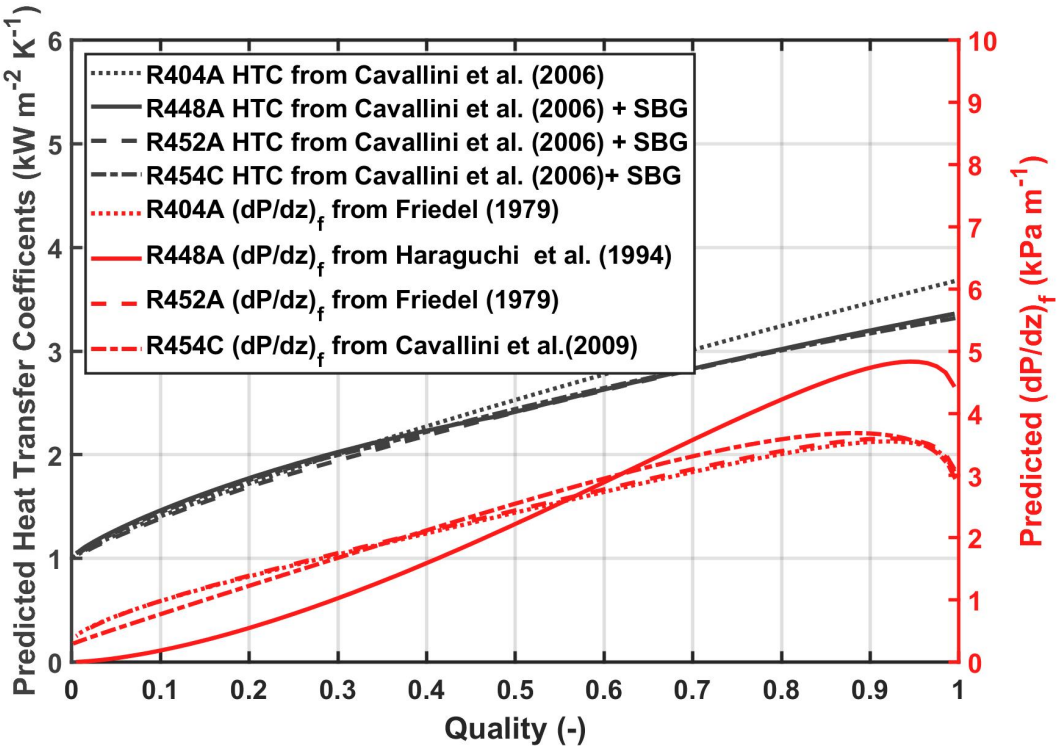

Figure 4.20: Heat transfer coefficients and pressure drop gradients for R404A, R448A, R452A and R454C at mass flow rates listed in Table 4.11 to produce 1 kW of cooling system in a condenser with ID = 4.7 mm and saturation temperature of 40 °C

coefficients and pressure drop gradients in a single condenser tube (with tube ID = 4.7 mm) operating at $T_{sat,avg}$ = 40 °C, using the correlations that were found to predict the data best. Figure 4.20 shows the results. Heat transfer coefficients of all four refrigerants are comparatively similar. The pressure drop of R404A, R452A, and R454C is approximately equal, and the pressure drop of R448A is on average 16% lower than that of R404A.

Therefore, even though R448A exhibits a higher pressure drop when compared to R404A at the same mass flux, it may actually have a lower pressure drop when

Table 4.11 R404A, R448A. R452A and R454C flow rates and corresponding mass fluxes required to produce 1 kW of cooling at 0 °C evaporating temperature and the associated latent heats of vaporization from REFPROP[70]

Refrigerant	**Latent Heat of Vaporization at 0** °C (kJ kg^{-1})	**Mass Flow Rate** ($g\ s^{-1}$)	**Mass flux in a tube with ID =4.7 mm** ($kg\ m^{-2}\ s^{-1}$)
R404A	166.3	6.0	343
R448A	206.1	4.9	277
R452A	164.5	6.1	347
R454C	189.2	5.3	305

compared on an equal cooling capacity. The pressure drop of R452A is consistently similar to that of the pressure drop of R404A. Overall, this analysis confirms that R448A, R452A and R454C may be considered as viable replacements for R404A.

4.5.3 R410A comparison

The performance of refrigerant R410A was compared to its proposed replacement candidate, R454B. The heat transfer for both the refrigerants was predicted using the Cavallini et al. [21] correlation and the results are shown in Figure 4.21 for different mass fluxes (G = 200 kg m^{-2} s^{-1} and 600 kg m^{-2} s^{-1}). The results show that on average R454B exhibits 11% higher heat transfer coefficients compared to R410A. This may be because R454B has an 18% higher liquid thermal conductivity compared to R404A (Table 4.12). Additionally, the mixture degradation for R454B is minimal, since its temperature glide is relatively low.

In addition, Figure 4.22 shows a pressure drop comparison for the two refrigerants at two different mass fluxes (G = 200 kg m^{-2} s^{-1} and 600 kg m^{-2} s^{-1}). The

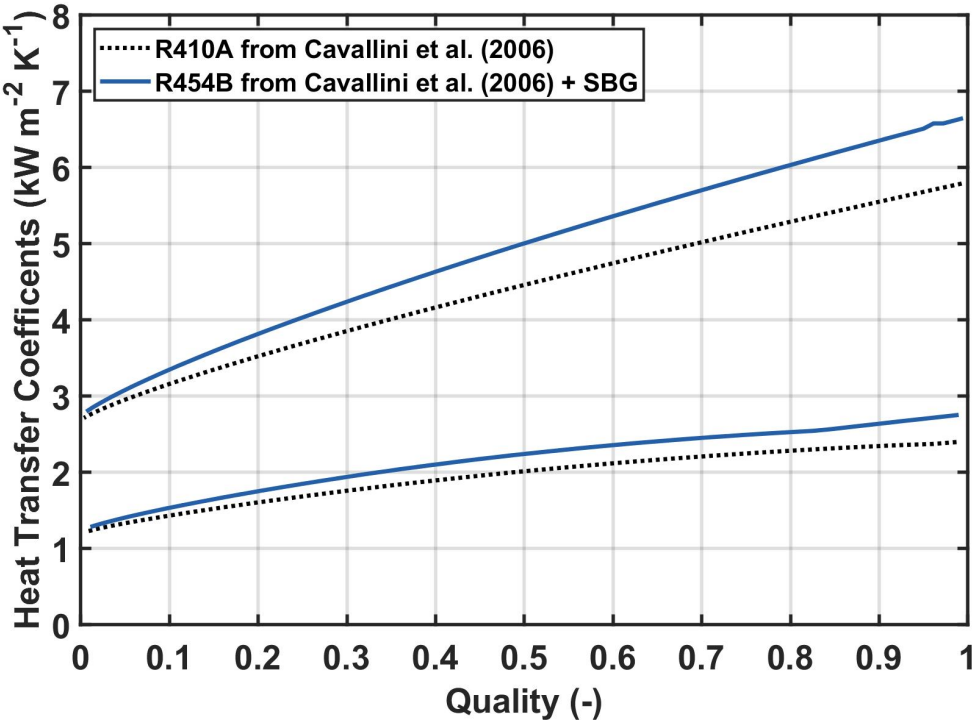

Figure 4.21: Condensation heat transfer coefficients of R410A and R454B at two different mass fluxes (G = 200 kg m^{-2} s^{-1} and 600 kg m^{-2} s^{-1}, $T_{sat,avg}$ = 60 °C) . The experimental data is compared with predictions from the Cavallini et al. [21] correlation for R404A, R448A and R452A

Table 4.12 Thermophysical Properties of R410A and R454B at $T_{sat,avg} = 60\,°C$, from REFPROP 10 [70]

	ΔT_{glide} °C	P_{sat} (kPa)	h_{fv} (kJ kg^{-1})	ρ_l (kg m^{-3})	ρ_v (kg m^{-3})	$\mu_l \times 10^6$ (kg m^{-1}s^{-1})	$\mu_v \times 10^6$ (kg m^{-1}s^{-1})	$k_l \times 10^3$ (W m^{-1} K^{-1})	$\sigma \times 10^3$ (N m^{-1})
R410A	0.1	3838	105	815	201	67	18	71	0.8
R454B	1.0	3582	142	786	147	70	16	84	1.4

Cavallini et al. [19] correlation was used for predicting the pressure drop of both the refrigerants. R454B exhibits a 39% higher pressure drop, primarily due to a higher liquid-vapor density ratio. In addition, R454B has a 35% higher latent heat of vaporization compared to R410A. In practical applications, this will result in different operating mass fluxes for the two fluids. Table 4.11 shows the mass flow rates of each refrigerant required to produce 1 kW of cooling assuming an evaporating temperature equal to 0 °C. Therefore, the heat transfer and pressure drop of R410A and R454B were also compared for equal cooling capacity. The results are shown in Figure 4.23. For equal cooling capacity, the heat transfer and pressure drop of R410A and R454B are similar. Therefore, from a condenser design perspective, R454B can be considered a viable substitute for R410A.

Table 4.13 R410A and R454B flow rates and corresponding mass fluxes required to produce 1 kW of cooling at 0 °C evaporating temperature and the associated latent heats of vaporization from REFPROP[70]

Refrigerant	**Latent Heat of Vaporization at 0** °C (kJ kg^{-1})	**Mass Flow Rate** (g s^{-1})	**Mass flux in a tube with ID =4.7 mm** (kg m^{-2} s^{-1})
R410A	221.3	4.5	260.4
R454B	260.9	3.8	220.9

4.6 Summary of the results

A facility capable of measuring the local heat transfer coefficients during condensation was constructed and rigorously validated. Experimental data were then collected at varying mass fluxes and saturation conditions during the condensation of five low

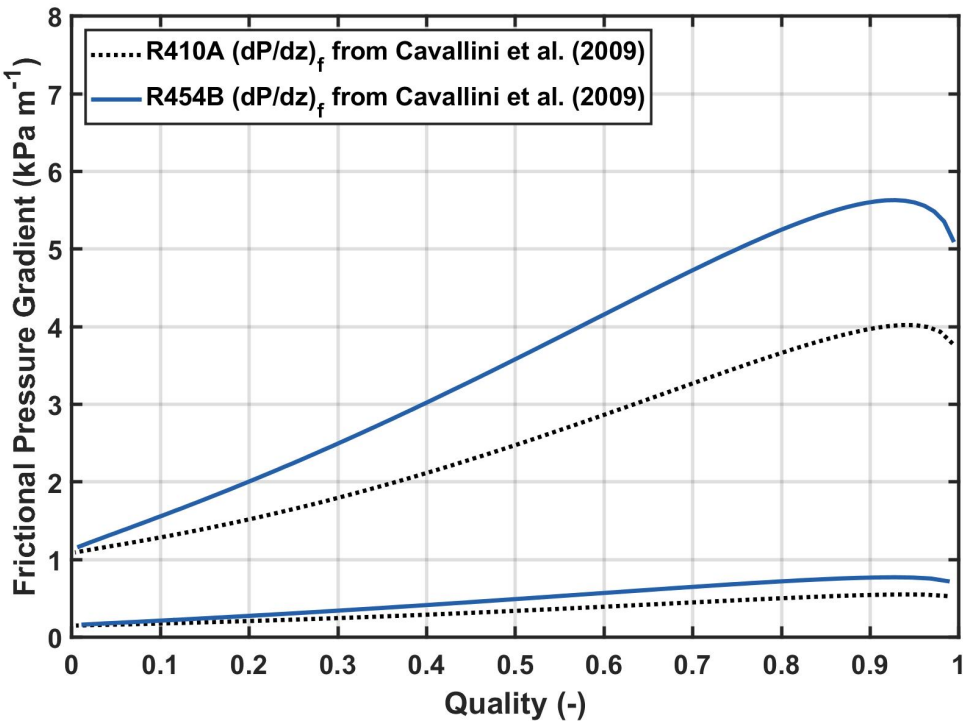

Figure 4.22: Predicted two-phase frictional pressure drop of R410A and R454B at two different mass fluxes (G = 200 kg m^{-2} s^{-1} and 600 kg m^{-2} s^{-1}, $T_{sat,avg}$ = 60 °C)

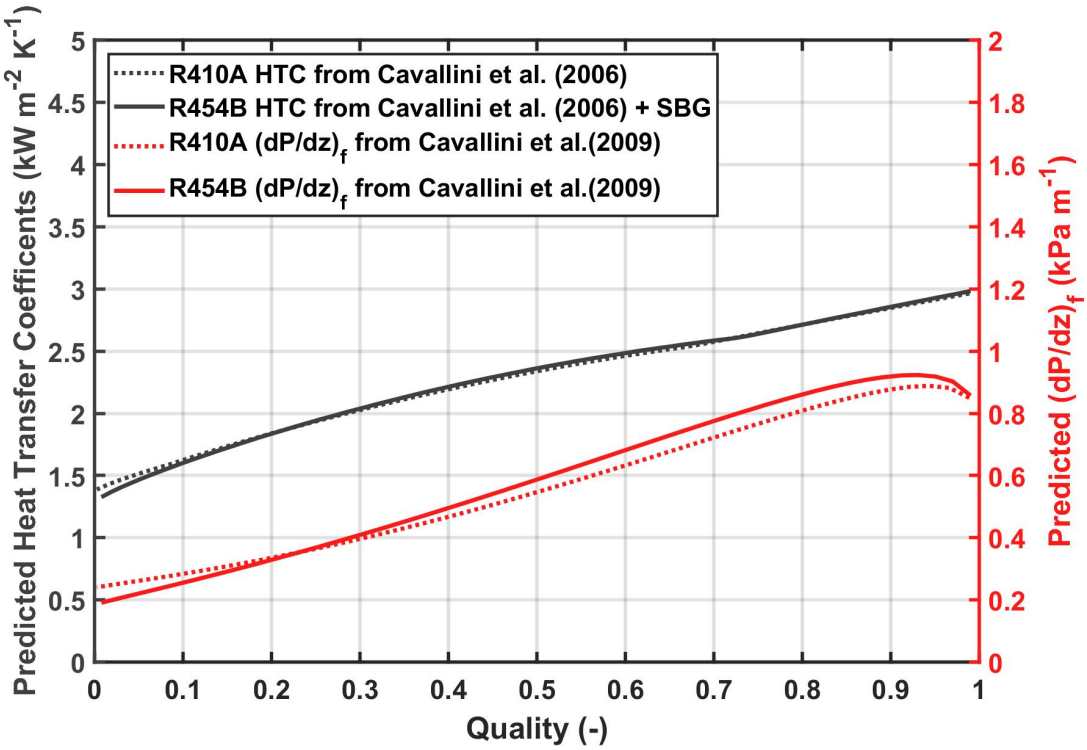

Figure 4.23: Heat transfer coefficients and pressure drop gradients for R410A and R454B at mass flow rates listed in Table 4.13 to produce 1 kW of cooling system in a condenser with ID = 4.7 mm and saturation temperature of 40 °C

GWP refrigerant mixtures: R448A(ΔT_{glide} = 4.3 °C), R450A (ΔT_{glide} = 0.6 °C), R452A (ΔT_{glide} = 3.0 °C), R454B (ΔT_{glide} = 1.2 °C) and R454C (ΔT_{glide} = 6.3 °C). The experimental pressure drop and local heat transfer coefficients are well predicted by the saturated two-phase models, after accounting for the mixture degradation using the SBG correlation. A comparison of the heat transfer and pressure drop of the new HFC/HFO mixtures indicates that they are similar to those of their HFC predecessors. Therefore, the low GWP mixtures may be considered as viable substitutes from a heat and momentum transport perspective. Additionally, the results

suggest that the non-equilibrium framework of Colburn and Drew [26] is not needed for these mixtures, greatly simplifying design and optimization of next generation systems.

Heat transfer data in the superheated and subcooled regions were compared to models of Kondou and Hrnjak [64], Agarwal and Hrnjak [3] and Xiao and Hrnjak [108]. However, inconsistencies between the modeling approaches and the need for an iterative solutions make them difficult to implement. While the agreement in the superheated regime with these models is reasonable, only the model of Kondou and Hrnjak [64] is accurately able to predict condensation in the saturated region. This is because Kondou and Hrnjak [64] suggested using the Cavallini et al. [21] correlation to predict the condensation in the saturation region, which predicts the saturated data in the present study very accurately (MAPE = 8%). In the superheated region, the model of Kondou and Hrnjak [64] is not based on real physical parameters, as it assumes an artificial constant quality of 0.9999. The heat transfer in the subcooled region was well predicted by the Gnielinski [46] single-phase heat transfer correlation (MAPE = 19%). The agreement with the Agarwal and Hrnjak [3] and Xiao and Hrnjak [108] model is poor, which shows that there is a need for a new condensation model for HFC/HFO refrigerants.

Chapter 5: Complete Condensation Model for HFC/HFO Mixtures

Thus far, this research has established that simplified equilibrium type models can be used to predict the heat transfer coefficient of new refrigerant mixtures in the saturated condensation regime. However, the results also show that the limited models available in the literature for complete condensation (superheated, saturated, and subcooled) generally do not translate well to refrigerant mixture heat transfer. Furthermore, the existing models are heavily empirical and difficult to implement. This greatly limits their usefulness in the design and optimization of new heat transfer equipment utilizing new low GWP fluids. Thus, this work aims to develop a physically-based condensation model, validated with the experimental data of the low GWP refrigerant mixtures.

This current model assumes that the mass transfer in the liquid and vapor phases is not limited i.e., the liquid and vapor compositions are in equilibrium at the saturation temperature and vapor bulk temperature, respectively. This allows the model to be much simpler and easier to implement compared to the Colburn and Drew [26] method, while still capturing the non-equilibrium effects due to superheated condensation. To account for the degradation due to the mixture effects, the Silver, Bell, and Ghaly [96, 12] correction must be applied to the heat transfer coefficients in the superheated and saturated regions.

5.1 Quality

A major challenge associated with predicting heat transfer during non-equilibrium condensation of mixtures is that the local qualities are difficult to evaluate. As established earlier, the thermodynamic qualities differ significantly from the actual qualities and therefore, can not be used as an approximate value. One way to track the actual quality, as the condensation proceeds, is to use the Colburn and Drew [26] framework. However, this non-equilibrium method is computationally challenging to implement and therefore, not accessible to many HVAC&R designers. An alternative approach was developed by Xiao and Hrnjak [108], which utilized the superficial quality (Equation 2.14).

The superficial quality is evaluated by first determining the locations where condensation starts and ends. There is a consensus among all the previous researchers on the criterion for determining the start of the condensation region: condensation starts when the tube wall temperature drops below the saturation temperature. For superheated vapor flow, the specific location along the length of the heat exchanger is determined by analyzing the inner tube wall temperatures along the length of the heat exchanger. If the flow is turbulent and occurs in a tube, the tube wall temperatures can be evaluated by applying Newton's law of cooling and the single-phase Gnielinski [46] correlation (Equation 5.1). The Churchill [25] or other appropriate correlations may be used as well for predicting the heat transfer in the laminar and transition regimes. The resulting expression is:

$$T_{wall} = T_b - \frac{q''}{\alpha_v} \tag{5.1}$$

where T_b is the bulk temperature of the vapor flow. The location and the refrigerant bulk temperature at the onset of condensation can be then be evaluated, which corresponds to the location where the tube wall is equal to the dew point temperature. The refrigerant onset bulk enthalpy can then be evaluated as a function of the pressure, bulk temperature, and bulk compositions:

$$h_{onset} = f(P,\ T_{b,onset},\ y_1,\ y_2...) \tag{5.2}$$

This onset enthalpy is then used as a reference in the evaluation of the quality. If the evaluated tube wall temperature at the inlet of the condenser (in the Equation 5.1) is lower than the dew point temperature, the superheated heat region begins at the inlet of the test section. In that case, the inlet temperature and bulk enthalpy should be used as the $T_{b,onset}$ and $h_{b,onset}$. The heat transfer analysis must then be repeated using the two-phase flow model (described in detail in the following section), instead of modeling it as single-phase flow.

To determine the end of condensation, Xiao and Hrnjak [108] introduced a semi-empirical expression for the location where the temperature in the subcooled film drops below the saturation temperature (Equation 2.16). However, as discussed in Section 4.4.5, the theoretical basis of this relationship is not clear. The difficulties in obtaining the heat flux to evaluate the Equation 2.16 in real practical situations were also discussed in Section 4.4.5. Furthermore, the enhancement in heat transfer in the subcooled region that Agarwal and Hrnjak [3] and Xiao and Hrnjak [108] described was not observed in the current study. Therefore, for the proposed model, two-phase effects in the subcooled region are assumed to be negligible, and the single-

phase heat transfer is assumed to be the dominant resistance. Furthermore, practical applications will usually operate with only a few degrees of subcooling, compared to tens of degrees (or more) of superheating. Thus, while the specific heat of the liquid phase is higher than the vapor, the subcooled region accounts for a smaller percentage of the total condensation load. In this study, on average, the subcooling load was 12% percent of the total heat load. Thus, a new parameter is introduced called the apparent quality:

$$x_{apparent} = \frac{h_b - h_l}{h_{onset} - h_l} \tag{5.3}$$

The $x_{apparent}$ uses the liquid saturation enthalpy as a reference for the end of condensation. Thus, the apparent quality is equal to 1 when condensation starts and equal to 0 when bulk enthalpy is equal to liquid saturation enthalpy. This simplifies the approach of Xiao and Hrnjak [108], by eliminating the need to determine a bulk enthalpy corresponding to the end of subcooled condensation.

5.2 Heat transfer in the superheated condensation region

Figure 5.1 shows a schematic of the heat transfer during superheated condensation. The total heat duty removed in this region is a combination primarily of the vapor sensible and latent components (Equation 5.4). In the superheated region, the liquid film is very thin, and thus, the contribution of liquid subcooling is neglected. The thermal resistances and the driving temperature differences associated with each of these modes of heat transfer are shown in Figure 5.1.

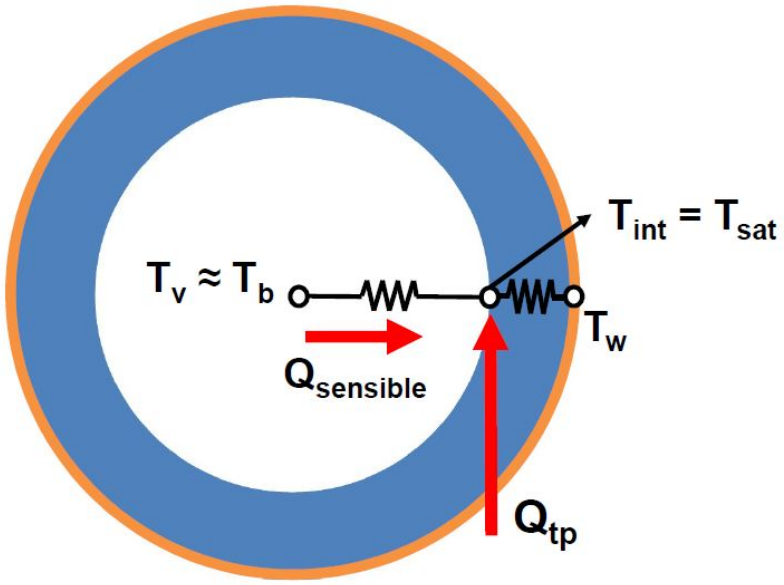

Figure 5.1: A schematic of heat transfer during superheated condensation.

$$\dot{q}''_{total} = \dot{q}''_{tp} + \dot{q}''_{v,sensible} \tag{5.4}$$

Recall that, the recent models have adopted two different techniques to evaluate the overall heat transfer coefficient associated with $\dot{q}''_{total}$ in Equation 5.4. Kondou and Hrnjak [64] and Agarwal and Hrnjak [3] defined the $\dot{q}''_{tp}$ as a product of the film heat transfer coefficient (evaluated using saturated two-phase correlations) and the temperature difference between the interface and the tube wall. Similarly, the sensible heat flux $\dot{q}''_{v,sensible}$, was evaluated by determining the single-phase vapor heat transfer coefficients and multiplying it by the temperature difference between the bulk fluid and the interface. The overall heat transfer coefficient was then evaluated by dividing the sum of $\dot{q}''_{tp}$ and $\dot{q}''_{v,sensible}$ by the temperature difference between the

refrigerant bulk temperature and the tube wall.

On the other hand, Xiao and Hrnjak [108] multiplied the film heat transfer coefficient with $(T_{sat} - T_{wall})/(T_b - T_{wall})$ to obtain the 'apparent' heat transfer coefficient associated with superheated condensation, which accounts for the resistance of the liquid film and the vapor core. The resulting expression was:

$$\alpha = \alpha_f \frac{T_{sat} - T_{wall}}{T_b - T_{wall}} \tag{5.5}$$

While the models of Hrnjak and co-workers are able to predict the superheated condensation data from the present study with a satisfactory agreement, they do not represent the actual physical phenomenon shown in the Figure 5.1. In their models, Kondou and Hrnjak [64], and Agarwal and Hrnjak [3] assume that the sensible and the latent heat transfer occur in parallel, instead of in series. Xiao and Hrnjak [108] assumed that the sensible and latent heat fluxes pass through both the thermal resistors. However, it is critical to note that the latent component of the heat duty is introduced at the liquid-vapor interface i.e., condensation happens at the interface. Thus, the resistance of the liquid film is the sole resistance to the latent heat flux.

Therefore, the model proposed in this study draws from the fundamentals from the literature that are illustrated in Figure 5.1. The sensible heat flux during superheated condensation can be predicted as:

$$q''_{v,sensible} = \alpha_v (T_v - T_i) \tag{5.6}$$

Similarly, the total heat flux through the liquid condensate film to the inner tube

wall can be written in terms of the film heat transfer coefficient and the respective driving temperature difference:

$$q''_{total} = \alpha_{TP}(T_i - T_w) \tag{5.7}$$

For most practical condenser applications utilizing zeotropic mixtures, the interface temperature is not known as it is a function of the local coupled heat and mass transfer. Therefore, the expression for sensible heat flux (Equation 5.6) can be rearranged to solve for the interface temperature and substituted into the Equation 5.7:

$$q''_{total} = \alpha_{TP}(T_v - \frac{q''_{v,sensible}}{\alpha_v} - T_w)$$

$$q''_{total} + \alpha_{TP}\frac{q''_{v,sensible}}{\alpha_v} = \alpha_{TP}(T_v - T_w)$$

$$q''_{total}\left(1 + \frac{\alpha_{TP}}{\alpha_v}\frac{q''_{v,sensible}}{q''_{total}}\right) = \alpha_{TP}(T_v - T_w)$$

$$q''_{total}\left(\frac{1}{\alpha_{TP}} + \frac{1}{\alpha_v}\frac{q''_{v,sensible}}{q''_{total}}\right) = (T_v - T_w)$$

$$q''_{total} = \left[\frac{1}{\alpha_{TP}} + \frac{1}{\alpha_v}\frac{q''_{v,sensible}}{q''_{total}}\right]^{-1}(T_v - T_w) \tag{5.8}$$

It is interesting to note here that the overall effective resistance has a similar form

as the SBG correction. This is because the challenges associated with superheated condensation are similar in nature to the problem of additional sensible heat transfer during mixture condensation i.e., the heat transfer schematic for mixture condensation is similar to the schematic for superheated condensation shown in Figure 5.1 [45].

The expression in Equation 5.8 can be further simplified by substituting in the expression for $q''_{v,sensible}$ from Equation 5.6 and assuming that the interface temperature is equal to the dew point temperature. In reality, the interface temperature is somewhere in between the T_{dew} and T_{bubble} temperatures for phase change of zeotropic mixtures. For superheated condensation, which occurs at the initial stages of condensation, the interface temperature will be closer to the dew point temperature. Furthermore, this is a conservative assumption which may result in slightly conservative design. The resulting expression for the heat transfer coefficient in the superheated region is:

$$\alpha_{superheated} \approx \left[\frac{1}{\alpha_{TP}} + \frac{T_v - T_{dew}}{q''_{total}}\right]^{-1} \tag{5.9}$$

The α_{TP} is predicted from the Cavallini et al. [21] correlation, using the apparent quality as an input. The q''_{total} in the Equation 5.9 is the total heat duty transferred. During the design of condensers, this variable is either known or is solved iteratively.

5.3 Heat transfer in the saturated condensation region

For heat transfer in the saturated region, the dominant thermal resistance to the process is due to the liquid condensate film. Therefore, the overall heat transfer coefficients in this region are simply equal to the film heat transfer coefficient.

$$\alpha_{saturated} = \alpha_{TP} \tag{5.10}$$

Similar to the superheated region, the film heat transfer coefficient is evaluated using the Cavallini et al. [21] correlation. The apparent quality is used as an input for the Cavallini et al. [21] correlation, instead of the thermodynamic quality, to obtain information about the local flow morphology.

5.4 Heat transfer in the subcooled region

The results described in Section 4.4.3 indicate the heat transfer in the subcooled region for the refrigerants in this study are well predicted by the single-phase Gnielinski [46] correlation. Therefore, for the proposed model, the latent effects in the subcooled region are assumed to be negligible and the Gnielinski [46] correlation is recommended for predicting the heat transfer for turbulent flows. If the flow is laminar, an appropriate single-phase heat transfer correlation may be used instead.

$$\alpha_{subcooled} = \alpha_{l} \tag{5.11}$$

5.5 Evaluation of the model

The model discussed above was used to predict the heat transfer coefficients for all the experimental conditions investigated in this study. In these experiments, condensation is assumed to begin at the test section inlet since the inner wall temperature in the first segment is always at least 15 °C lower than the saturation temperature. Therefore, the refrigerant inlet enthalpy is assumed to be the onset enthalpy. Table A.2 in Appendix A shows the details of how the proposed models can be used to predict the heat transfer coefficients for a sample experimental condition from this study. The predicted values were then compared with the measured values to assess the predictive capability of the proposed model.

The resulting comparison in the superheated region is shown in Figure 5.2. The model is able to provide very accurate predictions, with a MAPE value equal to 8%. Recall (from Chapter 4) that among the models of Hrnjak and co-workers, the Xiao and Hrnjak [108] model with the SBG correction exhibited the best agreement with the measured data, with a MAPE equal to 16%. The current model was able to improve predictive capability by 50%. This is achieved without incorporating any empirical constants and therefore, the model is expected to translate well to superheated condensation of other mixtures as well.

Figure 5.3 shows all the 962 data points collected in this study compared against the predictions from the proposed model. These data are representative of superheated, saturated, and subcooled condensation. Overall, the model is able to predict the data quite well, with a MAPE equal to 12%.

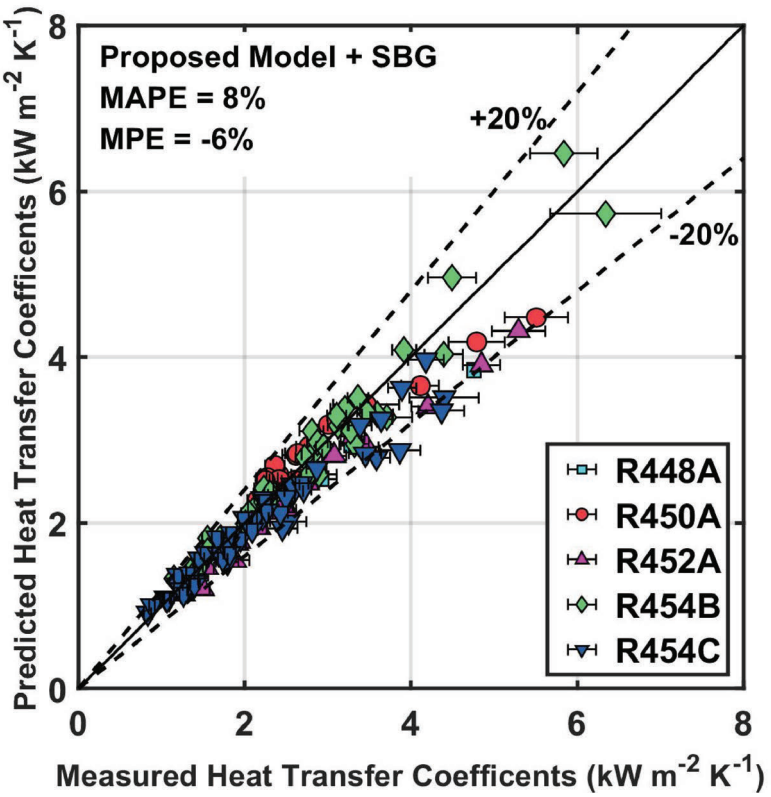

Figure 5.2: Predictive capability of the proposed model in the superheated region for R448A, R450A, R452A, R454B and R454C

5.5.1 Parametric evaluation of model

In addition to predicting the measured data accurately, a condensation heat transfer model should also provide an accurate representation of the phenomena. Therefore in this section, a parametric evaluation of the model was conducted for a range of conditions. The trends in the predictions were then analyzed to determine the effect of mass flux, diameter, fluid, and superheat. Table 5.1 lists of conditions that were investigated.

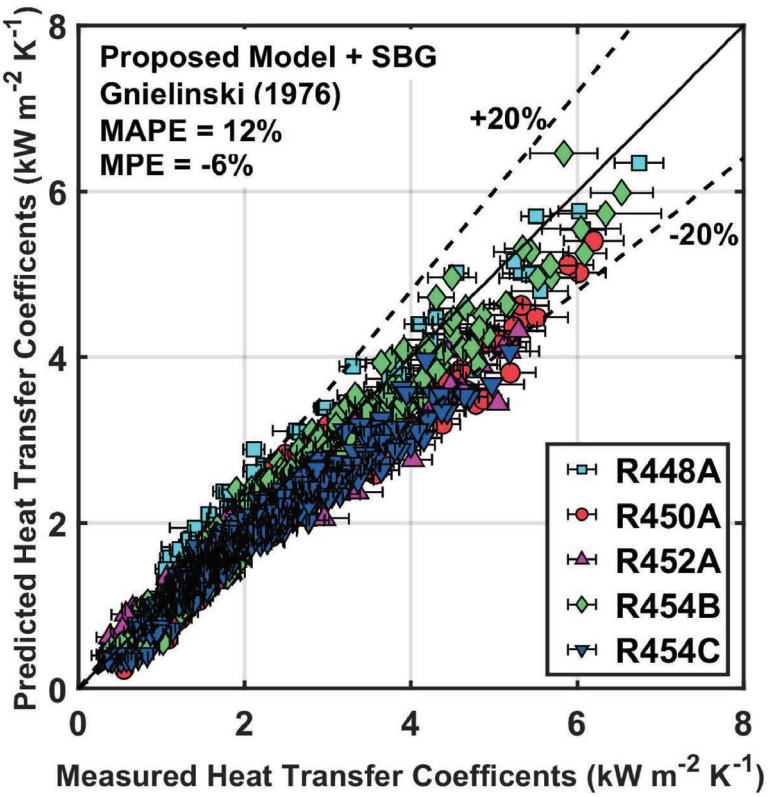

Figure 5.3: Predictive capability of the proposed model for complete condensation (superheated, saturated and subcooled) for R448A, R450A, R452A, R454B and R454C

Figures 5.4 and 5.5 show the effect of diameter and mass flux on the predicted heat transfer coefficient for condensing R454C with a 10 °C superheat. The heat transfer coefficient increases with increasing mass fluxes and decreasing tube diameters. The x-axis in Figures 5.4 and 5.5 show the apparent quality. In the saturated region, the heat transfer coefficients increase with the apparent quality, while the opposite is observed in the superheated condensation region. A discontinuity in the heat transfer coefficient is not observed during the transition from superheated to

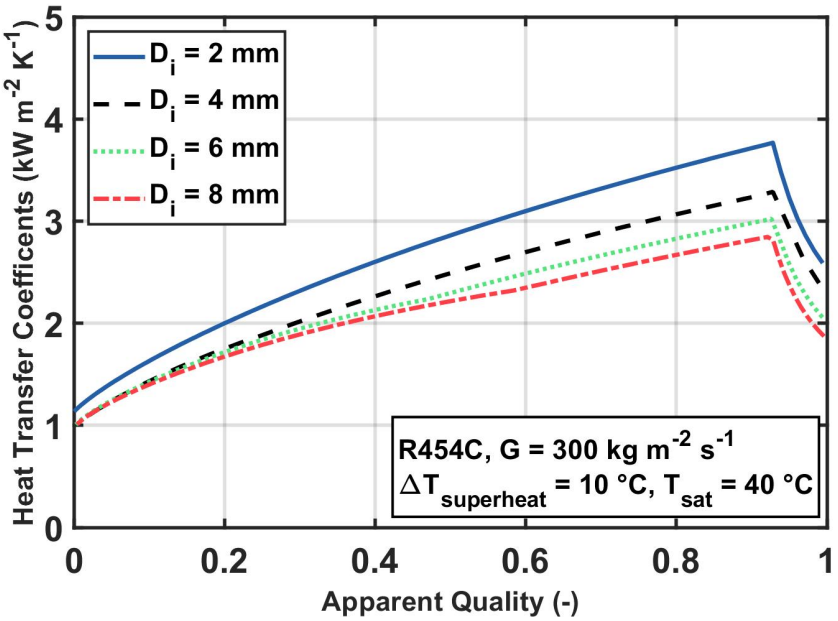

Figure 5.4: Effect of tube diameter for R454C

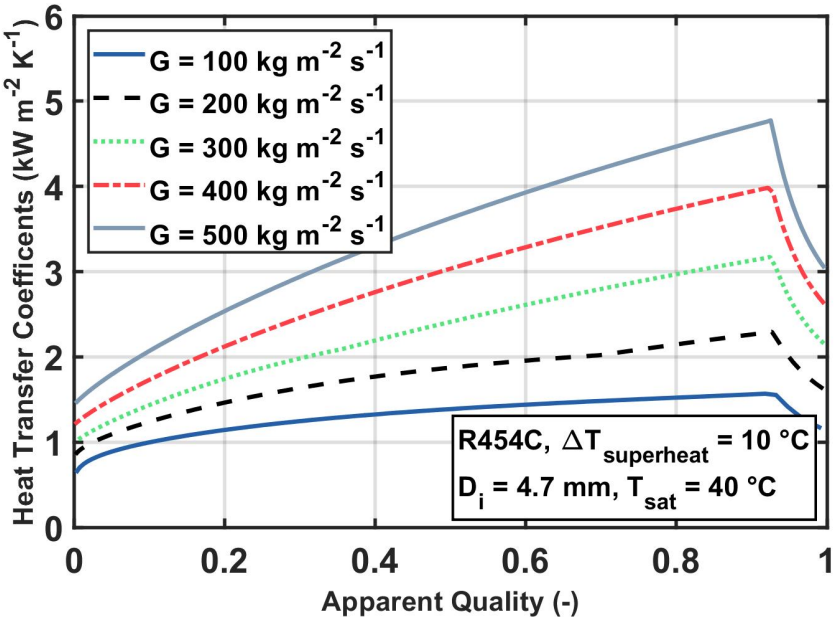

Figure 5.5: Effect of mass flux for R454C

Table 5.1 Conditions for the parametric evaluation of the model

Parameter Investigated	**Fluid**	**Diameter**	**Mass flux**	**Superheat**
	(-)	(mm)	(kg m^{-2} s^{-1})	(°C)
Diameter	R454C	2, 4, 6, 8	300	10
Mass flux	R454C	4.7	100, 200, 300, 400, 500	10
Superheat	R454C	4.7	300	5, 10, 15, 20, 25
Fluid	R1234yf, R1234ze(E), R448A, R450A, R452A, R454B, R454C, R455A	4.7	300	10

saturated condensation.

Figure 5.6 shows a comparison between heat transfer coefficients for different fluids. These include the mixtures investigated in the current study, as well as a high-temperature glide mixture, R455A ($\Delta T_{glide} = 10.5\,°C$). Additionally, predictions for pure HFO refrigerants, R1234yf, and R1234ze(E) are also included.

Finally, the effect of inlet superheat on the heat transfer coefficient and the apparent quality is shown in Figure 5.7. As expected, the superheated condensation effects become more pronounced with an increase in superheating. For the plot corresponding to 0 °C superheat, the superheated region does not exist and the apparent quality is equal to the thermodynamic quality. For flows with a comparatively lower superheat, the heat transfer coefficients are relatively similar in nature to those from a traditional two-phase model. However, this difference is more significant for the plot corresponding to 25 °C superheat. Specifically, the heat transfer coefficient for

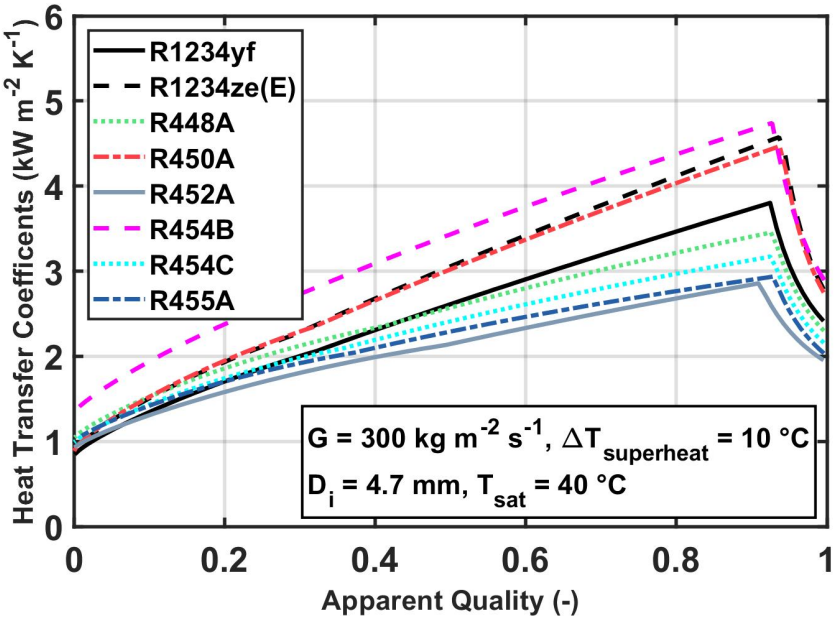

Figure 5.6: Predicted heat transfer coefficients for various fluids

25 °C superheat at a apparent quality equal to one is 58% lower than that for 0 °C superheat. Physically, this makes sense because the sensible thermal resistance is a function of the inlet superheating and is the dominant resistance for the process. Therefore, it limits the process despite the lower film condensation resistance at higher qualities.

In addition, Figure 5.7b shows that the apparent quality at the inlet of the saturated region (i.e, where bulk enthalpy is equal to vapor saturation enthalpy) is lowest in the plot for 25 °C superheat. This results in a 7% lower heat transfer coefficient at the inlet of the saturated condensation region, due to the greater volume of condensed liquid from the superheated region. Thus, this model provides a more accurate representation of the phenomenon compared to the earlier model of Hrnjak

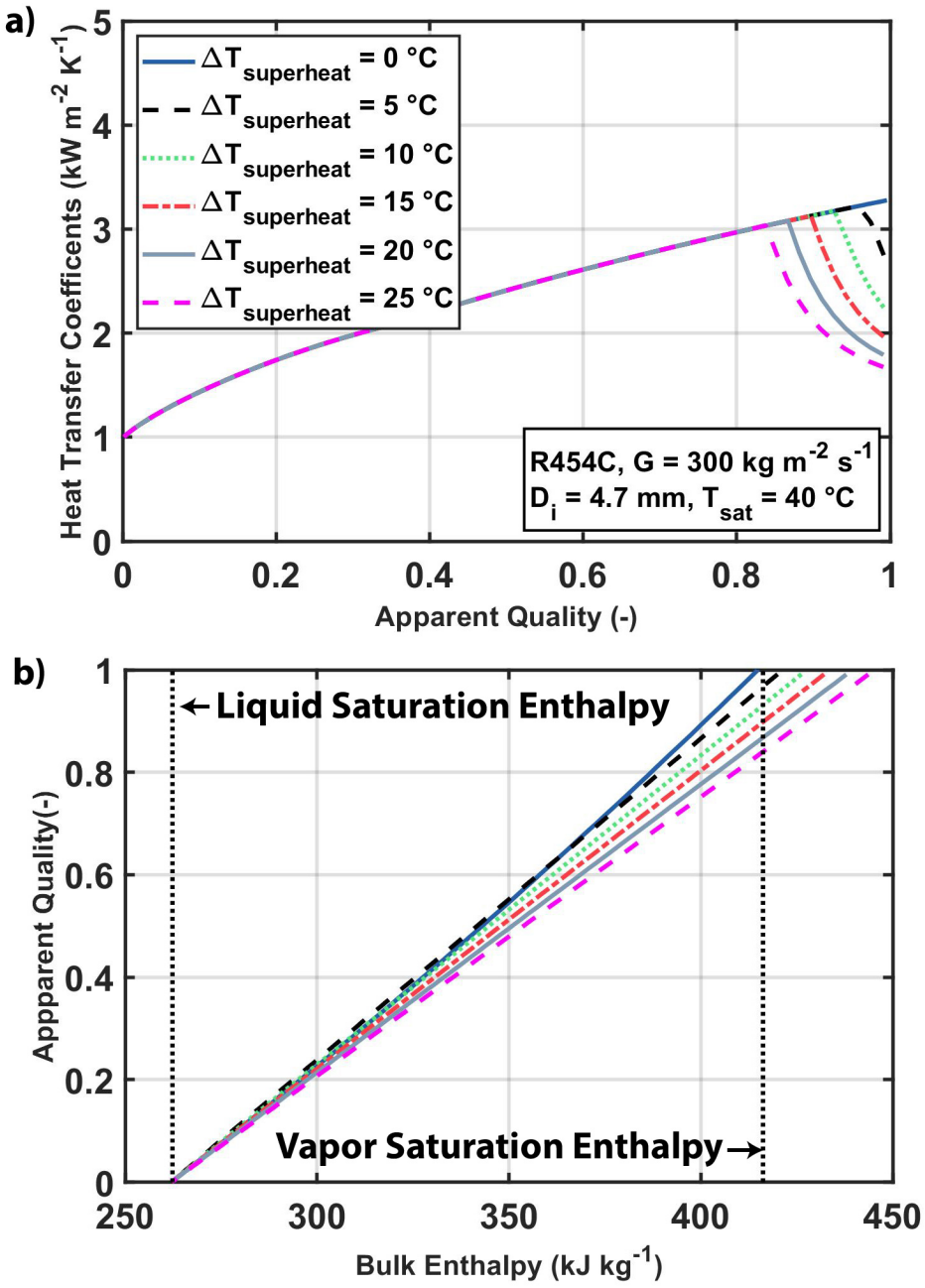

Figure 5.7: Effect of inlet superheat for R454C on a) heat transfer coefficients b) apparent quality

and co-workers Kondou and Hrnjak [64], Agarwal and Hrnjak [3], which assume that the quality is always the thermodynamic quality in the saturated region.

5.6 Impact of the model

It is clear from the earlier discussion that the heat transfer coefficients in the superheated region are not accurately predicted by the single-phase heat transfer correlations. In the current study, a new model was proposed which accurately models the underlying heat transfer phenomenon. Being able to accurately predict the heat transfer in this region offers an opportunity to design compact heat exchangers. This is demonstrated in this section by conducting design of a condenser. For the heat transfer in the condenser, two different approaches were tested: 1) the traditional approach which neglects the latent effects in the superheated and subcooled region, and 2) the non-equilibrium approach which predicts the heat transfer in the superheated and saturated regions using the proposed model. For both the approaches, the mixture degradation for low GWP zeotropic refrigerants was accounted for using the SBG correction. The resulting heat transfer areas corresponding to the two different approaches are then compared.

The system under consideration is a commercial refrigeration system with a 1055 kW (300 RT) cooling capacity. Currently, a majority of the commercial refrigeration systems utilize R404A as the working fluids. Some of the proposed low GWP replacements are R448A, R452A, and R454C. It is insightful to compare the performance of the three low GWP refrigerants with each other and with R404A. Therefore, the

analysis in this section was conducted for all four refrigerants.

The thermodynamic state points in the vapor compression cycle were selected to represent realistic operating conditions for these types of refrigeration systems. The refrigerant evaporates and condenses at 0 °C and 40 °C, respectively, with the ambient temperature equal to 25 °C. The refrigerant enters the condenser with a 10 °C superheat and leaves the condenser with a 5 °C subcooling. Table 4.10 shows a comparison of the thermophysical properties of all four refrigerants at $T_{sat,avg} = 40\,°C$, from REFPROP 10[70]. The latent heats of vaporization (h_{fv}) of the four refrigerants differ from each other, which would result in different mass flow rates in vapor compression systems utilizing these fluids. Therefore, the required flow rate for each refrigerant was evaluated by dividing the required cooling load (1055 kW) by the latent heat of vaporization at the evaporator temperature (0 °C).

For the condenser geometry, an A-frame air-cooled condenser (ACC) design was selected. A schematic of the ACC is shown in Figure 5.8. The ACC is cooled by air convection from an electrically driven fan. The size and geometry of the fins and tubes are informed by the investigation of Kays and London [61], who collected experimental data for air-cooled heat exchangers. The air-side heat transfer coefficient was evaluated to be 52 W m^{-2} K^{-1} [61], by assuming a constant air face velocity equal to 1 m s^{-1}.

For the tubes in the ACC, the heat transfer was further modeled by dividing the tubes further into 25 segments. Representative thermal resistance networks were set

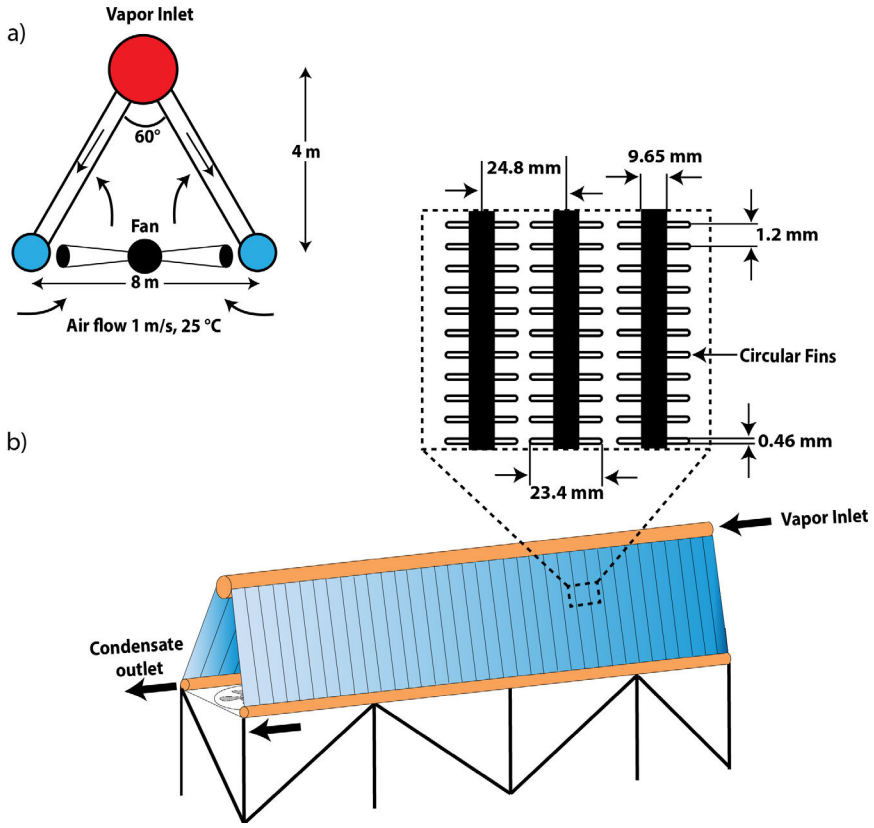

Figure 5.8: Schematic of the a) flow configuration in an A-frame ACC b) ACC system with tube geometries

up for each segment:

$$R_{total} = R_{air} + R_{conduction} + R_{refrigerant}$$

$$R_{total} = \frac{1}{h_{air} A_{so} \eta_{overall}} + \frac{ln\left(\frac{d_o}{d_i}\right)}{2\pi l k_{tube}} + \frac{1}{h_{refrigerant} A_{si}} \tag{5.12}$$

where $R_{air}, R_{conduction}$ and $R_{refrigerant}$ are the thermal resistances due to air-side convection across the finned surface, conduction through the tube and refrigerant

side convection, respectively.

The number of tubes, and consequently the refrigerant flow rate in each tube, was varied until the subcooling at the outlet was equal to 5 °C. The total refrigerant-side heat transfer area was then evaluated for each refrigerant and each approach. The results are shown in Figure 5.9. The application of the non-equilibrium model leads to 5% to 8% reduction in the heat exchanger area. This analysis clearly shows the advantage of the non-equilibrium approach. Note that for ACCs, the air-side resistance was the limiting resistance. For water-cooled condensers, this reduction in the area could be even more significant, as the condensation resistance becomes an increasingly significant percentage of the overall heat transfer resistance. Furthermore, the superheating load for this system was small, i.e. the superheating at the inlet was only 10 °C. For applications such as high-temperature heat pumps and heat pump water heaters, the refrigerant superheating from the compressor outlet may be as high as 35 °C [6]. For such systems, the understanding and implementation of superheated condensation models are even more critical as it would result in an even more significant reduction in condenser sizes.

The heat exchanger areas for R404A are 21% and 22% are lower than those for R454C for equilibrium and non-equilibrium approaches, respectively. R448A and R452A heat exchangers are smaller than those for R454C but bigger than those for R404A. For pure refrigerant condensation at equal mass fluxes, generally the refrigerants with the highest liquid thermal conductivity exhibit the highest heat transfer coefficients. However, this was not observed in our results for multi-component mixtures (Figure 5.9).

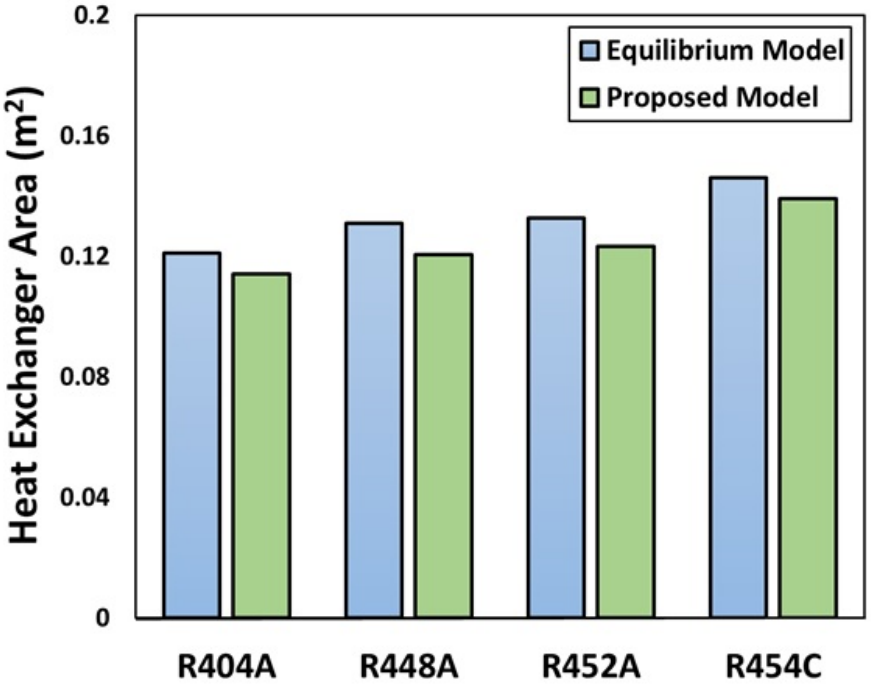

Figure 5.9: Refrigerant side heat exchanger area for R404A, R448A, R452A and R454C using the equilibrium and non-equilibrium models for constant cooling capacity (1055 kW)

There are two main reasons for the differences in the performance of these refrigerants. Firstly, R404A operates at a high mass flux, compared to other refrigerants, since it has the second-lowest latent heat of vaporization (Table 4.10). Consequently, the heat transfer coefficients of R404A are higher. Secondly, as discussed earlier, the degradation due to zeotropic condensation generally increases with the temperature glide. This explains why the R452A condenser is larger than that of R404A, despite having a higher liquid thermal conductivity and a slightly lower latent heat of vaporization. Furthermore, as zeotropic mixtures undergo condensation, the liquid/vapor interface temperature decreases, and subsequently, the driving temperature difference

to the process decreases, degrading heat transfer. In other words, the temperature difference between the interface and ambient at later stages of condensation (i.e. at lower qualities) for R454C is lower than that for R404A. This results in lower heat transfer rates for higher temperature glide mixtures. Thus, while R454C and R448A have a higher the latent heat capacity and a higher liquid thermal conductivity compared to R404A, the degradation due to heat zeotropic condensation is significant and must be considered during the design of next-generation condenser.

Chapter 6: Conclusions and Recommendations

6.1 Summary of the research scope

As international mandates continue to phase out refrigerants due to their environmental impact, near-azeotropic and zeotropic mixtures of HFCs and HFOs have emerged as potential replacements for conventional pure HFC refrigerants in the HVAC&R industry. While there have been several experimental and thermodynamic modeling studies focusing on the full system-level performance of these refrigerants, the research on their phase change heat transfer, specifically condensation, is limited. This information is critical for accurately designing next-generation condensers utilizing these fluids.

Furthermore, zeotropic mixtures are being proposed as working fluids in applications such as high-temperature heat pumps. For these applications, the superheating heat load at the condenser inlet is relatively higher compared to the traditional vapor compression systems. This leads to an increased contribution from superheated and subcooled condensation effects. These effects have traditionally been assumed to be negligible during condenser modeling, and these phenomenon have been relatively unaddressed in the literature. However, accurately predicting these phenomena opens up the possibility of minimizing the corresponding heat exchanger areas in these regions, and consequently designing more compact heat exchangers.

Therefore, the overarching goal of this study was to fill these gaps in the literature

by developing a better understanding of the zeotropic condensation phenomena in the superheated and subcooled condensation regions, along with the traditionally defined saturated region. Furthermore, this research was undertaken with the goal of providing HVAC&R designers with a modeling framework for predicting heat transfer in all three condensation regions.

6.2 Conclusions

Heat transfer and pressure drop measurements during in-tube condensation of five different low GWP refrigerants (R448A, R450A, R452A, R454B and R454C) were collected. These refrigerants are zeotropic mixtures, with temperature glides ranging from 0.6 °C to 6.3 °C. Condensation data were obtained in a 4.7 mm tube at a range of saturation conditions ($T_{sat,avg}$ = 40 – 60 °C) and at mass fluxes ranging from 100 kg m^{-2} s^{-1} to 500 kg m^{-2} s^{-1}.

An experimental facility with a 1.6 m long test section was designed and built to investigate the condensation heat transfer data these refrigerants. The test section is a tube-in-tube heat exchanger with the refrigerant flowing in the inner copper tube. The refrigerant is cooled by water counter-flowing in the tubing annulus. The test section is further divided into seven fully instrumented sub-segments to measure the quasi-local heat transfer coefficients along the length. The refrigerant enters the test section as a superheated vapor, completely completed condenses, and leaves as a subcooled fluid. This test section configuration allows for the investigation of superheated and subcooled condensation of refrigerant mixtures, in addition to the

traditionally defined saturated region.

The measured heat transfer data in the saturated region were in agreement with the general understanding of condensation behavior from the literature. The local heat transfer coefficients increase with mass flux and thermodynamic quality and decrease with saturation pressure. The average uncertainty in the measured heat transfer coefficients was 8%. The data for all five refrigerants were best predicted by the Cavallini et al. [21] correlation, after accounting for the mixture effects using the Silver [96], Bell and Ghaly [12] correction. The corresponding MAPE and MPE values were equal to 8% and 4% for the 704 saturated data points in this study. The correlations of Thome et al. [101], Del Col et al. [29] and Shah [91] were also able to sufficiently predict the data, with MAPE values lower than 15% after the mixture effects were accounted for. Thus, it was concluded that the non-equilibrium framework of Colburn and Drew [26] was not required for these mixtures. In addition, a comparison of the heat transfer and pressure drop of the new HFC/HFO mixtures against their HFC predecessors indicates that the low GWP mixtures may be considered as viable substitutes from a heat and momentum transport perspective.

In addition to the traditionally defined saturated region, heat transfer coefficients were also measured in the superheated condensation and subcooled regions. The measured data in these regions were compared to the previous models from the literature that had been developed for pure fluids. The resulting comparison indicates that the SBG correction is necessary to accurately capture the mixture effects in the superheated region. The superheated heat transfer coefficients were best predicted by the Xiao and Hrnjak [108] model with the SBG correction (MAPE = 16%).

However, the enhancement due to the latent effects in the subcooled region was not observed and the heat transfer coefficients in this region were accurately predicted by the single-phase Gnielinski [46] correlation (MAPE = 18%). Overall, only the model of Kondou and Hrnjak [64] was accurately able to predict the complete condensation (superheated, saturated, and subcooled) of refrigerant mixtures in this study (MAPE = 11%).

One of the reasons that the Kondou and Hrnjak [64] model performed so well was that they suggested using the Cavallini et al. [21] correlation in the saturated region, which was shown to predict the data in this study well. However, their model in the superheated region relies on simplifying assumptions that do not represent the actual heat transfer mechanisms. Therefore, a new condensation model was developed by considering the sensible and latent loads, and the evolution of the liquid and vapor mass fractions in the superheated region. The model provides predictions in the superheated and saturated regions, and the Gnielinski [46] correlation was recommended for predictions in the subcooled region. The model significantly improved the predictions in the superheated region (MAPE = 8%), without incorporating any empirical constants. In addition, the model is also able to predict the heat transfer for complete condensation with good accuracy (MAPE = 12%).

Being able to accurately predict the heat transfer in the superheated condensation region offers an opportunity to design compact condensers. To further illustrate this, an air-cooled condenser for a commercial refrigeration system, with a nominal cooling capacity equal to 1055 kW, was designed. This analysis was conducted for R404A, and three of its low GWP replacements (R448A, R450A, and R452A). The refrigerant

heat transfer was predicting using both, 1) the conventional approach which assumes single-phase vapor flow in the superheated region, and 2) the proposed model. The superheated at the condenser inlet was 10 °C. For all cases, the operating conditions were kept the same and the resulting heat exchangers areas were compared. The areas evaluated using the proposed model were 5% to 8% smaller. For liquid-cooled condensers and condensers with a higher inlet superheat (e.g. for high-temperature heat pumps), this difference will be even more significant.

Finally, while not the primary objective of this study, the frictional pressure drop for complete condensation was measured for the different refrigerants. On average, the two-phase frictional pressure drop was 79% of the measured value, with the average uncertainty in the calculated frictional pressure drop equal to 17%. The frictional pressure drop was compared to various pressure drop correlations from the literature. Overall, the Cavallini et al. [19] pressure drop correlation was able to predict the low GWP refrigerant data the best.

6.3 Contributions

This work will greatly facilitate the design of next-generation condensers for a wide range of applications and more broadly, aid in the adoption of low global warming potential technology. All the measured and calculated variables from this study have been made publicly available. This will aid future researchers in their investigations of single- and multi-component non-equilibrium condensation and guide the development of heat transfer models on the topic. These databases can be accessed using

the following links:

1. R450A[57, 58] – doi.org/10.6084/m9.figshare.7611674.v1
2. R448A and R452A[59, 60] – doi.org/10.6084/m9.figshare.10024739.v2
3. R454B [56] – doi.org/10.6084/m9.figshare.12921407
4. R454C [54] – doi.org/10.6084/m9.figshare.12235454.v1
5. R1233zd(E) [55, 53] – doi.org/10.6084/m9.figshare.11608359.v1

In addition to the public condensation database, a new heat transfer model was introduced, which incorporates the effects of superheated condensation. The implementation procedure for this model is much simpler than some of the earlier models on the topic. Thus, it is much more accessible to engineers and designers in the HVAC&R industry. Furthermore, the model will allow for the design of more compact condensers, which will require comparatively fewer resources to manufacture and have a smaller footprint.

6.4 Recommendations for future work

The current study was among the first to address superheated condensation of zeotropic refrigerant mixtures. During this research, we identified several relevant topics that can be expanded upon to further advance this field. A list of these topics is presented below.

- With the current experimental methodology, the investigation of heat transfer was prioritized. This is why the pressure taps along the length of the test section were not included, as they may disrupt the flow. Now that the heat transfer is better understood, an investigation of local two-phase frictional pressure drop in the superheated region is needed to understand how its effect on the condenser performance.

- The present investigation focused on heat transfer in the mini-channels. However, recently compact microchannel heat exchangers have become more prevalent in HVAC&R equipment due to the advances in manufacturing capabilities. Past investigations on saturated condensation have shown that the predictions methods developed for mini-channels translate poorly to heat transfer in micro-channel, due to more pronounced effects of fluid surface tension. Additional investigation is required to understand the effects of superheated condensation in micro-channel condensers. Furthermore, this investigation should also be extended to non-circular geometries.

- A flow visualization study will aid in understanding the influence of local flow structures on the condensation in the superheated and subcooled regions. It will also help inform the development of new flow regime maps which account for superheated and subcooled condensation.

- The present investigation tested condensation inside smooth tubes. This investigation should be extended to condensation inside enhanced tubes.

- The refrigerants tested in this study were directly obtained from manufactures

and had never been reclaimed or mixed with lubricants. For practical applications based on the vapor compression cycle, a lubricant is mixed with the refrigerants for the safe operation of the compressor. While oil separators are used to remove the lubricant before the refrigerant enters the condenser, past investigations have confirmed the presence of a trace amount of lubricants in the condensers. Similarly, a common issue that degrades the performance of vapor compression systems is the presence of non-condensable gases in the refrigerant stream. Therefore, it is critical to further investigate the superheated condensation of these new low GWP mixtures in the presence of lubricant and non-condensable gases.

- The current study has confirmed that accurately modeling superheated condensation provides an opportunity to design compact condensers. The next step would be to implement a condenser based on the current methodology in an actual vapor compression system and investigate its effect on the system COP and energy consumption.

Bibliography

[1] G. Ackermann. Combined heat and mass transfer in the same field at high temperature and partial pressure differences. *VDI-Forschungshef*, 8:1–16, 1937.

[2] Hasan M.M. Afroz, Akio Miyara, and Koutaro Tsubaki. Heat transfer coefficients and pressure drops during in-tube condensation of CO2/DME mixture refrigerant. *International Journal of Refrigeration*, 31(8):1458–1466, 12 2008. doi: 10.1016/j.ijrefrig.2008.02.009.

[3] Rahul Agarwal and Pega Hrnjak. Effect of sensible heat, condensation in superheated and subcooled region incorporated in unified model for heat rejection in condensers in horizontal round smooth tubes. *Applied Thermal Engineering*, 71(1):378–388, 2014. doi: 10.1016/j.applthermaleng.2014.05.071.

[4] Rahul Agarwal and Pega Hrnjak. Condensation in two phase and desuperheating zone for R1234ze(E), R134a and R32 in horizontal smooth tubes. *International Journal of Refrigeration*, 50(1991):172–183, 2015. doi: 10.1016/j.ijrefrig.2014.10.015.

[5] Ulf C. Andresen, Srinivas Garimella, Biswajit Mitra, Yirong Jiang, and Brian M. Fronk. Pressure drop during near-critical-pressure condensation of refrigerant blends. *International Journal of Refrigeration*, 59:1–13, 2015. doi: 10.1016/j.ijrefrig.2015.07.016.

[6] Cordin Arpagaus, Frédéric Bless, Michael Uhlmann, Jürg Schiffmann, and Stefan S. Bertsch. High temperature heat pumps: Market overview, state of the art, research status, refrigerants, and application potentials. *Energy*, 152:985–1010, 6 2018. doi: 10.1016/j.energy.2018.03.166.

[7] ASHRAE. *2017 ASHRAE handbook: Fundamentals*. American Society of Heating, Refrigeration and Air-Conditioning Engineers, Atlanta, GA, 2017.

[8] Marco Azzolin, Arianna Berto, Stefano Bortolin, Lorenzo Moro, and Davide Del Col. Condensation of ternary low GWP zeotropic mixtures inside channels. *International Journal of Refrigeration*, 103:77–90, 2019. doi: 10.1016/j.ijrefrig.2019.03.021.

[9] Ovid Baker. Design of Pipelines for the Simultaneous Flow of Oil and Gas. In *Fall Meeting of the Petroleum Branch of AIME*, Dallas, Texas, 4 1953. Society of Petroleum Engineers. doi: 10.2118/323-G.

[10] Todd M. Bandhauer, Akhil Agarwal, and Srinivas Garimella. Measurement and Modeling of Condensation Heat Transfer Coefficients in Circular Microchannels. *Journal of Heat Transfer*, 128(10):1050, 2006. doi: 10.1115/1.2345427.

[11] C. J. Baroczy. A systematic correlation for two-phase pressure drop. In *Chemical Engineering Progress symposium series No. 64*, page 232–249, 1966.

[12] KJ Bell and MA Ghaly. An approximate generalized design method for multicomponent/partial condenser. *American Institute of Chemical Engineers Symposium Series*, 69:72–79, 1973.

[13] A. E. Bergles, J. G. Collier, J. M. Delhaye, G. F. Hewitt, and F. Mayinger. *Two-phase flow and heat transfer in the power and process industries.* McGraw Hill, 1st edition, 1981.

[14] G. Breber, J. W. Palen, and J. Taborek. Prediction of Horizontal Tubeside Condensation of Pure Components Using Flow Regime Criteria. *Journal of Heat Transfer*, 102(3):471–476, 8 1980. doi: 10.1115/1.3244325.

[15] Van P. Carey. *Liquid-Vapor Phase-Change Phenomena.* Taylor & Francis, 2 edition, 2007.

[16] A. Cavallini, G. Censi, D Del Col, L. Doretti, G. A. Longo, L. Rossetto, D. Del Col, L. Doretti, G. A. Longo, and L. Rossetto. Experimental investigation on condensation heat transfer and pressure drop of new HFC refrigerants (R134a, R125, R32, R410A, R236ea) in a horizontal smooth tube. *International Journal of Refrigeration*, 24(1):73–87, 2001. doi: 10.1016/S0140-7007(00)00070-0.

[17] A. Cavallini, G. Censi, D. Del Col, L. Doretti, G. A. Longo, and L. Rossetto. A tube-in-tube water/zeotropic mixture condenser: Design procedure against experimental data. *Experimental Thermal and Fluid Science*, 25(7):495–501, 2002. doi: 10.1016/S0894-1777(01)00107-8.

[18] A. Cavallini, G. Censi, D. Del Col, L. Doretti, G. A. Longo, L. Rossetto, and C. Zilio. Condensation inside and outside smooth and enhanced tubes -a review of recent research, 2003.

[19] A. Cavallini, D. Del Col, M. Matkovic, and L. Rossetto. Frictional pressure drop during vapour-liquid flow in minichannels: Modelling and experimental evaluation. *International Journal of Heat and Fluid Flow*, 30(1):131–139, 2 2009. doi: 10.1016/j.ijheatfluidflow.2008.09.003.

[20] Alberto Cavallini, Giuseppe Censi, Davide Del Col, Luca Doretti, Giovanni A. Longo, and Luisa Rossetto. Condensation of halogenated refrigerants inside smooth tubes. *HVAC and R Research*, 8(4):429–451, 2002. doi: 10.1080/10789669.2002.10391299.

[21] Alberto Cavallini, Davide Del Col, Luca Doretti, Marko Matkovic, Luisa Rossetto, Claudio Zilio, and Giuseppe Censi. Condensation in horizontal smooth tubes: A new heat transfer model for heat exchanger design. *Heat Transfer Engineering*, 27(8):31–38, 2006. doi: 10.1080/01457630600793970.

[22] D. Chisholm. A theoretical basis for the Lockhart-Martinelli correlation for two-phase flow. *International Journal of Heat and Mass Transfer*, 10(12): 1767–1778, 12 1967. doi: 10.1016/0017-9310(67)90047-6.

[23] D. Chisholm and A. D. K. Laird. Two-Phase Flow in Rough Tubes. *Trans. ASME*, 80(2):276–286, 1958.

[24] Stuart W. Churchill. Friction-Factor Equation Spans All Fluid-Flow Regimes. *Chemical Engineering (New York)*, 84(24):91–92, 1977. doi: 10.3929/ETHZ-A-004613195.

[25] Stuart W. Churchill. Comprehensive Correlating Equations for Heat, Mass and Momentum Transfer in Fully Developed Flow in Smooth Tubes. *Industrial & Engineering Chemistry Fundamentals*, 16(1):109–116, 2 1977. doi: 10.1021/i160061a021.

[26] A P Colburn and T B Drew. The condensation of mixed vapours. *American Institute of Chemical Engineers*, 33(2):197–215, 1937.

[27] Hugh W. Coleman and W. Glenn Steele. *Experimentation, Validation, and Uncertainty Analysis for Engineers*. John Wiley & Sons, Inc., Hoboken, NJ, USA, 7 2009. doi: 10.1002/9780470485682.

[28] Crane Co. *Flow of Fluids Through Valves, Fittings, and Pipe - Technical Paper No. 410M*. Vervante, New York, 1982.

[29] D. Del Col, A. Cavallini, and J. R. Thome. Condensation of Zeotropic Mixtures in Horizontal Tubes: New Simplified Heat Transfer Model Based on Flow Regimes. *Journal of Heat Transfer*, 127(3):221, 2005. doi: 10.1115/1.1857951.

[30] D. Del Col, D. Torresin, and A. Cavallini. Heat transfer and pressure drop during condensation of the low GWP refrigerant R1234yf. *International Journal of Refrigeration*, 33(7):1307–1318, 11 2010. doi: 10.1016/j.ijrefrig.2010.07.020.

[31] Davide Del Col, Alberto Bisetto, Matteo Bortolato, Daniele Torresin, and Luisa Rossetto. Experiments and updated model for two phase frictional pressure drop inside minichannels. *International Journal of Heat and Mass Transfer*, 67:326–337, 12 2013. doi: 10.1016/j.ijheatmasstransfer.2013.07.093.

[32] Davide Del Col, Marco Azzolin, Alberto Bisetto, and Stefano Bortolin. Frictional Pressure Drop during Two-Phase Flow of Pure Fluids and Mixtures in Small Diameter Channels. *International Journal of Chemical Reactor Engineering*, 13(4):493–502, 2015. doi: 10.1515/ijcre-2014-0180.

[33] Davide Del Col, Marco Azzolin, Stefano Bortolin, and Claudio Zilio. Two-phase pressure drop and condensation heat transfer of R32/R1234ze(E) non-azeotropic mixtures inside a single microchannel. *Science and Technology for the Built Environment*, 21(5):595–606, 2015. doi: 10.1080/23744731.2015.1047718.

[34] Davide Del Col, Matteo Bortolato, Marco Azzolin, and Stefano Bortolin. Condensation heat transfer and two-phase frictional pressure drop in a single minichannel with R1234ze(E) and other refrigerants. *International Journal of Refrigeration*, 50:87–103, 2015. doi: 10.1016/j.ijrefrig.2014.10.022.

[35] F.W. Dittus and L.M.K. Boelter. Heat transfer in automobile radiators of the tubular type. *International Communications in Heat and Mass Transfer*, 12 (1):3–22, 1 1985. doi: 10.1016/0735-1933(85)90003-X.

[36] M. K. Dobson and J. C. Chato. Condensation in Smooth Horizontal Tubes. *Journal of Heat Transfer*, 120(1):193, 1998. doi: 10.1115/1.2830043.

[37] J. El Hajal, J R Thome, and A Cavallini. Condensation in horizontal tubes, part 1: Two-phase flow pattern map. *International Journal of Heat and Mass Transfer*, 46(18):3349–3363, 2003. doi: 10.1016/S0017-9310(03)00139-X.

[38] European Parliment and the Council of the European Union. Directive 2006/40/EC of the European Parliament and of the Council of 17 may 2006 relating to emissions from air conditioning systems in motor vehicles and amending council directive 70/156/EC. *Official Journal of the European Union*, 161: 1–11, 2006.

[39] L. Friedel. Improved friction pressure drop correlations for horizontal and vertical two phase pipe flow. In *Proc. of European Two-Phase Flow Group Meet*, page Paper E2, Ispra, Italy, 1979.

[40] Brian M. Fronk. *Coupled heat and mass transfer during condensation of high-temperature-glide zeotropic mixtures in small diameter channels*. PhD thesis, Georgia Institute of Technology, 2014.

[41] Brian M. Fronk and Srinivas Garimella. In-tube condensation of zeotropic fluid mixtures: A review. *International Journal of Refrigeration*, 36(2):534–561, 3 2013. doi: 10.1016/j.ijrefrig.2012.11.030.

[42] Brian M. Fronk and Srinivas Garimella. Condensation of ammonia and high-temperature-glide zeotropic ammonia/water mixtures in minichannels – Part II: Heat transfer models. *International Journal of Heat and Mass Transfer*, 101:1357–1373, 2016. doi: 10.1016/j.ijheatmasstransfer.2016.05.048.

[43] Brian M. Fronk and Srinivas Garimella. Condensation of ammonia and high-temperature-glide ammonia/water zeotropic mixtures in minichannels – Part I: Measurements. *International Journal of Heat and Mass Transfer*, 101:1343–1356, 10 2016. doi: 10.1016/j.ijheatmasstransfer.2016.05.049.

[44] Brian M. Fronk and Srinivas Garimella. Condensation of carbon dioxide in microchannels. *International Journal of Heat and Mass Transfer*, 100:150–164, 2016. doi: 10.1016/j.ijheatmasstransfer.2016.03.083.

[45] Srinivas Garimella and Brian M. Fronk. *Encyclopedia of Two-Phase Heat Transfer and Flow I: Fundamentals and Methods – Volume 2: Condensation Heat Transfer*, volume 2. World Scientific, 10 2016. doi: 10.1142/9310-vol2.

[46] V. Gnielinski. New Equations for Heat and Mass Transfer in Turbulent Pipe and Channel Flow. *International Chemical Engineering*, 1976.

[47] E. Granryd. Heat transfer in flow evaporation (and condensation) of mixtures. Technical report, Oak Ridge National Laboratory, Oak Ridge, Tennessee, USA, 1989.

[48] Hidetaka Haraguchi, Shigeru Koyama, and Tetsu Fujii. Condensation of Refrigerants HCF C 22, HFC 134a and HCFC 123 in a Horizontal Smooth Tube. 1st Report, Proposals of Empirical Expressions for the Local Frictional Pressure Drop. *Transactions of the Japan Society of Mechanical Engineers Series B*, 60(574):2111–2116, 1994. doi: 10.1299/kikaib.60.2111.

[49] Hidetaka Haraguchi, Shigeru Koyama, and Tetsu Fujii. Condensation of Refrigerants HCFC 22, HFC 134a and HCFC 123 in a Horizontal Smooth Tube. 2nd Report, Proposals of Empirical Expressions for Local Heat Transfer Coefficient. *Transactions of the Japan Society of Mechanical Engineers Series B*, 60(574):2117–2124, 1994. doi: 10.1299/kikaib.60.2117.

[50] C. C. Heald. *Cameron Hydraulic Data*. Flowserve Corp., 19th editi edition, 2002.

[51] M Anowar Hossain, Yoji Onaka, and Akio Miyara. Experimental study on condensation heat transfer and pressure drop in horizontal smooth tube for R1234ze(E), R32 and R410A. *International Journal of Refrigeration*, 35(4): 927–938, 2012. doi: 10.1016/j.ijrefrig.2012.01.002.

[52] F. Illán-Gómez, A. López-Belchí, J R García-Cascales, and F Vera-García. Experimental two-phase heat transfer coefficient and frictional pressure drop inside mini-channels during condensation with R1234yf and R134a. *International Journal of Refrigeration*, 51:12–23, 2015. doi: 10.1016/j.ijrefrig.2014.11.014.

[53] Tabeel A. Jacob and Brian M. Fronk. Experimental Investigation of Low GWP Alternative R1233zd(E) for Use in Organic Rankine Cycle Condensers. In *Rankine 2020 - Advances in Cooling, Heating and Power Generation*, page (Accepted), Glasgow, 2020. doi: 10.18462/iir.rankine.2020.1122.

[54] Tabeel A. Jacob and Brian M. Fronk. In-tube condensation data of R454C in a horizontal 4.7 mm ID tube. *Figshare*, page Dataset, 2020. doi: 10.6084/m9.figshare.12235454.v1.

[55] Tabeel A. Jacob and Brian M. Fronk. In-tube condensation data of R1233zd(E) in a horizontal 4.7 mm ID tube. *figshare*, 2020. doi: 10.6084/m9.figshare.11608359.v1.

[56] Tabeel A. Jacob and Brian M. Fronk. In-tube condensation data of R454B in a horizontal 4.7 mm ID tube. *Figshare*, page Dataset, 2020. doi: 10.6084/m9.figshare.12921407.

[57] Tabeel A. Jacob, Ethan P. Matty, and Brian M. Fronk. In-tube condensation data of R134a and R450A in a horizontal 4.7 mm ID tube, Figshare. *Figshare*, 2019. doi: 10.6084/m9.figshare.7611674.v1.

[58] Tabeel A. Jacob, Ethan P. Matty, and Brian M. Fronk. Experimental investigation of in-tube condensation of low GWP refrigerant R450A using a fiber optic distributed temperature sensor. *International Journal of Refrigeration*, 103:274–286, 7 2019. doi: 10.1016/j.ijrefrig.2019.04.021.

[59] Tabeel A. Jacob, Ethan P. Matty, and Brian M. Fronk. In-tube condensation data of R404A, R448A, and R452A in a horizontal 4.7 mm ID tube. *Figshare*, 2019. doi: 10.6084/m9.figshare.10024739.v1.

[60] Tabeel A. Jacob, Ethan P. Matty, and Brian M. Fronk. Comparison of R404A condensation heat transfer and pressure drop with low global warming potential replacement candidates R448A and R452A. *International Journal of Refrigeration*, 116:9–22, 8 2020. doi: 10.1016/j.ijrefrig.2020.03.014.

[61] William M. Kays and Alexander L. London. *Compact Heat Exchangers*. McGraw Hill, New York, 3rd ed. edition, 1984.

[62] Sung Min Kim and Issam Mudawar. Universal approach to predicting heat transfer coefficient for condensing mini/micro-channel flow. *International Journal of Heat and Mass Transfer*, 56(1-2):238–250, 2013. doi: 10.1016/j.ijheatmasstransfer.2012.09.032.

[63] SJ Kline and FA McClintock. Describing uncertainties in single-sample experiments. *Mechanical Engineering*, 75:3–8, 1953.

[64] Chieko Kondou and Pega Hrnjak. Condensation from superheated vapor flow of R744 and R410A at subcritical pressures in a horizontal smooth tube. *International Journal of Heat and Mass Transfer*, 55(11-12):2779–2791, 2012. doi: 10.1016/j.ijheatmasstransfer.2012.01.030.

[65] Chieko Kondou, Fumiya Mishima, and Shigeru Koyama. Condensation and evaporation of R32/R1234ze(E) and R744/R32/R1234ze(E) flow in horizontal microfin tubes. *Science and Technology for the Built Environment*, 21(5):564–577, 2015. doi: 10.1080/23744731.2015.1023163.

[66] S Koyama. Condensation Heat Transfer of Binary Mixture Refrigerants of R22 and R114 Inside a Horizontal Tube. *International Journal of Refrigeration*, 13 (4):256–263, 1988. doi: 10.1016/0140-7007(90)90038-X.

[67] Shigeru Koyama, Ken Kuwahara, Kouichi Nakashita, and Ken Yamamoto. An experimental study on condensation of refrigerant R134a in multi-port extruded tube. *International Journal of Refrigeration*, 26(4):425–432, 2003. doi: 10.1016/S0140-7007(02)00155-X.

[68] S.Z. Kuhn, V.E. Schrock, and P.F. Peterson. An investigation of condensation from steam–gas mixtures flowing downward inside a vertical tube. *Nuclear Engineering and Design*, 177(1-3):53–69, 12 1997. doi: 10.1016/S0029-5493(97)00185-4.

[69] Bruce E. Larock, Roland E. Jeppson, and Gary Z. Watters. *Hydraulics of Pipeline Systems*. CRC Press, 1st editio edition, 1999.

[70] Eric W. Lemmon, Ian H Bell, Marcia L Huber, and Mark O Mclinden. NIST Standard Reference Database 23: Reference Fluid Thermodynamic and Transport Properties-REFPROP, Version 10, 2018.

[71] Kuo-Shing Liang and Peter-Griffith. Experimental and analytical study of direct contact condensation of steam in water. *Nuclear Engineering and Design*, 147(3):425–435, 4 1994. doi: 10.1016/0029-5493(94)90225-9.

[72] R W Lockhart and R C Martinelli. Proposed correlation of data for isothermal two-phase two component flow in pipes. *Chemical Engineering Progress*, 45(1):39–48, 1949.

[73] Malcolm Macdonald and Srinivas Garimella. Modeling of In-Tube Condensation of Zeotropic Mixtures. *Journal of Heat Transfer*, 138(9):091502, 9 2016. doi: 10.1115/1.4033352.

[74] J.M. Mandhane, G.A. Gregory, and K. Aziz. A flow pattern map for gas—liquid flow in horizontal pipes. *International Journal of Multiphase Flow*, 1(4):537–553, 10 1974. doi: 10.1016/0301-9322(74)90006-8.

[75] R C Martinelli and D B Nelson. Prediction of pressure drop during forced circulation boiling of water. *Trans. ASME*, 70:695–702, 1948.

[76] Marko Matkovic, Alberto Cavallini, Davide Del Col, and Luisa Rossetto. Experimental study on condensation heat transfer inside a single circular minichannel. *International Journal of Heat and Mass Transfer*, 52(9-10):2311–2323, 2009. doi: 10.1016/j.ijheatmasstransfer.2008.11.013.

[77] Melissa Meyer and Pega Hrnjak. Flow regimes during condensation in superheated zone. *International Journal of Refrigeration*, 84:336–343, 12 2017. doi: 10.1016/j.ijrefrig.2017.04.010.

[78] K. Mishima and T. Hibiki. Some characteristics of air-water two-phase flow in small diameter vertical tubes. *International Journal of Multiphase Flow*, 22 (4):703–712, 8 1996. doi: 10.1016/0301-9322(96)00010-9.

[79] Akio Miyara, Ken Kuwahara, and Shigeru Koyama. Correlation of Frictional Pressure Loss of Two-Phase Flow Including Effects of Tube Diameter and Mass Velocity. *The Proceedings of Conference of Kyushu Branch*, 2004.57:117–118, 2004. doi: 10.1299/jsmekyushu.2004.57.117.

[80] Adrián Mota-Babiloni, Joaquín Navarro-Esbrí, Ángel Barragán-Cervera, Francisco Molés, and Bernardo Peris. Experimental study of an R1234ze(E)/R134a mixture (R450A) as R134a replacement. *International Journal of Refrigeration*, 51:52–58, 2015. doi: 10.1016/j.ijrefrig.2014.12.010.

[81] Adrián Mota-Babiloni, Joaquín Navarro-Esbrí, Bernardo Peris, Francisco Molés, and Gumersindo Verdú. Experimental evaluation of R448A as R404A lower-GWP alternative in refrigeration systems. *Energy Conversion and Management*, 105:756–762, 11 2015. doi: 10.1016/j.enconman.2015.08.034.

[82] Adrián Mota-Babiloni, Jorge Haro-Ortuño, Joaquín Navarro-Esbrí, and Ángel Barragán-Cervera. Experimental drop-in replacement of R404A for warm countries using the low GWP mixtures R454C and R455A. *International Journal of Refrigeration*, 2018. doi: 10.1016/j.ijrefrig.2018.05.018.

[83] H. Müller-Steinhagen and K. Heck. A simple friction pressure drop correlation for two-phase flow in pipes. *Chemical Engineering and Processing: Process Intensification*, 20(6):297–308, 11 1986. doi: 10.1016/0255-2701(86)80008-3.

[84] W. Nusselt. Die Oberflächenkondensation des Wasserdampfes. *Zeitschrift des Vereins Deutscher Ingenieure*, 60:541–546, 1916.

[85] J E Park, F Vakili-Farahani, L Consolini, and J R Thome. Experimental study on condensation heat transfer in vertical minichannels for new refrigerant R1234ze(E) versus R134a and R236fa. *Experimental Thermal and Fluid Science*, 35(3):442–454, 2011. doi: 10.1016/j.expthermflusci.2010.11.006.

[86] BC Price and KJ Bell. Design of binary vapor condensers using the Colburn-Drew equations, 1973.

[87] S.A. Klein. Engineering Equation Solver (EES), Version 10. *F-Chart Software*, 2019.

[88] M Schulz and D Kourkoulas. Regulation (EU) No 517/2014 of the European Parliament and of the Council of 16 April 2014 on fluorinated greenhouse gases and repealing Regulation (EC) No 842/2006. *Official Journal of the European Union*, 2014.

[89] M. Mohammed Shah. An Improved and Extended General Correlation for Heat Transfer During Condensation in Plain Tubes. *HVAC&R Research*, 15 (5):889–913, 9 2009. doi: 10.1080/10789669.2009.10390871.

[90] Mirza M. Shah. A general correlation for heat transfer during film condensation inside pipes. *International Journal of Heat and Mass Transfer*, 22(4):547–556, 1979. doi: 10.1016/0017-9310(79)90058-9.

[91] Mirza M. Shah. Comprehensive correlations for heat transfer during condensation in conventional and mini/micro channels in all orientations. *International Journal of Refrigeration*, 67:22–41, 7 2016. doi: 10.1016/j.ijrefrig.2016.03.014.

[92] Mirza Mohammed Shah. General correlation for heat transfer during condensation in plain tubes: Further development and verification. In *ASHRAE Transactions*, pages 13–001, 2013.

[93] D. W. Shao and E. Granryd. Experimental and theoretical study on flow condensation with non-azeotropic refrigerant mixtures of R32/R134a. *International Journal of Refrigeration*, 21(3):230–246, 1998. doi: 10.1016/S0140-7007(98)00015-2.

[94] Jeong Seob Shin and Moo Hwan Kim. An experimental study of condensation heat transfer inside a mini-channel with a new measurement technique. *International Journal of Multiphase Flow*, 30(3):311–325, 2004. doi: 10.1016/j.ijmultiphaseflow.2003.11.012.

[95] Mansoor Siddique, Michael W. Golay, and Mujid S. Kazimi. Local Heat Transfer Coefficients for Forced-Convection Condensation of Steam in a Vertical Tube in the Presence of a Noncondensable Gas. *Nuclear Technology*, 102(3): 386–402, 6 1993. doi: 10.13182/NT93-A17037.

[96] L. Silver. Gas cooling with aqueous condensation. *Transactions of the Institution of Chemical Engineers*, 25:30–42, 1947.

[97] F. J. Smit, J. R. Thome, and J. P. Meyer. Heat Transfer Coefficients During Condensation of the Zeotropic Refrigerant Mixture HCFC-22/HCFC-142b. *Journal of Heat Transfer*, 124(6):1137, 2002. doi: 10.1115/1.1484108.

[98] M. Soliman, J. R. Schuster, and P. J. Berenson. A General Heat Transfer Correlation for Annular Flow Condensation. *Journal of Heat Transfer*, 90(2): 267–274, 5 1968. doi: 10.1115/1.3597497.

[99] Yemada Taitel and A. E. Dukler. A model for predicting flow regime transitions in horizontal and near horizontal gas-liquid flow. *AIChE Journal*, 22(1):47–55, 1976. doi: 10.1002/aic.690220105.

[100] T. N. Tandon, H. K. Varma, and C. P. Gupta. Generalized correlation for condensation of binary mixtures inside a horizontal tube. *International Journal of Refrigeration*, 9(3):134–136, 1986. doi: 10.1016/0140-7007(86)90062-9.

[101] J. R. Thome, J. El Hajal, and A. Cavallini. Condensation in horizontal tubes, part 2: New heat transfer model based on flow regimes. *International Journal of Heat and Mass Transfer*, 46(18):3365–3387, 2003. doi: 10.1016/S0017-9310(03)00140-6.

[102] Michael A. Vanderputten, Tabeel A. Jacob, Maria Sattar, Nouman Ali, and Brian M. Fronk. Two-phase flow regimes of condensing R-134a at low mass flux in rectangular microchannels. *International Journal of Refrigeration*, 84: 92–103, 12 2017. doi: 10.1016/j.ijrefrig.2017.08.021.

[103] L Wang, C Dang, and E Hihara. Experimental and Theoretical Study on Condensation Heat Transfer of Nonazeotropic Refrigerant Mixtures R1234yf / R32 Inside a Horizontal Smooth Tube. In *International Refrigeration and Air Conditioning COnference*, page Paper 1308, 2012.

[104] R. L. Webb. Convective condensation of superheated vapor. *Journal of Heat Transfer*, 120(2):418–421, 1998. doi: 10.1115/1.2824266.

[105] Mao Yu Wen, Ching Yen Ho, and Jome Ming Hsieh. Condensation heat transfer and pressure drop characteristics of R-290 (propane), R-600 (butane), and a mixture of R-290/R-600 in the serpentine small-tube bank. *Applied Thermal Engineering*, 26(16):2045–2053, 2006. doi: 10.1016/j.applthermaleng.2005.10.001.

[106] Jiange Xiao. *Non-equilibrium effects on in-tube condensation from superheated vapor*. PhD thesis, University of Illinois at Urbana-Champaign, 2019.

[107] Jiange Xiao and Pega Hrnjak. Heat transfer and pressure drop of condensation from superheated vapor to subcooled liquid. *International Journal of Heat and Mass Transfer*, 103:1327–1334, 2016. doi: 10.1016/j.ijheatmasstransfer.2016.08.036.

[108] Jiange Xiao and Pega Hrnjak. A heat transfer model for condensation accounting for non-equilibrium effects. *International Journal of Heat and Mass Transfer*, 111:201–210, 2017. doi: 10.1016/j.ijheatmasstransfer.2017.03.019.

[109] Jiange Xiao and Pega Hrnjak. A new flow regime map and void fraction model based on the flow characterization of condensation. *International Journal of Heat and Mass Transfer*, 108:443–452, 2017. doi: 10.1016/j.ijheatmasstransfer.2016.11.104.

[110] Jiange Xiao and Pega Hrnjak. Flow regimes during condensation from superheated vapor. *International Journal of Heat and Mass Transfer*, 132:301–308, 2019. doi: 10.1016/j.ijheatmasstransfer.2018.12.016.

[111] Jiange Xiao and Pega Hrnjak. A flow regime map for condensation in macro and micro tubes with non-equilibrium effects taken into account. *International Journal of Heat and Mass Transfer*, 130:893–900, 2019. doi: 10.1016/j.ijheatmasstransfer.2018.10.081.

[112] S. M. Zivi. Estimation of Steady-State Steam Void-Fraction by Means of the Principle of Minimum Entropy Production. *Journal of Heat Transfer*, 86(2): 247–251, 5 1964. doi: 10.1115/1.3687113.

Nomenclature

Symbols

c_p	specific heat capacity	J $kg^{-1}K^{-1}$
D	diameter	m
G	mass flux	kg $m^{-2}s^{-1}$
h	specific enthalpy	kJ kg^{-1}
h_{lv}	latent heat of vaporization	kJ kg^{-1}
k	thermal conductivity	W m^{-1} K^{-1}
l	length of a segment	m
ln	natural logarithm	-
$\dot{m}$	mass flow rate	kg s^{-1}
P	pressure	kPa
ΔP	differential pressure drop	kPa
$\dot{Q}$	heat duty	kW
q''	heat flux	kW m^{-2}

T	temperature	°C
U	uncertainty	-
V	velocity	m s^{-1}
x	thermodynamic quality	-
$\tilde{x}$	molar concentration in liquid phase	-
y	bulk mass concentration	-
$\tilde{y}$	molar concentration in the vapor phase	-

Greek Letters

α	heat transfer coefficient	W m^{-2} K^{-1}
α_c	convective heat transfer coefficient	W m^{-2} K^{-1}
α_f	film heat transfer coefficient	W m^{-2} K^{-1}
β	experimental data that were within ± 20% of the predicted value	%
μ	dynamic viscosity	kg m^{-1} s^{-1}
ρ	density	kg m^{-3}
σ	surface tension	N m^{-1}

Subscripts

bubble bubble temperature

avg average

cond condensation

deceleration deceleration pressure gain

dew dew temperature

fric frictional pressure drop

i test section segment #

in inlet

inner inner diameter

int liquid/vapor interface

l liquid phase

measured experimentally measured value

Mix mixture

out outlet

outer outer diameter

rand random uncertainty

ref refrigerant

s	sensible heat duty
sat	evaluated at saturation conditions
sys	systematic uncertainty
T	total heat duty
tot	total uncertainty
v	vapor phase
w	water
$wall$	wall

APPENDICES

Appendix A: Sample Calculations

This appendix provides representative analysis/sample calculations for a data point from this study. The working fluid for this data point is R454C, with nominal mass flux equal to 300 kg m^{-2} s^{-1} and saturation temperature equal to 50 °C. Sample Heat transfer and pressure drop calculations for this experiment are presented in Tables A.1 and A.3, respectively. In addition, Table A.2 shows in detail the procedure to implement the model that was developed in this study for the sample experiment.

Table A.1 Sample heat transfer calculation

R454C, T = 50 °C @ G = 300 kg m^{-2} s^{-1}		
Input(s)	**Equation(s)**	**Result(s)**
Mass flux and experimental conditions		
$d_{ii} = 0.0047[m]$(measured) $\dot{m}_{ref} = 0.005164[kg\ s^{-1}]$(measured) P_{ref} = 2031 [kPa] (measured) $y_1 = 0.215$ (R32 mass composition) $y_1 = 0.785$ (R1234yf mass composition)	$A_i = \frac{\pi}{4} d_{ii}^2$ $G = \frac{\dot{m}_{ref}}{A_i}$ $T_{dew} = f(P_{ref}, y_1, y_2, x = 1)$ $T_{bubble} = f(P_{ref}, y_1, y_2, x = 0)$	$A_i = 0.00001753[m^2]$ G = 294.6 [kg m^{-2} s^{-1}] T_{dew} = 53.44 [°C] T_{bubble} = 47.14 [°C]
Heat transfer in the tee before Segment 1		
P_w =137.5 [kPa] (measured) $\dot{m}_w$ =0.02892 [kg s^{-1}] (measured) $T_w[1]$ = 25.70 [C] (measured) $T_w[2]$ = 24.79 [C] (measured)	$h_w[1] = f(P_w, T_w[1])$ $h_w[2] = f(P_w, T_w[2])$ $\dot{Q}[1] = \dot{m}_w(h_w[1] - h_w[2])$	$h_w[1]$ = 107.9 [kJ kg^{-1}] $h_w[2]$ = 104.1[kJ kg^{-1}] $\dot{Q}[1]$ = 0.1096 [kW]
P_{ref} = 2031 [kPa] (measured) $\dot{m}_{ref} = 0.005164[kg\ s^{-1}]$(measured) $y_1 = 0.215$ (R32 mass composition) $y_2 = 0.785$ (R1234yf mass composition) $T_{ref}[1]$ = 85.37 [°C](measured) $\dot{Q}[1]$ = 0.1096 [kW]	$h_{ref}[1] = f(P_{ref}, T_{ref}[1], y_1, y_2)$ $h_{ref}[2] = h_{ref}[1] - \frac{Q[1]}{\dot{m}_{ref}}$ $T_{ref}[2] = f(P_{ref}, h_{ref}[2], y_1, y_2)$ $h_{ref,avg}[1] = \frac{h_{ref,avg}[1] + h_{ref,avg}[2]}{2}$ $T_{ref,avg}[1] = f(P_{ref}, h_{ref,avg}[1], y_1, y_2)$	$h_{ref}[1]$ = 460.3 [kJ kg^{-1}] $h_{ref}[2]$ = 439.1 [kJ kg^{-1}] $T_{ref}[2]$ = 68.41[°C] $h_{ref,avg}[1]$ = 449.7 [kJ kg^{-1}] $T_{ref,avg}[1]$ = 76.75 [°C]

Heat transfer in Segment 1		
P_w=137.5 [kPa] (measured) $\dot{m}_w$=0.02892 [kg s^{-1}] $T_w[2]$ = 24.79 [C] (measured) $T_w[3]$ = 23.33 [C] (measured) $h_w[2]$ = 104.1[kJ kg^{-1}]	$h_w[3] = f(P_w, T_w[3])$ $\dot{Q}[2] = \dot{m}_w(h_w[2] - h_w[3])$	$h_w[3]$ = 97.98 [kJ kg^{-1}] $\dot{Q}[2] = 0.1763$ [kW]
P_{ref} = 2031 [kPa] (measured) $\dot{m}_{ref} = 0.005164[kg\ s^{-1}]$(measured) $y_1 = 0.215$ (R32 mass composition) $y_1 = 0.785$ (R1234yf mass composition) $T_{ref}[2] = 68.41$ [°C] $\dot{Q}[2] = 0.1763$ [kW] $h_{ref}[2] = 439.1$ [kJ kg^{-1}]	$h_{ref}[3] = h_{ref}[2] - \frac{Q[2]}{\dot{m}_{ref}}$ $T_{ref}[3] = f(P_{ref}, h_{ref}[3], y_1, y_2)$	$h_{ref}[3] = 405$ [kJ kg^{-1}] $T_{ref}[3] = 52.84$[°C]
$d_{ii} = 0.004724$ [m] d_{oi}=0.00635 [m] $l[1] = 0.1773$ [m] $k_c = 0.3961$[kW m^{-1} k^{-1}] $\dot{Q}[2] = 0.1763$ [kW] $T_{c,outter}[1] = 29.94$[°C]	$T_{c,inner}[1] = T_{c,outer}[1] + \frac{\dot{Q}[2]\ln(d_{ii}/d_{oi})}{2\pi l[1]k_c}$	$T_{c,inner}[1] = 30.06$ [°C]
P_{ref} = 2031 [kPa] (measured) $y_1 = 0.215$ (R32 mass composition) $y_1 = 0.785$ (R1234yf mass composition) $A_i = 0.00001753[m^2]$ $\dot{Q}[2] = 0.1763$ [kW] $h_{ref}[2] = 439.1$ [kJ kg^{-1}] $h_{ref}[3] = 405$ [kJ kg^{-1}] $T_{c,inner}[1] = 30.06$ [°C]	$h_{ref,avg}[2] = \frac{h_{ref,avg}[2] + h_{ref,avg}[3]}{2}$ $T_{ref,avg}[2] = f(P_{ref}, h_{ref,avg}[2], y_1, y_2)$ $\alpha_{ref}[1] = \frac{\dot{Q}[2]/A_i}{T_{ref,avg}[2] - T_{c,inner}[1]}$	$h_{ref,avg}[2] = 422.1$ [kJ kg^{-1}] $T_{ref,avg}[2] = 55.92$[°C] $\alpha_{ref}[1] = 2.591$ [kW m^{-2} k^{-1}]

Heat transfer in Segment 2		
P_w =137.5 [kPa] (measured) $\dot{m}_w$ =0.02892 [kg s^{-1}] $T_w[3]$ = 23.33 [°C] (measured) $T_w[4]$ = 21.92 [°C] (measured) $h_w[3]$ = 97.98[kJ kg^{-1}]	$h_w[4] = f(P_w, T_w[4])$ $\dot{Q}[3] = \dot{m}_w(h_w[3] - h_w[4])$	$h_w[4]$ = 92.09 [kJ kg^{-1}] $\dot{Q}[3]$ = 0.1705 [kW]
P_{ref} = 2031 [kPa] (measured) $\dot{m}_{ref}$ = 0.005164[$kg\ s^{-1}$](measured) y_1 = 0.215 (R32 mass composition) y_1 = 0.785 (R1234yf mass composition) $T_{ref}[3]$ = 52.84 [°C] $\dot{Q}[3]$ = 0.1705 [kW] $h_{ref}[3]$ = 405 [kJ kg^{-1}]	$h_{ref}[4] = h_{ref}[3] - \frac{Q[3]}{\dot{m}_{ref}}$ $T_{ref}[4] = f(P_{ref}, h_{ref}[4], y_1, y_2)$	$h_{ref}[4]$ = 372 [kJ kg^{-1}] $T_{ref}[4]$ = 51.31[°C]
d_{ii} = 0.004724 [m] d_{oi} =0.00635 [m] $l[2]$ = 0.1773 [m] k_c = 0.3961[kW m^{-1} k^{-1}] $\dot{Q}[3]$ = 0.1705 [kW] $T_{c,outter}[2]$ = 27.74[°C]	$T_{c,inner}[2] = T_{c,outer}[2] + \frac{\dot{Q}[3]\ln(d_{ii}/d_{oi})}{2\pi l[2]k_c}$	$T_{c,inner}[2]$ = 27.86 [°C]
P_{ref} = 2031 [kPa] (measured) y_1 = 0.215 (R32 mass composition) y_1 = 0.785 (R1234yf mass composition) A_i = 0.00001753[m^2] $\dot{Q}[3]$ = 0.1705 [kW] $h_{ref}[3]$ = 405 [kJ kg^{-1}] $h_{ref}[4]$ = 372 [kJ kg^{-1}] $T_{c,inner}[2]$ = 27.86 [°C]	$h_{ref,avg}[3] = \frac{h_{ref,avg}[3] + h_{ref,avg}[4]}{2}$ $T_{ref,avg}[3] = f(P_{ref}, h_{ref,avg}[3], y_1, y_2)$ $\alpha_{ref}[2] = \frac{\dot{Q}[3]/A_i}{T_{ref,avg}[3] - T_{c,inner}[2]}$ $x_{ref,avg}[2] = f(P_{ref}, h_{ref,avg}[3], y_1, y_2)$	$h_{ref,avg}[3]$ = 388.5[kJ kg^{-1}] $T_{ref,avg}[3]$ = 50.62[°C] $\alpha_{ref}[2]$ = 2.675 [kW m^{-2} k^{-1}] $x_{ref,avg}[2]$ = 0.7648[–]

Heat transfer in Segment 3		
P_w =137.5 [kPa] (measured) $\dot{m}_w$ =0.02892 [kg s^{-1}] $T_w[4]$ = 21.92 [°C] (measured) $T_w[5]$ = 20.67 [°C] (measured) $h_w[4]$ = 92.09[kJ kg^{-1}]	$h_w[5] = f(P_w, T_w[5])$ $\dot{Q}[4] = \dot{m}_w(h_w[4] - h_w[5])$	$h_w[5]$ = 86.86 [kJ kg^{-1}] $\dot{Q}[4]$ = 0.1513 [kW]
P_{ref} = 2031 [kPa] (measured) $\dot{m}_{ref}$ = 0.005164[$kg\ s^{-1}$](measured) y_1 = 0.215 (R32 mass composition) y_1 = 0.785 (R1234yf mass composition) $T_{ref}[4]$ = 51.31 [°C] $\dot{Q}[4]$ = 0.1513 [kW] $h_{ref}[4]$ = 372 [kJ kg^{-1}]	$h_{ref}[5] = h_{ref}[4] - \frac{Q[4]}{\dot{m}_{ref}}$ $T_{ref}[5] = f(P_{ref}, h_{ref}[5], y_1, y_2)$	$h_{ref}[5]$ = 342.7 [kJ kg^{-1}] $T_{ref}[5]$ = 49.93 [°C]
d_{ii} = 0.004724 [m] d_{oi} =0.00635 [m] $l[3]$ = 0.1773 [m] k_c = 0.3961[kW m^{-1} k^{-1}] $\dot{Q}[4]$ = 0.1513 [kW] $T_{c,outter}[3]$ = 23.37[°C]	$T_{c,inner}[3] = T_{c,outer}[3] + \frac{\dot{Q}[4]\ln(d_{ii}/d_{oi})}{2\pi l[3]k_c}$	$T_{c,inner}[3]$ = 23.47 [°C]
P_{ref} = 2031 [kPa] (measured) y_1 = 0.215 (R32 mass composition) y_1 = 0.785 (R1234yf mass composition) A_i = 0.00001753[m^2] $\dot{Q}[4]$ = 0.1513 [kW] $h_{ref}[4]$ = 372 [kJ kg^{-1}] $h_{ref}[5]$ = 342.7 [kJ kg^{-1}] $T_{c,inner}[3]$ = 23.47 [°C]	$h_{ref,avg}[4] = \frac{h_{ref,avg}[4] + h_{ref,avg}[5]}{2}$ $T_{ref,avg}[4] = f(P_{ref}, h_{ref,avg}[4], y_1, y_2)$ $\alpha_{ref}[3] = \frac{\dot{Q}[4]/A_i}{T_{ref,avg}[4] - T_{c,inner}[3]}$ $x_{ref,avg}[3] = f(P_{ref}, h_{ref,avg}[4], y_1, y_2)$	$h_{ref,avg}[4]$ = 357.3 [kJ kg^{-1}] $T_{ref,avg}[4]$ = 50.62[°C] $\alpha_{ref}[3]$ = 2.118 [kW m^{-2} k^{-1}] $x_{ref,avg}[3]$ = 0.531[–]

Heat transfer in Segment 4		
P_w =137.5 [kPa] (measured) $\dot{m}_w$ =0.02892 [kg s^{-1}] $T_w[5]$ = 20.67 [°C] (measured) $T_w[6]$ = 19.61 [°C] (measured) $h_w[5]$ = 86.86 [kJ kg^{-1}]	$h_w[6] = f(P_w, T_w[6])$ $\dot{Q}[5] = \dot{m}_w(h_w[5] - h_w[6])$	$h_w[6]$ = 82.39 [kJ kg^{-1}] $\dot{Q}[5]$ = 0.1291 [kW]
P_{ref} = 2031 [kPa] (measured) $\dot{m}_{ref}$ = 0.005164[$kg\ s^{-1}$](measured) y_1 = 0.215 (R32 mass composition) y_1 = 0.785 (R1234yf mass composition) $T_{ref}[5]$ = 49.93 [°C] $\dot{Q}[5]$ = 0.1291 [kW] $h_{ref}[5]$ = 342.7 [kJ kg^{-1}]	$h_{ref}[6] = h_{ref}[5] - \frac{Q[5]}{\dot{m}_{ref}}$ $T_{ref}[6] = f(P_{ref}, h_{ref}[6], y_1, y_2)$	$h_{ref}[6]$ = 317.7 [kJ kg^{-1}] $T_{ref}[6]$ = 48.78 [°C]
d_{ii} = 0.004724 [m] d_{oi} =0.00635 [m] $l[4]$ = 0.1773 [m] k_c = 0.3961[kW m^{-1} k^{-1}] $\dot{Q}[5]$ = 0.1291 [kW] $T_{c,outter}[4]$ = 22.34[°C]	$T_{c,inner}[4] = T_{c,outer}[4] + \frac{\dot{Q}[5]\ln(d_{ii}/d_{oi})}{2\pi l[4]k_c}$	$T_{c,inner}[4]$ = 22.42 [°C]
P_{ref} = 2031 [kPa] (measured) y_1 = 0.215 (R32 mass composition) y_1 = 0.785 (R1234yf mass composition) A_i = 0.00001753[m^2] $\dot{Q}[5]$ = 0.1291 [kW] $h_{ref}[5]$ = 342.7 [kJ kg^{-1}] $h_{ref}[6]$ = 317.7 [kJ kg^{-1}] $T_{c,inner}[4]$ = 22.42 [°C]	$h_{ref,avg}[5] = \frac{h_{ref,avg}[5] + h_{ref,avg}[6]}{2}$ $T_{ref,avg}[5] = f(P_{ref}, h_{ref,avg}[5], y_1, y_2)$ $\alpha_{ref}[4] = \frac{\dot{Q}[5]/A_i}{T_{ref,avg}[5] - T_{c,inner}[4]}$ $x_{ref,avg}[4] = f(P_{ref}, h_{ref,avg}[5], y_1, y_2)$	$h_{ref,avg}[5]$ = 330.2 [kJ kg^{-1}] $T_{ref,avg}[5]$ = 49.35[°C] $\alpha_{ref}[4]$ = 1.822 [kW m^{-2} k^{-1}] $x_{ref,avg}[4]$ = 0.3371[–]

Heat transfer in Segment 5		
P_w =137.5 [kPa] (measured) $\dot{m}_w$ =0.02892 [kg s^{-1}] $T_w[6]$ = 19.61 [°C] (measured) $T_w[7]$ = 18.78 [°C] (measured) $h_w[6]$ = 82.39 [kJ kg^{-1}]	$h_w[7] = f(P_w, T_w[7])$ $\dot{Q}[6] = \dot{m}_w(h_w[6] - h_w[7])$	$h_w[7]$ = 78.92 [kJ kg^{-1}] $\dot{Q}[6]$ = 0.1004 [kW]
P_{ref} = 2031 [kPa] (measured) $\dot{m}_{ref}$ = 0.005164[$kg\ s^{-1}$](measured) y_1 = 0.215 (R32 mass composition) y_1 = 0.785 (R1234yf mass composition) $T_{ref}[6]$ = 48.78 [°C] $\dot{Q}[5]$ = 0.1004 [kW] $h_{ref}[6]$ = 317.7 [kJ kg^{-1}]	$h_{ref}[7] = h_{ref}[6] - \frac{Q[6]}{\dot{m}_{ref}}$ $T_{ref}[7] = f(P_{ref}, h_{ref}[7], y_1, y_2)$	$h_{ref}[7]$ = 298.2 [kJ kg^{-1}] $T_{ref}[7]$ = 47.92 [°C]
d_{ii} = 0.004724 [m] d_{oi} =0.00635 [m] $l[5]$ = 0.1773 [m] k_c = 0.3961[kW m^{-1} k^{-1}] $\dot{Q}[6]$ = 0.1004 [kW] $T_{c,outter}[5]$ = 22.51[°C]	$T_{c,inner}[5] = T_{c,outer}[5] + \frac{\dot{Q}[6]\ln(d_{ii}/d_{oi})}{2\pi l[5]k_c}$	$T_{c,inner}[5]$ = 22.58 [°C]
P_{ref} = 2031 [kPa] (measured) y_1 = 0.215 (R32 mass composition) y_1 = 0.785 (R1234yf mass composition) A_i = 0.00001753[m^2] $\dot{Q}[6]$ = 0.1004 [kW] $h_{ref}[6]$ = 317.7 [kJ kg^{-1}] $h_{ref}[7]$ = 298.2 [kJ kg^{-1}] $T_{c,inner}[5]$ = 22.58 [°C]	$h_{ref,avg}[6] = \frac{h_{ref,avg}[6] + h_{ref,avg}[7]}{2}$ $T_{ref,avg}[6] = f(P_{ref}, h_{ref,avg}[6], y_1, y_2)$ $\alpha_{ref}[5] = \frac{\dot{Q}[6]/A_i}{T_{ref,avg}[6] - T_{c,inner}[5]}$ $x_{ref,avg}[5] = f(P_{ref}, h_{ref,avg}[6], y_1, y_2)$	$h_{ref,avg}[6]$ = 308 [kJ kg^{-1}] $T_{ref,avg}[6]$ = 48.35 [°C] $\alpha_{ref}[5]$ = 1.481 [kW m^{-2} k^{-1}] $x_{ref,avg}[5]$ = 0.1849[–]

Heat transfer in Segment 6		
P_w =137.5 [kPa] (measured) $\dot{m}_w$ =0.02892 [kg s^{-1}] $T_w[7]$ = 18.78 [°C] (measured) $T_w[8]$ = 18.05 [°C] (measured) $h_w[7]$ = 78.92 [kJ kg^{-1}]	$h_w[8] = f(P_w, T_w[8])$ $\dot{Q}[7] = \dot{m}_w(h_w[7] - h_w[8])$	$h_w[8]$ = 75.88 [kJ kg^{-1}] $\dot{Q}[7]$ = 0.0879 [kW]
P_{ref} = 2031 [kPa] (measured) $\dot{m}_{ref}$ = 0.005164[$kg\ s^{-1}$](measured) y_1 = 0.215 (R32 mass composition) y_1 = 0.785 (R1234yf mass composition) $T_{ref}[7]$ = 47.92 [°C] $\dot{Q}[7]$ = 0.0879 [kW] $h_{ref}[7]$ = 298.2 [kJ kg^{-1}]	$h_{ref}[8] = h_{ref}[7] - \frac{Q[7]}{\dot{m}_{ref}}$ $T_{ref}[8] = f(P_{ref}, h_{ref}[8], y_1, y_2)$	$h_{ref}[8]$ = 281.2 [kJ kg^{-1}] $T_{ref}[8]$ = 47.2 [°C]
d_{ii} = 0.004724 [m] d_{oi} =0.00635 [m] $l[6]$ = 0.1773 [m] k_c = 0.3961[kW m^{-1} k^{-1}] $\dot{Q}[7]$ = 0.0879 [kW] $T_{c,outter}[6]$ = 21.07[°C]	$T_{c,inner}[6] = T_{c,outer}[6] + \frac{\dot{Q}[7]\ln(d_{ii}/d_{oi})}{2\pi l[6]k_c}$	$T_{c,inner}[6]$ = 21.13 [°C]
P_{ref} = 2031 [kPa] (measured) y_1 = 0.215 (R32 mass composition) y_1 = 0.785 (R1234yf mass composition) A_i = 0.00001753[m^2] $\dot{Q}[7]$ = 0.0879 [kW] $h_{ref}[7]$ = 298.2 [kJ kg^{-1}] $h_{ref}[8]$ = 281.2 [kJ kg^{-1}] $T_{c,inner}[6]$ = 21.13 [°C]	$h_{ref,avg}[7] = \frac{h_{ref,avg}[7] + h_{ref,avg}[8]}{2}$ $T_{ref,avg}[7] = f(P_{ref}, h_{ref,avg}[7], y_1, y_2)$ $\alpha_{ref}[6] = \frac{\dot{Q}[7]/A_i}{T_{ref,avg}[7] - T_{c,inner}[6]}$ $x_{ref,avg}[6] = f(P_{ref}, h_{ref,avg}[6], y_1, y_2)$	$h_{ref,avg}[7]$ = 289.7 [kJ kg^{-1}] $T_{ref,avg}[7]$ = 47.56 [°C] $\alpha_{ref}[6]$ = 1.264 [kW m^{-2} k^{-1}] $x_{ref,avg}[6]$ = 0.0643 [–]

Heat transfer in Segment 7		
P_w =137.5 [kPa] (measured) $\dot{m}_w$ =0.02892 [kg s^{-1}] $T_w[8]$ = 18.05 [°C] (measured) $T_w[9]$ = 17.41 [°C] (measured) $h_w[8]$ = 75.88 [kJ kg^{-1}]	$h_w[9] = f(P_w, T_w[9])$ $\dot{Q}[8] = \dot{m}_w(h_w[8] - h_w[9])$	$h_w[8]$ = 73.21 [kJ kg^{-1}] $\dot{Q}[8]$ = 0.0773 [kW]
P_{ref} = 2031 [kPa] (measured) $\dot{m}_{ref}$ = 0.005164[$kg\ s^{-1}$](measured) y_1 = 0.215 (R32 mass composition) y_1 = 0.785 (R1234yf mass composition) $T_{ref}[8]$ = 47.2 [°C] $\dot{Q}[8]$ = 0.0773 [kW] $h_{ref}[8]$ = 281.2 [kJ kg^{-1}]	$h_{ref}[9] = h_{ref}[8] - \frac{Q[8]}{\dot{m}_{ref}}$ $T_{ref}[9] = f(P_{ref}, h_{ref}[9], y_1, y_2)$	$h_{ref}[9]$ = 266.2 [kJ kg^{-1}] $T_{ref}[9]$ = 43.63 [°C]
d_{ii} = 0.004724 [m] d_{oi} =0.00635 [m] $l[7]$ = 0.1773 [m] k_c = 0.3961[kW m^{-1} k^{-1}] $\dot{Q}[8]$ = 0.0773 [kW] $T_{c,outter}[7]$ = 20.01[°C]	$T_{c,inner}[7] = T_{c,outer}[7] + \frac{\dot{Q}[8]\ln(d_{ii}/d_{oi})}{2\pi l[7]k_c}$	$T_{c,inner}[7]$ = 21.07 [°C]
P_{ref} = 2031 [kPa] (measured) y_1 = 0.215 (R32 mass composition) y_1 = 0.785 (R1234yf mass composition) A_i = 0.00001753[m^2] $\dot{Q}[8]$ = 0.0773 [kW] $h_{ref}[8]$ = 281.2 [kJ kg^{-1}] $h_{ref}[9]$ = 266.2 [kJ kg^{-1}] $T_{c,inner}[7]$ = 21.07 [°C]	$h_{ref,avg}[8] = \frac{h_{ref,avg}[8] + h_{ref,avg}[9]}{2}$ $T_{ref,avg}[8] = f(P_{ref}, h_{ref,avg}[8], y_1, y_2)$ $\alpha_{ref}[7] = \frac{\dot{Q}[8]/A_i}{T_{ref,avg}[8] - T_{c,inner}[7]}$	$h_{ref,avg}[8]$ = 273.7 [kJ kg^{-1}] $T_{ref,avg}[8]$ = 43.63 [°C] $\alpha_{ref}[7]$ = 1.246 [kW m^{-2} k^{-1}]

Table A.2 Sample prediction procedure for the proposed model

R454C, T = 50 °C @ G = 300 kg m^{-2} s^{-1}

Input(s)	Equation(s)	Result(s)
Predictions in the segment 1		
$T_{c,inner}[1] = 30.06$ [°C] $h_{ref}[1] = 460.3$ [kJ kg^{-1}]	Condensation begins when the tube wall temperature is lower than the saturation temperature. Condensation is assumed to begin at test section inlet since inner wall temperature in the first segment is at least 15 °C lower than saturation temperature. Therefore, refrigerant inlet enthalpy is onset enthalpy.	$h_{onset} = 460.3$[kJ kg^{-1}]
$h_v = 418.4$ [kJ kg^{-1}] $h_l = 279.8$ [kJ kg^{-1}] $h_{onset} = 460.3$[kJ kg^{-1}] $h_{ref,avg}[2] = 422.1$ [kJ kg^{-1}] (superheated segment)	$x_{apparent}[2] = \frac{h_{ref,avg}[2] - h_l}{h_{onset} - h_l}$	$x_{apparent}[2] = 0.788$
$\rho_{l,sat} = 939.8$ [kg m^{-3}] $\rho_{v,sat} = 100.7$ [kg m^{-3}] $\mu_{l,sat} = 0.00009673$ [Pa s] $\mu_{v,sat} = 0.00001409$ [Pa s] $k_l = 0.0000668$ [kW m^{-1} °C^{-1}] $Pr_l = 2.542$ [-] $G = 294.6$ [kg m^{-2} s^{-1}] $d_{ii} = 0.004724$ [m] $g = 9.82$ [m s^{-2}] $x_{apparent}[2] = 0.788$	Cavallini *et al.* (2006) Correlation: $X_{tt} = \left[\frac{1-x_{apparent}}{x_{apparent}}\right]^{0.9}\left[\frac{\rho_{v,sat}}{\rho_{l,sat}}\right]^{0.5}\left[\frac{\mu_{l,sat}}{\mu_{v,sat}}\right]^{0.1}$ $J_G^T = \left[\left[\frac{7.5}{4.3X_{tt}^{1.111}+1}\right]^{-3} + 2.6^{-3}\right]^{-1/3}$ $J_G = \frac{x_{apparent} G}{\sqrt{g d_{ii} \rho_v (\rho_l - \rho_v)}}$ $\alpha_{LO} = 0.023 \frac{k_l}{d_{ii}}\left[G d_{ii}/\mu_{l,sat}\right]^{0.8} Pr_l^{0.4}$ If $(J_G > J_G^T)$ then: $\alpha_{cav} = \alpha_{LO}\left[1+1.128 x_{apparent}^{0.817}(\rho_l/\rho_v)^{0.3685}(\mu_l/\mu_v)^{0.236}\right.$ $\left.\times(1-\mu_v/\mu_v)^{2.144} Pr_l^{-0.1}\right.$ If $(J_G \leq J_G^T)$ then:	$\alpha_{cav}[1] = 3.172$ [kW m^{-2} k^{-1}]

	$\alpha_{Strat} = \left\langle \begin{array}{l} 0.725\left\{1+0.741[(1-x)/x]^{0.3321}\right\}^{-1} \\ \times\left[k_l^3\rho_l(\rho_l-\rho_v)gh_{lv}/(\mu_l d_{ii}\Delta T)\right]^{0.25} \\ +(1-x^{0.87})\alpha_{LO} \end{array} \right\rangle$ $\alpha_{cav} = \left[\alpha_A (J_G^T/J_G)^{0.8} - \alpha_{Strat}\right](J_G/J_G^T)+\alpha_{Strat}$	
$\alpha_{cav}[1] = 3.172$ [kW m^{-2} k^{-1}] $T_{dew} =$ 53.44 [˚C] $A_i = 0.00001753[m^2]$ $\dot{Q}[2] = 0.1763$ [kW] $T_{ref,avg}[2] =$ 55.92[˚C]	$\alpha_{jacob}[1] = \left[\frac{1}{\alpha_{cav}[1]} + \frac{T_{ref,avg}[2]-T_{dew}}{\dot{Q}[2]/A_i}\right]^{-1}$	$\alpha_{jacob}[1] = 2.838$ [kW m^{-2} k^{-1}]
$G = 294.6$ [kg m^{-2} s^{-1}] $d_{ii} = 0.004724$ [m] $\mu_{v,sat} = 0.00001409$ [Pa s] $c_{p,v,sat} = 1.518$ [kJ/kg-C] $\mathrm{Pr}_v = 1.115$ [-] $T_{dew} =$ 53.44 [˚C] $T_{bubble} =$ 47.14 [˚C] $A_i = 0.00001753[m^2]$ $k_v = 0.00001919$ [kW m^{-1} ˚C^{-1}] $\alpha_{jacob}[1] = 2.838$ [kW m^{-2} k^{-1}] $x_{apparent}[2] = 0.788$	Silver (1947), Bell & Ghaly (1973) : $\mathrm{Re}_v = G x_{apparent} d_{ii}/\mu_{v,sat}$ $Z = x_{apparent} c_{p,v,sat} \frac{(T_{dew}-T_{bubble})}{h_v - h_l}$ $\alpha_v = 0.023(k_v/d_{ii})\,\mathrm{Re}_v^{0.8}\,\mathrm{Pr}_v^{0.4}$ $\alpha_{jacob,sbg} = \left(\frac{1}{\alpha_{jacob}} + \frac{Z}{\alpha_v}\right)^{-1}$	$\alpha_{jacob,sbg}[1] =$ 2.38[kW m^{-2} k^{-1}]

Predictions in the segment 2		
$h_v = 418.4$ [kJ kg^{-1}] $h_l = 279.8$ [kJ kg^{-1}] $h_{onset} = 460.3$[kJ kg^{-1}] $h_{ref,avg}[3] = 388.5$ [kJ kg^{-1}] (saturated segment)	$x_{apparent}[3] = \frac{h_{ref,avg}[3] - h_l}{h_{onset} - h_l}$	$x_{apparent}[3] = 0.602$
$\rho_{l,sat} = 939.8$ [kg m^{-3}] $\rho_{v,sat} = 100.7$ [kg m^{-3}] $\mu_{l,sat} = 0.00009673$ [Pa s] $\mu_{v,sat} = 0.00001409$ [Pa s] $k_l = 0.0000668$ [kW m^{-1} °C^{-1}] $Pr_l = 2.542$ [-] $G = 294.6$ [kg m^{-2} s^{-1}] $d_{ii} = 0.004724$ [m] $g = 9.82$ [m s^{-2}] $x_{apparent}[3] = 0.602$	Cavallini *et al.* (2006) Correlation	$\alpha_{cav}[2] = 2.743$ [kW m^{-2} k^{-1}]
$\alpha_{cav}[2] = 2.743$ [kW m^{-2} k^{-1}]	$\alpha_{jacob}[2] = \alpha_{cav}[2]$	$\alpha_{jacob}[2] = 2.743$[kW m^{-2} k^{-1}]
$G = 294.6$ [kg m^{-2} s^{-1}] $d_{ii} = 0.004724$ [m] $\mu_{v,sat} = 0.00001409$ [Pa s] $c_{p,v,sat} = 1.518$ [kJ/kg-C] $Pr_v = 1.115$ [-] $T_{dew} = 53.44$ [°C] $T_{bubble} = 47.14$ [°C] $A_i = 0.00001753[m^2]$ $k_v = 0.00001919$ [kW m^{-1} °C^{-1}] $\alpha_{jacob}[2] = 2.743$[kW m^{-2} k^{-1}] $x_{apparent}[3] = 0.602$	Silver (1947), Bell & Ghaly (1973)	$\alpha_{jacob,sbg}[2] =$ 2.33[kW m^{-2} k^{-1}]

Predictions in the segment 3		
$h_v = 418.4$ [kJ kg^{-1}] $h_l = 279.8$ [kJ kg^{-1}] $h_{onset} = 460.3$[kJ kg^{-1}] $h_{ref,avg}[4] = 357.3$ [kJ kg^{-1}] (saturated segment)	$x_{apparent}[4] = \frac{h_{ref,avg}[4] - h_l}{h_{onset} - h_l}$	$x_{apparent}[4] = 0.4294$
$\rho_{l,sat} = 939.8$ [kg m^{-3}] $\rho_{v,sat} = 100.7$ [kg m^{-3}] $\mu_{l,sat} = 0.00009673$ [Pa s] $\mu_{v,sat} = 0.00001409$ [Pa s] $k_l = 0.0000668$ [kW m^{-1} °C^{-1}] $Pr_l = 2.542$ [-] $G = 294.6$ [kg m^{-2} s^{-1}] $d_{ii} = 0.004724$ [m] $g = 9.82$ [m s^{-2}] $x_{apparent}[4] = 0.4294$	Cavallini *et al.* (2006) Correlation	$\alpha_{cav}[3] = 2.323$ [kW m^{-2} k^{-1}]
$\alpha_{cav}[3] = 2.323$ [kW m^{-2} k^{-1}]	$\alpha_{jacob}[3] = \alpha_{cav}[3]$	$\alpha_{jacob}[3] = 2.323$ [kW m^{-2} k^{-1}]
$G = 294.6$ [kg m^{-2} s^{-1}] $d_{ii} = 0.004724$ [m] $\mu_{v,sat} = 0.00001409$ [Pa s] $c_{p,v,sat} = 1.518$ [kJ/kg-C] $Pr_v = 1.115$ [-] $T_{dew} = 53.44$ [°C] $T_{bubble} = 47.14$ [°C] $A_i = 0.00001753[m^2]$ $k_v = 0.00001919$ [kW m^{-1} °C^{-1}] $\alpha_{jacob}[3] = 2.323$[kW m^{-2} k^{-1}] $x_{apparent}[4] = 0.4294$	Silver (1947), Bell & Ghaly (1973)	$\alpha_{jacob,sbg}[3] =$ 2.038[kW m^{-2} k^{-1}]

Predictions in the segment 4		
$h_v = 418.4$ [kJ kg^{-1}] $h_l = 279.8$ [kJ kg^{-1}] $h_{onset} = 460.3$[kJ kg^{-1}] $h_{ref,avg}[5] = 330.2$ [kJ kg^{-1}] (saturated segment)	$x_{apparent}[5] = \frac{h_{ref,avg}[5] - h_l}{h_{onset} - h_l}$	$x_{apparent}[5] = 0.2791$
$\rho_{l,sat} = 939.8$ [kg m^{-3}] $\rho_{v,sat} = 100.7$ [kg m^{-3}] $\mu_{l,sat} = 0.00009673$ [Pa s] $\mu_{v,sat} = 0.00001409$ [Pa s] $k_l = 0.0000668$ [kW m^{-1} °C^{-1}] $Pr_l = 2.542$ [-] $G = 294.6$ [kg m^{-2} s^{-1}] $d_{ii} = 0.004724$ [m] $g = 9.82$ [m s^{-2}] $x_{apparent}[5] = 0.2791$	Cavallini *et al.* (2006) Correlation	$\alpha_{cav}[4] = 1.971$ [kW m^{-2} k^{-1}]
$\alpha_{cav}[4] = 1.971$ [kW m^{-2} k^{-1}]	$\alpha_{jacob}[4] = \alpha_{cav}[4]$	$\alpha_{jacob}[4] = 1.971$ [kW m^{-2} k^{-1}]
$G = 294.6$ [kg m^{-2} s^{-1}] $d_{ii} = 0.004724$ [m] $\mu_{v,sat} = 0.00001409$ [Pa s] $c_{p,v,sat} = 1.518$ [kJ/kg-C] $Pr_v = 1.115$ [-] $T_{dew} = 53.44$ [°C] $T_{bubble} = 47.14$ [°C] $A_i = 0.00001753[m^2]$ $k_v = 0.00001919$ [kW m^{-1} °C^{-1}] $\alpha_{jacob}[4] = 1.971$[kW m^{-2} k^{-1}] $x_{apparent}[5] = 0.2791$	Silver (1947), Bell & Ghaly (1973)	$\alpha_{jacob,sbg}[4] =$ 1.777[kW m^{-2} k^{-1}]

Predictions in the segment 5		
$h_v = 418.4$ [kJ kg^{-1}] $h_l = 279.8$ [kJ kg^{-1}] $h_{onset} = 460.3$[kJ kg^{-1}] $h_{ref,avg}[6] = 308$ [kJ kg^{-1}] (saturated segment)	$x_{apparent}[6] = \frac{h_{ref,avg}[6] - h_l}{h_{onset} - h_l}$	$x_{apparent}[6] = 0.156$
$\rho_{l,sat} = 939.8$ [kg m^{-3}] $\rho_{v,sat} = 100.7$ [kg m^{-3}] $\mu_{l,sat} = 0.00009673$ [Pa s] $\mu_{v,sat} = 0.00001409$ [Pa s] $k_l = 0.0000668$ [kW m^{-1} °C^{-1}] $Pr_l = 2.542$ [-] $G = 294.6$ [kg m^{-2} s^{-1}] $d_{ii} = 0.004724$ [m] $g = 9.82$ [m s^{-2}] $x_{apparent}[6] = 0.156$	Cavallini *et al.* (2006) Correlation	$\alpha_{cav}[5] = 1.623$ [kW m^{-2} k^{-1}]
$\alpha_{cav}[5] = 1.623$ [kW m^{-2} k^{-1}]	$\alpha_{jacob}[5] = \alpha_{cav}[5]$	$\alpha_{jacob}[5] = 1.623$ [kW m^{-2} k^{-1}]
$G = 294.6$ [kg m^{-2} s^{-1}] $d_{ii} = 0.004724$ [m] $\mu_{v,sat} = 0.00001409$ [Pa s] $c_{p,v,sat} = 1.518$ [kJ/kg-C] $Pr_v = 1.115$ [-] $T_{dew} = 53.44$ [°C] $T_{bubble} = 47.14$ [°C] $A_i = 0.00001753[m^2]$ $k_v = 0.00001919$ [kW m^{-1} °C^{-1}] $\alpha_{jacob}[5] = 1.623$[kW m^{-2} k^{-1}] $x_{apparent}[6] = 0.156$	Silver (1947), Bell & Ghaly (1973)	$\alpha_{jacob,sbg}[5] =$ 1.503[kW m^{-2} k^{-1}]

Predictions in the segment 6		
$h_v = 418.4$ [kJ kg^{-1}] $h_l = 279.8$ [kJ kg^{-1}] $h_{onset} = 460.3$[kJ kg^{-1}] $h_{ref,avg}[7] = 289.7$ [kJ kg^{-1}] (saturated segment)	$x_{apparent}[7] = \frac{h_{ref,avg}[7] - h_l}{h_{onset} - h_l}$	$x_{apparent}[7] = 0.05505$
$\rho_{l,sat} = 939.8$ [kg m^{-3}] $\rho_{v,sat} = 100.7$ [kg m^{-3}] $\mu_{l,sat} = 0.00009673$ [Pa s] $\mu_{v,sat} = 0.00001409$ [Pa s] $k_l = 0.0000668$ [kW m^{-1} °C^{-1}] $Pr_l = 2.542$ [-] $G = 294.6$ [kg m^{-2} s^{-1}] $d_{ii} = 0.004724$ [m] $g = 9.82$ [m s^{-2}] $x_{apparent}[7] = 0.05505$	Cavallini *et al.* (2006) Correlation	$\alpha_{cav}[6] = 1.276$ [kW m^{-2} k^{-1}]
$\alpha_{cav}[6] = 1.276$ [kW m^{-2} k^{-1}]	$\alpha_{jacob}[6] = \alpha_{cav}[6]$	$\alpha_{jacob}[6] = 1.276$ [kW m^{-2} k^{-1}]
$G = 294.6$ [kg m^{-2} s^{-1}] $d_{ii} = 0.004724$ [m] $\mu_{v,sat} = 0.00001409$ [Pa s] $c_{p,v,sat} = 1.518$ [kJ/kg-C] $Pr_v = 1.115$ [-] $T_{dew} = 53.44$ [°C] $T_{bubble} = 47.14$ [°C] $A_i = 0.00001753[m^2]$ $k_v = 0.00001919$ [kW m^{-1} °C^{-1}] $\alpha_{jacob}[6] = 1.276$[kW m^{-2} k^{-1}] $x_{apparent}[7] = 0.055$	Silver (1947), Bell & Ghaly (1973)	$\alpha_{jacob,sbg}[6] =$ 1.214[kW m^{-2} k^{-1}]
Predictions in the segment 7		
$\mu_l = 0.0001022$ [Pa s] $Pr_l = 2.538[-]$ $d_{ii} = 0.004724$ [m] $G = 294.6$ [kg m^{-2} s^{-1}] $h_{ref,avg}[7] = 289.7$ [kJ kg^{-1}] (subcooled segment)	Gnielinski (1976) Correlation: $f_b = [1.82\log_{10}(Gd_{ii}/\mu_v) - 1.64]$ $\alpha_v = \left(\frac{k_v}{d_{ii}}\right)\frac{(f_b/8)(Gd_{ii}/\mu_v - 1000)\,Pr_v}{1 + 12.7(f_b/8)^{1/2}(Pr_v^{2/3} - 1)}$	$f_b = 0.02888$ $\alpha_{jacob}[7] = 1.01$ [kW m^{-2} k^{-1}]

Table A.3 Sample pressure drop calculation

R454C, T = 50 °C @ G = 300 kg m^{-2} s^{-1}

Input(s)	Equation(s)	Result(s)
Determine the lengths associated with two-phase and single-phase regions		
$x_{ref}[2...7] = [0.8934, 0.6394, 0.4252, 0.2508, 0.1202, 0.009186]$ (From heat transfer calculations) $L[2...7] = [0.3429, 0.5334, 0.7239, 0.9144, 1.105, 1.295]$ (Measured)	$x_{ref}(L) = aL^2 + bL + c$	$a = 0.5163$ $b = -1.769$ $c = 1.438$ Coefficient of determination: $R^2 = 1$
$x_{ref}(L) = 1$	$x_{ref}(L) = 0.5163L^2 - 1.769L + 1.438$	$L_v = 0.269\,m$
$x_{ref}(L) = 0$ $L_v = 0.269\,m$	$x_{ref}(L) = 0.5163L^2 - 1.769L + 1.438$ $L_{tp} = L(x=0) - L_v$	$L_{tp} = 1.033\,m$
$L_v = 0.269\,m$ $L_{tp} = 1.033\,m$ $L_{total} = 1.676\,m\,(measured)$	$L_l = L_{total} - L_{tp} - L_v$	$L_l = 0.374\,m$
Evaluate the minor loses		
$d_{ii} = 0.0047[m]$(measured) P_{ref} = 2031 [kPa] (measured) μ_{in} =0.00001533 [kg m^{-1} s^{-1}] ρ_{in} = 77.76 [kg m^{-3}] $\dot{V}_{in}$ = 3.788 [m s^{-1}] $L_v = 0.269\,m$	Churchill (1977) correlation: $\mathrm{Re} = Gd_{ii} / \mu_{in}$ $B = \left(\frac{37530}{\mathrm{Re}}\right)^{16}$ $A = \left(2.457 \ln\left[\frac{1}{\left(\frac{7}{\mathrm{Re}}\right)^{0.9} + 0.27RR}\right]\right)^{16}$ $f = 8\left\{\left(\frac{8}{\mathrm{Re}}\right)^{12} + [A+B]^{-1.5}\right\}^{1/12}$ $\Delta P_v = f\left(\frac{l_v}{d_{ii}}\right)\frac{\rho_{in}V^2}{2}$	$\Delta P_v = 0.647$ [kPa]

$d_{ii} = 0.0047[m]$(measured) P_{ref} = 2031 [kPa] (measured) $\mu_{out} = 0.0001193$ [kg m^{-1} s^{-1}] $\rho_{out} = 1015$ [kg m^{-3}] $\dot{V}_{out} = 0.2902$ [m s^{-1}] $L_l = 0.374\,m$	Churchill (1977) correlation:	$\Delta P_l = 0.1035$ [kPa]
$\rho_{in} = 77.76$ [kg m^{-3}] $\dot{V}_{in} = 3.788$ [m s^{-1}] $\rho_{out} = 1015$ [kg m^{-3}] $\dot{V}_{out} = 0.2902$ [m s^{-1}]	$\Delta P_{decceleration} = \rho_{in}\dot{V}_{in}^2 - \rho_{out}\dot{V}_{out}^2$	$\Delta P_{decceleration} = 0.770$ [kPa]
Evaluate two-phase Frictional Pressure Drop		
$\Delta P_{measured} = 1.46$ [kPa] $\Delta P_v = 0.647$ [kPa] $\Delta P_l = 0.1035$ [kPa] $\Delta P_{decceleration} = 0.770$ [kPa]	$\Delta P_{friction} = \Delta P_{measured} - \Delta P_v - \Delta P_l - \Delta P_{decceleration}$	$\Delta P_{friction} = 1.479$ [kPa]